

AFRL-IF-RS-TR-1998-170
Final Technical Report
August 1998



ADAPTIVE SPREAD SPECTRUM SYSTEMS USING FILTERBANKS AND THE DISCRETE WAVELET TRANSFORM

Rensselaer Polytechnic Institute

G.J. Saulnier, K.J. Hetling, and P.K. Das

APPROVED FOR PUBLIC RELEASE; DISTRIBUTION UNLIMITED.

19981015 097

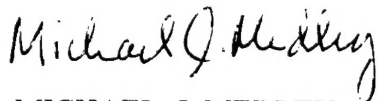
**AIR FORCE RESEARCH LABORATORY
INFORMATION DIRECTORATE
ROME RESEARCH SITE
ROME, NEW YORK**

DTIC QUALITY INSPECTED 4

This report has been reviewed by the Air Force Research Laboratory, Information Directorate, Public Affairs Office (IFOIPA) and is releasable to the National Technical Information Service (NTIS). At NTIS it will be releasable to the general public, including foreign nations.

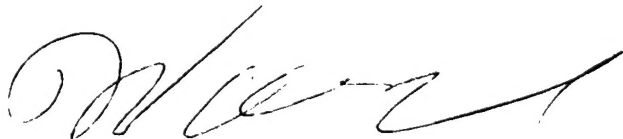
AFRL-IF-RS-TR-1998-170 has been reviewed and is approved for publication.

APPROVED:



MICHAEL J. MEDLEY
Project Engineer

FOR THE DIRECTOR:



WARREN H. DEBANY, JR., Technical Advisor
Information Grid Division
Information Directorate

If your address has changed or if you wish to be removed from the Air Force Research Laboratory Rome Research Site mailing list, or if the addressee is no longer employed by your organization, please notify AFRL/IFGC, 525 Brooks Road, Rome, NY 13441-4505. This will assist us in maintaining a current mailing list.

Do not return copies of this report unless contractual obligations or notices on a specific document require that it be returned.

REPORT DOCUMENTATION PAGE			Form Approved OMB No. 0704-0188	
Public reporting burden for this collection of information is estimated to average 1 hour per response, including the time for reviewing instructions, searching existing data sources, gathering and maintaining the data needed, and completing and reviewing the collection of information. Send comments regarding this burden estimate or any other aspect of this collection of information, including suggestions for reducing this burden, to Washington Headquarters Services, Directorate for Information Operations and Reports, 1215 Jefferson Davis Highway, Suite 1204, Arlington, VA 22202-4302, and to the Office of Management and Budget, Paperwork Reduction Project (0704-0188), Washington, DC 20503.				
1. AGENCY USE ONLY (Leave blank)	2. REPORT DATE August 1998	3. REPORT TYPE AND DATES COVERED Final Sep 95 - Jan 98		
4. TITLE AND SUBTITLE ADAPTIVE SPREAD SPECTRUM SYSTEMS USING FILTERBANKS AND THE DISCRETE WAVELET TRANSFORM		5. FUNDING NUMBERS C - 30602-95-C-0167 PE - 62702F PR - 4519 TA - 42 WU - 91		
6. AUTHOR(S) G. J. Saulnier, K. J. Hetling, and P. K. Das				
7. PERFORMING ORGANIZATION NAME(S) AND ADDRESS(ES) Rensselaer Polytechnic Institute 110 Eighth Street Troy NY 12180-3590		8. PERFORMING ORGANIZATION REPORT NUMBER N/A		
9. SPONSORING/MONITORING AGENCY NAME(S) AND ADDRESS(ES) AFRL/IFGC 525 Brooks Road Rome NY 13440-4505		10. SPONSORING/MONITORING AGENCY REPORT NUMBER AFRL-IF-RS-TR-1998-170		
11. SUPPLEMENTARY NOTES AFRL Project Engineer: Michael J. Medley/IFGC/(315) 330-4830				
12a. DISTRIBUTION AVAILABILITY STATEMENT Approved for public release; distribution unlimited.		12b. DISTRIBUTION CODE		
13. ABSTRACT (Maximum 200 words) This report discusses the development of new approaches for providing anti-jam, multipath resistant, multi-user communications based on filterbank and wavelet techniques. The first portion considers the synthesis of spreading waveforms using full binary tree multi-rate filterbank design techniques. Non-binary spreading waveforms are produced that are optimized for multi-user, multipath and interference channels and shown to out-perform some conventional spreading sequences. The second part of the report describes and evaluates a spread spectrum version of Orthogonal Frequency Division Multiplexing (OFDM) wherein the same information is transmitted on multiple orthogonal carriers, creating both time and frequency diversity. In the receiver, time domain and transform domain excision are used to improve performance in pulsed wideband or narrowband jamming, respectively. In addition, the report considers replacing the inverse and forward FFT's commonly used in OFDM systems with inverse and forward Modulated Lapped Transforms (MLT's). Performance results demonstrate the effectiveness of the techniques. For both the spreading waveform design and OFDM work, simulations were performed using the Signal Processing WorkSystem (SPW) from AltaGroup of Cadence Design Systems, Inc.				
14. SUBJECT TERMS Multipath Propagation, Interference Suppression, Jamming, OFDM, Multi-Carrier, Spreading Sequences, Gold Codes, Excision		15. NUMBER OF PAGES 148		
		16. PRICE CODE		
17. SECURITY CLASSIFICATION OF REPORT UNCLASSIFIED	18. SECURITY CLASSIFICATION OF THIS PAGE UNCLASSIFIED	19. SECURITY CLASSIFICATION OF ABSTRACT UNCLASSIFIED	20. LIMITATION OF ABSTRACT UL	

Contents

1	Introduction	1
1.1	Overview	1
1.2	Publications	2
1.3	Report Organization	3
2	Hetling Ph.D. Thesis	4
3	Proceedings of the SPIE, 1997	111
3	IEEE DSP Workshop, 1996	124
4	ICC, 1997	129
5	MILCOM, 1997	135

Chapter 1

Introduction

1.1 Overview

The primary objective of this effort was to develop new approaches for providing anti-jam, multipath resistant, multi-user communications based on filterbank and wavelet techniques. The investigation was primarily simulation-based, where the new techniques were implemented using the Signal Processing WorkSystem (SPW) from the Alta Group or Cadence Design Systems. Monte Carlo simulation using these SPW implementations was used to characterize system behavior and to obtain performance results.

The investigation focused on two major areas. The first area was the synthesis of new spreading waveforms using multi-rate filterbank design techniques. The spreading waveforms are produced by designing a full binary tree filterbank with properties that are determined by the desired properties of the signal. The spreading waveforms themselves are simply the impulse responses of the individual paths through the tree. The waveforms are non-binary and can be designed to optimize performance for the given channel conditions, including multi-user interference, multipath propagation, intentional interference (jamming) or a combination thereof. Performance results are provided for a number of spreading waveform sets which have been designed for different channels.

The second area of investigation concerns the use of Orthogonal Frequency Division Multiplexing (OFDM) in a military environment. Conventional OFDM signaling sends a data stream by breaking it into a number of lower-rate streams and sending each of these lower-rate streams on a different orthogonal carrier. The carriers are usually generated using an inverse Fast Fourier Transform (FFT) and demodulated using a forward FFT. This investigation focused on using OFDM as a spread spectrum modulation wherein the same information is sent on all of the carriers and both time and frequency diversity can be built into the signal. Frequency diversity occurs simply because the same infor-

mation is sent on many carriers of different frequencies. Time diversity can be obtained by sending the same data bit on each of the carriers but sending them at different times. In a simple implementation a particular data bit is sent on the first carrier in the first data bit interval, then on the second carrier during the second data bit interval followed by the third carrier during the next data bit interval, etc. In a more complicated implementation, a pseudo-random hopping pattern can be used to determine which carrier is occupied by which data bit at a given time. At the receiver, the energy from each of the carriers can be combined coherently prior to making decisions, providing processing gain equal to the number of carriers. In the case of narrowband interference, carriers that are jammed can be eliminated from the combining stage, effectively implementing interference excision. Another aspect of the work considered replacing the inverse and forward FFT's in the OFDM system with inverse and forward Modulated Lapped Transforms (MLT's). The MLT has the advantage of having greater time support and providing better spectral containment than a FFT of the same order. In the case of narrowband interference, the MLT-based system was able to provide better performance than the FFT due to this better spectral containment. In the presence of pulsed wideband interference, time segments of the received signal, i.e. the signal consisting of the sum of all the carriers, are excised in an attempt to suppress the interference. The use of time diversity greatly improved performance under these conditions, but the use of the MLT resulted in some performance loss. This loss is due to the greater time support of the MLT which resulted in the removal of time segments of the signal affecting more received data bits.

1.2 Publications

A number of publications have resulted from this effort:

- K. J. Hetling, "Multirate Filter Banks for Spread Spectrum Waveform Design", Ph.D. Thesis, Rensselaer Polytechnic Institute, Troy, NY, August 1996.
- K. J. Hetling, G. J. Saulnier and P. K. Das, "Performance of Filter Bank-Based Spreading Codes for Cellular and Micro-Cellular Channels," *Proceeding of the SPIE, Wavelet Applications IV*, Harold H. Szu, Ed. Vol. 3078, March 1997, pp. 635-646.
- G. J. Saulnier, V. A. A. Whyte, and M. J. Medley, "An OFDM Spread Spectrum System Using Lapped Transforms and Partial Band Interference Suppression," *Proceedings of the 1996 IEEE Digital Signal Processing Workshop*, Loen, Norway, September 1996.

- G. J. Saulnier, V. A. A. Whyte, and M. J. Medley, "OFDM Spread Spectrum Communications Using Lapped Transforms and Interference Excision," IEEE International Conference on Communications Conference Record, IEEE Publication 97CH36067, Montreal, Canada, June 1997, pp. 944-948.
- G. J. Saulnier, M. Mettke and M. J. Medley, "Performance of an OFDM Spread Spectrum Communications System Using Lapped Transforms," IEEE Military Communications Conference, Monterey, CA, November 1997.

1.3 Report Organization

The remainder of the report consists of appendices containing the publications cited above in the order given. The first two publications document the work on filterbank-based spreading codes while the remaining three document the work performed on spread spectrum OFDM with the MLT.

Appendix A: Hetling Ph.D. Thesis

Multirate Filter Banks for Spread Spectrum
Waveform Design

Kenneth J. Hetling
Ph.D. Thesis
Electrical Engineering
Rensselaer Polytechnic Institute
Troy, NY 12180-3590

Contents

1	Introduction and Background	14
1.1	Spread Spectrum Systems	14
1.2	Multuser Systems and CDMA	16
1.3	Multipath Channels and Spread Spectrum Communications	18
1.4	Pseudo-Noise Sequences for DSSS	19
1.5	Generalized Representation of Spreading Sequences	20
1.5.1	Cross Correlation Properties of Spreading Codes	21
1.6	Scope	23
2	PR-QMF Based Spreading Codes	26
2.1	Block Transforms and Multirate Filter Banks	27
2.2	Matrix Representation of Multirate Filter Banks	28
2.2.1	Polyphase Matrix Representation	29
2.2.2	Time-Domain Matrix Representation	30
2.3	The Two-Channel Subband Filter Bank	32
2.3.1	Subband Tree Structures	35
2.4	Progressive Optimality and Filter Bank Design	38
2.5	Subband Tree Applications	39
2.6	Properties of PR-QMF Based Spreading Codes	40

2.6.1	Generation of the PR-QMF Based Spreading Codes	40
2.6.2	Orthogonality Between Spreading Codes	44
2.6.3	Autocorrelation Properties of PR-QMF Spreading Codes	47
3	Optimized Filter Design for PR-QMF Based Spreading Codes	49
3.1	Optimized Filter Design for Anti-Jam Communications	50
3.2	Optimization Functions for the Multiuser Channel	53
3.2.1	The Two User Channel	54
3.2.2	Channels With Few Users	55
3.2.3	Channels With Many Users	57
3.3	Multiuser Channel With Coarse Synchronization	58
3.3.1	Alternate Representation of Spreading Code Shifts	59
3.3.2	Objective Functions for Coarse Synchronization	61
3.4	Optimized Filter Design for Multipath Channels	65
3.5	Optimized Filter Design for Composite Channels	66
3.6	Objective Functions for Other Interference Sources	67
4	Performance Analysis and Results	68
4.1	Performance in the Presence of Stationary Interference	69
4.1.1	Analysis	69
4.1.2	Results	71
4.2	Multiuser Channel	76
4.2.1	Analysis	76
4.2.2	Multiuser/Multipath Interference Results	80
5	Conclusions	95

5.1	Summary of Work	95
5.2	Conclusions	96
5.3	Future Directions	97
6	Bibliography	98
	APPENDICES	103
A	Matrix Notation and Operations	103
A.1	Notation and Specialized Matrices	103
A.2	Shift Operations on Vectors and Matrices	105
B	Filter Coefficients of the Subband Trees	106
B.1	Filter Coefficients for Section 4.1.2	107
B.2	Filter Coefficients for Section 4.2.2.1	108
B.3	Filter Coefficients for Section 4.2.2.4	108
B.4	Filter Coefficients for Section 4.2.2.6	109

List of Figures

1.1	Simplified DSSS Transmitter	15
1.2	Time Domain DSSS Receivers	16
1.3	Time-Frequency Plane for TDMA and FDMA	17
1.4	Time-Frequency Plane for CDMA	17
1.5	Spreading Code Generation Via Transforms	20
1.6	Data Bit Polarities	22
2.1	Multirate Subband Filter Bank	27
2.2	Two-Channel Subband Filter Bank	33
2.3	Quadrature Mirror Filter Frequency Responses	33
2.4	Full Binary Tree Structure	35
2.5	Normalized Frequency Response of an Ideal L-Stage Full Binary Tree . .	36
2.6	Dyadic Tree Structure	36
2.7	Normalized Frequency Response of an Ideal L-Stage Dyadic Subband Tree	37
2.8	The <i>Noble Identities</i> for Decimation and Interpolation	37
2.9	Four Band Tree Using Product Filters	38
2.10	Progressively Optimized Filter Banks - Level 1	38
2.11	Progressively Optimized Filter Banks - Level 2A	39
2.12	Progressively Optimized Filter Banks - Level 2B	39

2.13 Spreading Code Branches	45
3.1 Demodulation of a Signal Plus Interference	51
3.2 Interchange of a Filter and Downsampler	52
3.3 Interference Channel With N Users	57
3.4 Comparison of Gaussian Approximation Objective Function Argument	58
3.5 Mobile to Base Communications System	59
3.6 Branch Split at Stage 1	61
3.7 Spreading Code Branches	63
3.8 Final Stage Split	65
4.1 Magnitude Responses of the 3rd Stage Subbands	72
4.2 Performance Against 10dB Jamming	73
4.3 Frequency Spectrum of the PR-QMF Based System	74
4.4 Results Using a Reduced Code Pool, JSR=15dB	75
4.5 Results for a Single Tone Jammer, $\omega=0.687$, JSR=10dB	75
4.6 Sample Histogram of Cross Correlation Values	77
4.7 Frequency Response of Multiuser Codes	82
4.8 Cross Correlation Values of Sample Codes	84
4.9 Histograms of Cross Correlation Values	85
4.10 Multiuser Computer Simulation Results	86
4.11 Multiuser BER Results	87
4.12 Capacity for Various Weighting Factors	88
4.13 Sample Frequency Responses, $\alpha = 1.0$ and $\alpha = 0.6$	89
4.14 Sample Frequency Responses, $\alpha = 1.0$ and $\alpha = 0.4$	90
4.15 Capacity Inaccurate Power Control	91

4.16	Cross Correlation Results for Codes With Partial Synchronization	92
4.17	Capacity Results for Codes With Partial Synchronization	93
4.18	Frequency Response of Codes With Partial Synchronization	94
4.19	Cross Correlations of Two Codes Designed For Partial Synchronization .	94

Acknowledgement

I wish to thank a number of people who have helped me complete this thesis. First, I would like to thank Professor Gary Saulnier for his advice and support throughout my years here at RPI. Also, thanks go to Professor Pankaj Das for his multitude of research ideas many of which found their way into this thesis. I owe a great deal of gratitude to Michael Medley for his friendship, patience, and many hours of discussion on wavelets, filterbanks, and any other topic I wished to talk about.

I also owe thanks to Rome Laboratory at Griffiss AFB in Rome New York for the financial support under contracts #F30602-94-C-0142 and #F30602-95-C-0167 which provided the funding for the work contained in this thesis.

I would like to thank my family for their support especially my parents who have passed on to me the love and values they inherited from their parents. Additionally, my father, has provided me with the best example of engineering excellence which I will always try to achieve. I also wish to thank Alice Torda who was my unofficial advisor throughout all of my education.

Most importantly, this undertaking would not have been possible without the constant love and support from my wife Edi. She has done more for me than she will ever realize and taught me more than any university ever could. It is to you, Edi, that this thesis is dedicated. I love you.

Finally, I wish to thank God who makes all good things possible.

Abstract

A foundation for the generation of spreading codes based upon multirate filter banks is introduced. This new class of spreading codes is proposed as an alternative to the m -sequences which are the traditional choice for a direct sequence spread spectrum system. Unlike m -sequences, the new codes are not limited to being binary valued and their construction is based upon specific known channel characteristics.

After describing the generation of the codes from a given multirate filter bank, several important properties and characteristics of the codes are formulated in terms of the subband tree filters. A methodology for designing the filters is then presented. The filter tap weights are generated by solving a multivariable constrained optimization problem. The optimization problem incorporates the properties of the codes as well as channel characteristics. Objective functions and constraints are presented for three interference channels common to a mobile communications environment: stationary interference, multiuser interference, and multipath interference.

Expressions are then developed for analyzing the bit error rate performance of the spreading codes under various channel conditions. These expressions can be used to determine the capacity, in terms of number of users in the channel, of a system using the newly developed spreading codes. Filter banks are then designed for the various channel types. Designs for the multiuser channel include synchronous and asynchronous multiuser systems, as well as, a system with partial synchronization.

Comparisons are then made with the m -sequences and the Gold codes. It is shown that the newly developed spreading codes outperform the m -sequences and Gold codes when used in channels for which the new codes were designed. It is shown that two limiting cases of spreading codes based upon multirate subband filter banks result in FDMA and TDMA systems and the remainder of the class of codes provides a tradeoff of performance in various interference scenarios.

Chapter 1

Introduction and Background

1.1 Spread Spectrum Systems

Spread Spectrum (SS) communications is a technique whereby the transmission bandwidth employed is much larger than that normally required to transmit at the given data rate. The use of this excess bandwidth provides the system with advantages in the areas of Anti-Jam (AJ) communications, high resolution ranging, resistance to multipath fading, and Low Probability of Intercept/Detection (LPI/D) of the transmissions. Because of these properties, the evolution of spread spectrum techniques has primarily been concerned with military applications. Recently, however, there has been a shift of focus with interest in spread spectrum moving towards commercial applications, especially in the fields of mobile communications (cellular telephony) and Personal Communications Systems (PCS) [36]. This shift has occurred largely because of techniques whereby spread spectrum, employed in a multiuser channel, can provide nearly, if not more, spectral efficiency than traditional (narrowband) techniques [12].

This, however, is not the only reason for the commercialization trend. The other system advantages mentioned above have also contributed. For example, the multipath channel is commonly encountered in mobile communications and a system which has an inherent advantage against the resulting fading is obviously desirable [9]. Channels are also encountered where the available bandwidth must be shared by both spread spectrum and narrowband signals [21]. In this case, the AJ property and the low power spectral density exhibited by the spread signal result in little interference between the users. Still other systems take advantage of the high resolution ranging property of spread spectrum [4].

Although there are many different methods of spreading a digital signal, the one most commonly used and proposed for use in commercial systems is known as Direct

Sequence Spread Spectrum (DSSS). A typical DSSS transmitter is shown in Figure 1.1. After modulation, the signal is further modulated with a pseudo-noise (PN) sequence

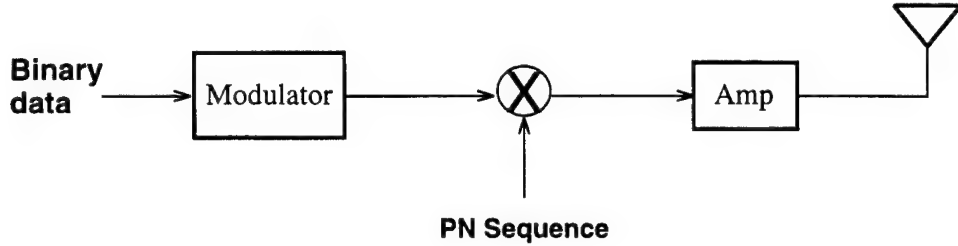


Figure 1.1: Simplified DSSS Transmitter

whose bandwidth is much greater than that of the baseband digital signal. The result of this secondary modulation is that the spectrum of the transmitted signal is that of the PN sequence and is wideband or spread. If the power of the spreading code (the PN sequence) is normalized such that the transmitted power is unaltered, then the increase in bandwidth will create a signal with a low power spectral density giving rise to the LPI/D property mentioned above.

The AJ property of spread spectrum systems is commonly discussed using a figure of merit known as the *processing gain*. If B_{ss} and B_D are the bandwidths of the PN sequence and the data sequence respectively, then the processing gain, G_P can be approximated by [33]

$$G_P \approx \frac{B_{ss}}{B_D}. \quad (1.1)$$

The processing gain can now be applied to determine effectiveness against jamming. Let E_s be the energy of the signal and E_J be the energy of the jammer or interference. Assuming the noise is dominated by the interference noise energy (as opposed to thermal noise), then the Signal to Noise Ratio (SNR) after despreading can be calculated by

$$SNR = \frac{E_s}{E_J} G_P. \quad (1.2)$$

There are two different common receiver structures used with DSSS systems as shown in Figure 1.2. In the first structure, the receiver simply multiplies the incoming signal with a copy of the PN sequence synchronized in phase with the PN sequence in the received signal. The copy of the PN sequence can either be locally generated or sent to the receiver over a different channel. The result of the multiplication is integrated over each data bit and the result is then compared to a threshold to make a message bit decision. The second receiver structure uses a *sliding correlator* which performs a

complete cross correlation between the received sequence and the PN code. The output of the sliding correlator is then sampled at the appropriate time and the result is sent to the threshold device.

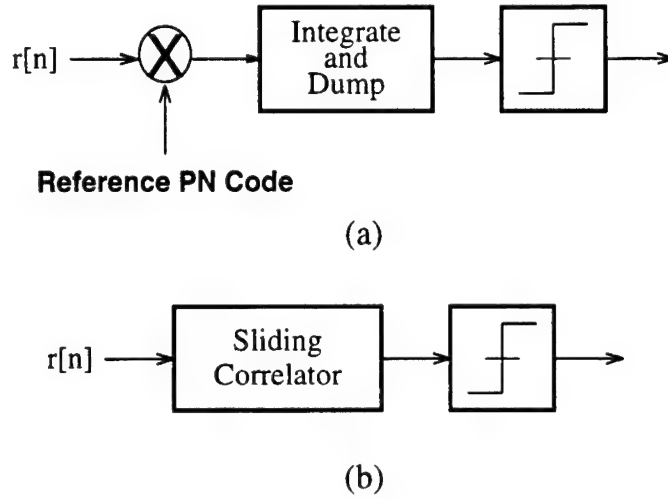


Figure 1.2: Time Domain DSSS Receivers

1.2 Multiuser Systems and CDMA

As mentioned above, the shift towards the use of spread spectrum in commercial systems has largely occurred in the area of multiple access and multiuser channels. The goal of a multiple access channel is to maximize the number of users while maintaining a certain despread SNR such that acceptable performance is retained. This is accomplished by ensuring that the energy transmitted by the users causes minimal interference to others in the communications channel. In other words, each of the transmissions should, ideally, be completely orthogonal to each other. One simple method of accomplishing this, known as Time Division Multiple Access (TDMA), requires that each user transmit during a separate time interval [16]. A pictorial view of this on the time-frequency plane is shown in Figure 1.3a. Since these time intervals do not overlap, orthogonality between user transmissions is ensured. Another method applies the same principle in the frequency domain. The available spectrum is divided into non-overlapping frequency bands and each user is assigned a band as shown in Figure 1.3b. This is known as Frequency Division Multiple Access (FDMA) [15]. In each of these cases, strict orthogonality cannot be attained since finite length transmissions require infinite bandwidth and, conversely, a band limited signal requires an infinitely long transmission time. Therefore, in order to

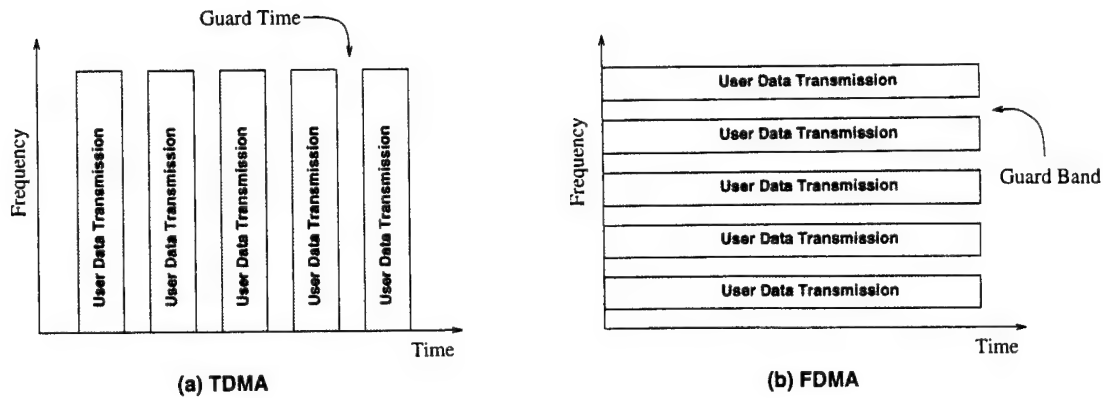


Figure 1.3: Time-Frequency Plane for TDMA and FDMA

increase the orthogonality between users, guard zones are inserted. In the TDMA system, *guard time* is placed between the transmissions of different users where no transmitting is permitted. Likewise, in FDMA, *guard bands* are implemented between the user bands.

A third and more complex method of allowing multiple users to share a given time-frequency space is called Code Division Multiple Access (CDMA) [9]. The time-frequency plane for CDMA is shown in Figure 1.4. A CDMA system is a spread spectrum system

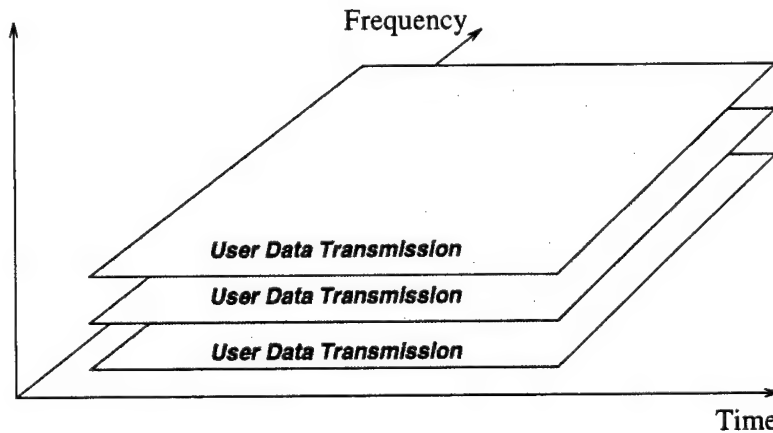


Figure 1.4: Time-Frequency Plane for CDMA

in which each user is assigned a unique spreading code. Ideally, the cross correlations between the spreading codes should be zero. Under such conditions, upon correlation in the receiver, all other user transmissions will be uncorrelated with the desired signal and

no interference will be encountered. Such complete orthogonality, however, is impossible to attain with finite length transmissions. Therefore, spreading codes are chosen for which the cross correlations are small between the codes thus providing minimal impact on the Bit Error Rate (BER) of the users.

Like the FDMA system, there is very little control required for CDMA once the users are assigned their spreading codes. Synchronization of the users is not required as is necessary in the TDMA system. Additionally, the performance of the channel gracefully degrades as the number of users increases[9]. Finally, the other advantages of a spread spectrum systems mentioned above are inherently achieved with the CDMA system making it an attractive choice for the multiuser channel.

1.3 Multipath Channels and Spread Spectrum Communications

Multipath interference results when multiple copies of the transmitted signal arrive at the receiver with different delays. This interference is usually the result of reflections in the channel. Land-mobile and mobile-satellite channels, among others, generally introduce some multipath interference. The net result of the multipath interference is that the composite received signal undergoes random amplitude and phase perturbations. As a result, the effect is often called *multipath fading*. In cases where the maximum delay difference between the paths is sufficiently small, the multipath fading is the same for all frequencies in the signal of interest and the fading is called *frequency non-selective*. The size of the band of frequencies which undergo essentially the same fading is determined by the *coherence bandwidth* [34] of the channel, which is inversely proportional to the maximum delay difference between the various paths. For frequency non-selective fading, the amplitude of the total desired signal will vary, resulting in periods when the total received signal is very small. When the bandwidth of the signal of interest is greater than the coherence bandwidth, the amplitude and phase variations for different portions of the signal will be somewhat uncorrelated and the fading is called *frequency selective*. In this case, it is likely that when the amplitude of a portion of the signal becomes small, the amplitude of another portion remains high and reliable reception of the signal is still possible. As a consequence, broadband signals, such as spread spectrum signals, have an advantage over narrowband signals in a multipath interference environment when the transmission bandwidth can be made larger than the coherence bandwidth.

1.4 Psuedo-Noise Sequences for DSSS

Clearly, the effectiveness of any given spread spectrum system is dependent upon the spreading codes used to modulate the data. The most common PN sequences used in DSSS are known as *maximal length sequences* or *m-sequences*. These were chosen because they have good randomness properties and are very easy to generate [37]. An *m-sequence* consists of a pattern of zeros and ones which are converted to plus and minus ones, respectively, prior to modulation of the signal. Some of the main properties of the *m-sequences* are: [54]

- The length of the sequence is always $N = 2^n - 1$ where n is an integer
- There are $\frac{N+1}{2}$ ones in the sequence $\frac{N+1}{2} - 1$ zeros
- Any circular shift of the sequence added to itself (modulo-2) is another *m-sequence*
- The cyclic autocorrelation of the sequence with itself after conversion to plus and minus ones is $\theta(k) = N$ for $k = lN$ and $\theta(k) = -1$ for $k \neq lN$ where l is an integer.

Each value of the PN sequence is known as a *chip* and the rate at which the PN sequence is transmitted is called the *chip rate*. When used in a DSSS system, the conversion of the zero chips to minus ones prior to modulation of the data results in a small DC component for large sequences. Finally, due to properties not mentioned above, the frequency spectrum of a modulated DSSS signal using an *m-sequence* has the shape of $\sin(x)/x$. The main lobe of the spectrum has a width of twice the chip rate.

Since cross correlations between spreading codes is critical for CDMA performance, a set of sequences with good cross correlation properties are used as spreading codes. The most common of these are known as Gold Codes [13]. Specifically, for any positive integer, n , not divisible by 4, there exists a set of $2^n + 1$ Gold codes whose length is $2^n - 1$. The normalized cross correlation between any pair of Gold Codes may result in one of three values given by [54]

$$\begin{aligned} & -\frac{1}{N}t(n) \\ & -\frac{1}{N} \\ & \frac{1}{N}[t(n) - 2] \end{aligned} \tag{1.3}$$

where N is the length of the code and

$$t(n) = \begin{cases} 1 + 2^{\frac{(n+1)}{2}} & \text{for } n \text{ odd} \\ 1 + 2^{\frac{(n+2)}{2}} & \text{for } n \text{ even} \end{cases} \tag{1.4}$$

1.5 Generalized Representation of Spreading Sequences

Each different class of spreading sequences, such as the PN codes discussed above, can be represented as a transformation on a “unit” vector. For example consider the system shown in Figure 1.5. Let \mathbf{x}_n be a column vector which consists of all zeros except for



Figure 1.5: Spreading Code Generation Via Transforms

the n th element which is a one. The spreading code, \mathbf{c}_n , is generated by taking a linear transformation on the vector \mathbf{x}_n . This linear transform can be represented by a matrix, \mathbf{T} , which contains the spreading codes in its columns so that

$$\mathbf{T} = [\mathbf{t}_0 \ \mathbf{t}_1 \ \dots \ \mathbf{t}_{N-1}]. \quad (1.5)$$

where $\mathbf{t}_0, \mathbf{t}_1, \dots, \mathbf{t}_{N-1}$ are column vectors each of which is a spreading code. The transformation shown in Figure 1.5 can now be represented by

$$\mathbf{c}_n = \mathbf{T}\mathbf{x}_n. \quad (1.6)$$

There is no restriction on \mathbf{T} except that it must be a linear transformation. The number of users (or number of spreading codes needed) determines the number of columns of \mathbf{T} while the length of the codes is equal to the number of rows in \mathbf{T} .

As a simple example, consider a system in which there are four users each using a different 7 chip binary valued sequence as a spreading code. The transformation matrix is

$$\mathbf{T} = \begin{bmatrix} 1 & 1 & 1 & -1 \\ 1 & -1 & -1 & -1 \\ -1 & 1 & -1 & 1 \\ -1 & -1 & 1 & 1 \\ 1 & 1 & 1 & -1 \\ -1 & 1 & 1 & 1 \\ 1 & -1 & -1 & -1 \end{bmatrix}. \quad (1.7)$$

Note that the spreading codes given in the matrix are not m -sequences. In order to extract the third code in the matrix (which is an m -sequence), the matrix is multiplied by the unit vector $\mathbf{x}_3 = [0 \ 0 \ 1 \ 0]^T$.

The multiuser systems discussed in Section 1.2 can now be fit into this framework. For a TDMA system, the transformation uses the standard basis [1] and \mathbf{T} becomes the identity matrix. A pure FDMA system would use an unrealizable matrix in which the columns are of infinite length and consist of equally spaced sinusoids. In each of these two cases, the transformation is a unitary transformation and $\mathbf{T}^T \mathbf{T} = \mathbf{I}$ where \mathbf{I} is the identity matrix. An example of a non-unitary transformation is a CDMA system using the Gold codes. In this case, the transformation matrix, \mathbf{T}_g , contains the Gold codes in its columns.

1.5.1 Cross Correlation Properties of Spreading Codes

As mentioned in Section 1.2 the cross correlation properties between two spreading codes is critical for good performance in a multiuser environment. There are three categories of multiuser channels which must be considered. The first category considered is known as the *synchronous* multiuser channel and occurs when all user transmissions are using the same clock to key the data. In this situation, the beginning of each spreading code occurs at the same time. Two examples of synchronous multiuser systems are the transmultiplexer [2] [46] [47] and the base to mobile channel in cellular telephony [23]. The second situation is known as the *asynchronous* multiuser channel and occurs in the mobile to base channel of a cellular environment [16]. Under these conditions, no restriction is placed upon the start time of user transmissions. This lack of synchronization occurs for two reasons. The first is that each user is operating from a different clock. Therefore, the composite signal from all user transmissions will consist of transmissions with different delays associated with them. The second reason is due to the different propagation paths from the mobile users to the base hub. Since these paths are all different and constantly changing, the received signal is modeled as an asynchronous multiuser channel. Therefore, when determining the cross correlations and resulting interference between users, random delays must be accounted for. The third case which will be considered, is when the users attain partial synchronization. In this situation, each of the user's transmissions are timed to a common clock, however, different propagation paths from the mobile users to the hub still causes some uncertainty in the relative delay between the transmissions. Throughout this thesis, the only delays which are integer multiples of a chip duration will be considered.

The relationship between the user's data and the interfering data is shown in Figure 1.6. There are two different cases which must be considered depending upon whether the interference data bit changes polarity during the user's bit period. The two codes under consideration are labeled c_n and c_m with the polarity of the transmitted code, and therefore the message bit, indicated by the sign. The message signal is represented by c_n and the interfering user is represented by c_m . In case one, the data bit polarity of the interference does not change between the two bits. In case two, the two data bits have

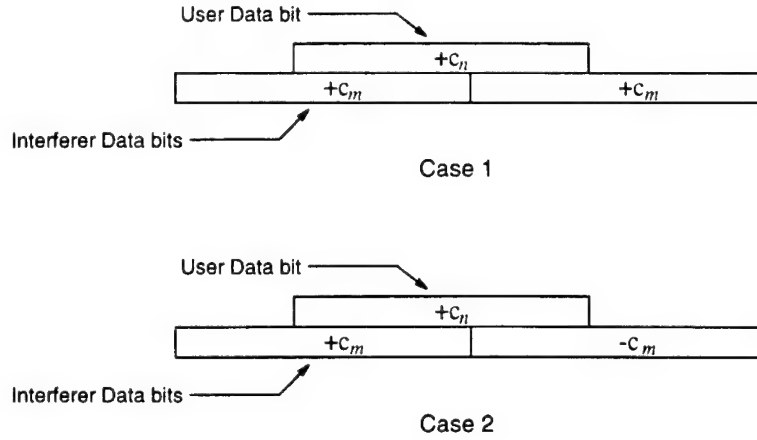


Figure 1.6: Data Bit Polarities

opposite polarities. The cross correlations of all other polarity combinations differ only in sign from one of these two cases and, since it is the cross correlation magnitude which is of interest, they need not be considered separately.

If \mathbf{c}_n and \mathbf{c}_m represent two different spreading codes, the cross correlation between them can be calculated as

$$\rho_\delta = (\mathbf{c}_n)_\delta^T \mathbf{c}_m \quad (1.8)$$

where $(\mathbf{c}_n)_\delta$ is a circular shift down of the vector \mathbf{c}_n by δ positions (see Appendix A). In a similar fashion, the cross correlations for case two can be represented by

$$\rho_\delta^- = (\mathbf{c}_n)_\delta^T \mathbf{K}_\delta \mathbf{c}_m \quad (1.9)$$

where \mathbf{K}_δ a diagonal matrix whose first δ diagonal elements are negative one and the remaining elements are positive one. Expanding Equation 1.8 using Equation 1.6 gives

$$\begin{aligned} \rho_\delta &= (\mathbf{c}_n)_\delta^T \mathbf{c}_m \\ &= (\mathbf{T}\mathbf{x}_n)_\delta^T \mathbf{T}\mathbf{x}_m \\ &= \mathbf{x}_n^T (\mathbf{T})_\delta^T \mathbf{T}\mathbf{x}_m \end{aligned} \quad (1.10)$$

If δ is zero (i.e. a synchronous system) and \mathbf{T} is a unitary transformation, then the cross correlations between any two codes is identically zero. For the asynchronous case, however, it is impossible (with finite length codes) for ρ_δ to be zero for all delays. The objective, therefore, is to design a transform \mathbf{T} such that the elements of $(\mathbf{T})_\delta^T \mathbf{T}$ are as small as possible for all shifts δ .

One method of trying to accomplish this is to employ the Gold codes discussed in Section 1.4. Since the Gold codes are known to have good cross correlation properties,

it has been suggested to use them as the input to a unitary transformation in Figure 1.5 for Multitone [11] and CDMA [31] applications. In terms of the notation of Equation 1.6 the transformed codes are

$$\begin{aligned}\mathbf{c}_{gn} &= \mathbf{T}\mathbf{x}_{gn} \\ \mathbf{c}_{gm} &= \mathbf{T}\mathbf{x}_{gm}\end{aligned}\tag{1.11}$$

where \mathbf{x}_{gn} and \mathbf{x}_{gm} are Gold codes. If these are implemented in a synchronous system the cross correlation between the transformed codes is

$$\begin{aligned}\rho &= \mathbf{c}_{gn}^T \mathbf{c}_{gm} \\ &= (\mathbf{T}\mathbf{x}_{gn})^T \mathbf{T}\mathbf{x}_{gm} \\ &= \mathbf{x}_{gn}^T \mathbf{T}^T \mathbf{T}\mathbf{x}_{gm} \\ &= \mathbf{x}_{gn}^T \mathbf{x}_{gm}\end{aligned}\tag{1.12}$$

which is the cross correlations between the Gold codes. Notice, however, that this holds only for the synchronous case. As an example, consider Case 1 of Figure 1.6. Performing the cross correlation calculation now results in

$$\begin{aligned}\rho_\delta &= (\mathbf{c}_{gn})_\delta^T \mathbf{c}_{gm} \\ &= (\mathbf{T}\mathbf{x}_{gn})_\delta^T \mathbf{T}\mathbf{x}_{gm} \\ &= \mathbf{x}_{gn}^T (\mathbf{T})_\delta^T \mathbf{T}\mathbf{x}_{gm}\end{aligned}\tag{1.13}$$

Since $(\mathbf{T})_\delta^T \mathbf{T}$ is not always equal to the identity matrix, the above result is not equal to the cross correlation result given by Equation 1.12. Equation 1.13 can further be expanded as

$$\begin{aligned}\rho_\delta &= \mathbf{x}_{gn}^T (\mathbf{T})_\delta^T \mathbf{T}\mathbf{x}_{gm} \\ &= \mathbf{x}_n^T \mathbf{T}_g^T (\mathbf{T})_\delta^T \mathbf{T}\mathbf{x}_m \\ &= \mathbf{x}_n^T (\mathbf{T}\mathbf{T}_g)_\delta^T \mathbf{T}\mathbf{x}_m \\ &= \mathbf{x}_n^T (\mathbf{P})_\delta^T \mathbf{P}\mathbf{x}_m\end{aligned}\tag{1.14}$$

with $\mathbf{P} = \mathbf{T}\mathbf{T}_g$ and \mathbf{T}_g being a transformation matrix with Gold codes as its columns. This result is identical to Equation 1.10 and the problem once again reduces to designing a matrix \mathbf{P} (or \mathbf{T}) which will minimize the cross correlations over all time shifts. The spreading codes can then be easily extracted from this matrix.

1.6 Scope

As previously mentioned, one reason for the use of m -sequences as spreading codes is their ease of generation. An $N = 2^n - 1$ chip sequence can be generated with a length n shift

register and a simple feedback network of modulo-2 adders [54]. This kept the complexity and cost of early spread spectrum systems low. Recently, advances in microprocessor technology, electronic storage devices, and modulation circuitry have decreased the cost and complexity of each respective area thereby making alternatives to the m -sequences worth considering. In fact several other branches of research, unrelated to the proposed research contained herein, are also exploring this idea [17, 53, 35, 51]. A main feature of these new proposals is that the spreading codes are not limited to being binary valued.

The simplest of these systems shapes the chips of a PN sequence using [53]

$$sprd(t) = p(t) \left[A_1 + A_2 \sin\left(\frac{2\pi}{T_c}t\right) + A_3 \cos\left(\frac{2\pi}{T_c}t\right) \right] \quad (1.15)$$

where T_c is the chip period, $p(t)$ is the PN sequence, and A_1 , A_2 , and A_3 are weighting coefficients. By choosing the weighting coefficients correctly, the resulting spreading code, $sprd(t)$, can be shaped so that its power spectrum is flat with low sidelobes, thereby making efficient use of the available bandwidth in which to spread the signal.

The other areas of investigation cited above originated in wavelet research, particularly Haar wavelet based systems. In the Geometric Harmonic Modulation [17], a composite signal is constructed by multiplying harmonically related sinusoids. Applications are being sought in the area of local area wireless communications. The other wavelet based codes use weighted rotations of the Haar Wavelet Coefficient Matrix [35]. The codes are then matched to a noise background to provide an LPI/D spreading system. Recently, these same codes were studied for use in a CDMA system [30]. Finally, in Fractal Modulation [51], a wavelet basis is used to modulate the data for a use in a channel with unknown bandwidth and unknown duration. Under this scheme, the data bit is modulated with each basis function. These are then added together and the composite waveform is transmitted.

The objective of the research in this proposal is to initiate the development of a new class of alternative spreading codes. This new class will be based upon the recent developments in subband filter banks and related topics in multirate digital signal processing. Specifically, the transforms discussed in Section 1.5 will be replaced by a multirate subband filter bank and the codes will be constructed from a frequency domain standpoint. Unlike the m -sequences discussed above, this new class of spreading codes, called Perfect Reconstruction Quadrature Mirror Filter (PR-QMF) Based Spreading Codes, will not be limited to being binary valued. Instead, the values of the chips will be determined by the properties which the codes should obey. Example codes will be developed for three different types of interference sources: stationary interference, multipath interference, and multiuser interference.

An overview of this thesis is as follows. In Chapter 2, an m -band multirate subband filter bank is introduced. It is shown how the transforms discussed in Section 1.5 can

be implemented by employing this m -band multirate subband structure using the unit vector as an input to the synthesis bank. An alternative receiver structure, useful for the conceptual development of the design procedure, is introduced which utilizes the subband filter bank in place of the traditional receivers discussed in Section 1.1. Next, the conditions on the filter bank are examined such that a property known as perfect reconstruction can be achieved. Particular emphasis is placed on the simple two-band filter bank and it is shown how the m -band structures can be constructed from the two-band building block using a progressively optimal approach. Finally, the formulation of the spreading codes is developed and, using this formulation, several important properties about the codes are examined.

Chapter 3 uses the results of Chapter 2 to formulate the design of the spreading codes. The design method uses an optimization procedure and objective functions are developed for various types of channel interference. A method for the design of codes for composite interference channels is introduced. Finally, the general procedure is summarized for extensions to channel interference not covered by this thesis.

In Chapter 4, an analysis of systems using the codes is presented along with some results. For each type of interference, an example subband multirate filter bank is designed and a set of spreading codes is generated. Using these codes, several interesting results are achieved which include the duality between the multiuser and multipath codes and their relationship to FDMA and TDMA systems.

Finally, Chapter 5 presents a summary of the work presented in this thesis. The reasoning behind using the multirate filter bank approach is reviewed and the use of the PR-QMF based codes is discussed. The important contributions are highlighted and some directions for future research in the area are proposed.

Chapter 2

PR-QMF Based Spreading Codes

In Chapter 1 it was shown how a set of spreading codes can be generated by performing a linear transformation on a set of unit vectors such that

$$\mathbf{c}_n = \mathbf{T}\mathbf{x}_n \quad (2.1)$$

where \mathbf{x}_n is a unit vector, \mathbf{T} is a linear transform, and \mathbf{c}_n is the resulting spreading code. One possible method of performing these transforms is to employ a multirate subband filter bank shown in Figure 2.1. In a multirate filter bank system, the discrete time signal $r(n)$ is filtered by a set of Finite Impulse Response (FIR) filters $H_0(z)$ through $H_{M-1}(z)$ and the output of each filter is then downsampled by a factor of N . This process of filtering and downsampling is known as *decimation* and the combination of a filter and downsampler is known as a *decimator* [6]. The result of the decimation is that the signal, $r(n)$, is split into M *subbands* which can be processed independently. A filter bank which decomposes a signal into subbands is known as an *analysis stage*. Likewise, the *synthesis stage* recombines the processed subbands into a signal $\hat{r}(n)$. It does this by using an *interpolator* on each subband which consists of upsampling the signal by N and then filtering with an FIR filter $G_m(z)$. The output of each interpolator is added together to form $\hat{r}(n)$.

In this chapter it will be shown that the transformation discussed in Section 1.5 can be implemented via the synthesis stage of the multirate filter bank shown in Figure 2.1. The matrix representation of filter banks (both the time-domain and z -domain) will be discussed with particular emphasis on the perfect reconstruction property and its connection to a unitary matrix transformation. A simplified two-channel filter bank will then be introduced and it will be shown that an m -band structure can be constructed using the two-band case as a building block and a technique called *progressive optimality*. Finally the formulation of the spreading codes which result from using filter banks will be presented and expressions for two important properties, the cross correlations and the autocorrelations, will be developed.

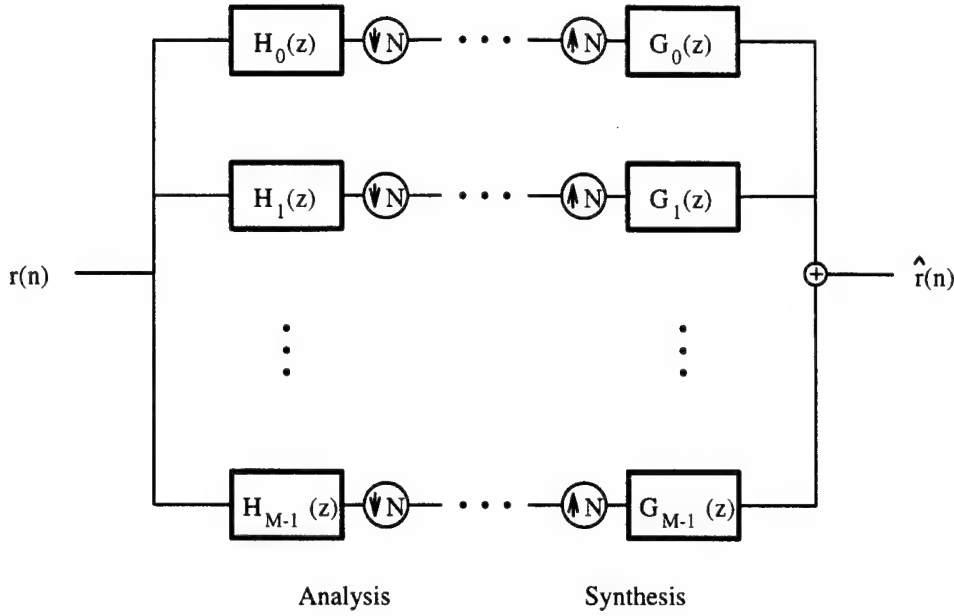


Figure 2.1: Multirate Subband Filter Bank

2.1 Block Transforms and Multirate Filter Banks

Consider a matrix \mathbf{T} whose columns contain a set of spreading codes such that

$$\mathbf{T} = [\mathbf{t}_0 \ \mathbf{t}_1 \ \dots \ \mathbf{t}_{M-1}]. \quad (2.2)$$

where $\mathbf{t}_0, \mathbf{t}_1, \dots, \mathbf{t}_{M-1}$ are the spreading codes. Let the synthesis filters of Figure 2.1 each contain, as their filter coefficients, one column of \mathbf{T} (i.e. one particular spreading code) so that

$$g_{m,n} = \mathbf{t}_m(N-n) \quad (2.3)$$

where $g_{m,n}$ is the n th element of the impulse response of $G_m(z)$ and $\mathbf{t}_m(n)$ is the n th element of the vector \mathbf{t}_m . Let \mathbf{x}_m be a unit vector of all zeros except for the m th element which contains a one. If \mathbf{x}_m is processed by the synthesis filter bank, the output will be the impulse response of $G_m(z)$ and the filter bank will implement

$$\mathbf{t}_m = \mathbf{T}\mathbf{x}_m \quad (2.4)$$

where \mathbf{t}_m is the desired spreading code. The properties of the spreading codes contained in \mathbf{T} , therefore, can be directly related to the properties of the subbands of a multirate filter bank. The properties of the subbands, in turn, can be determined by properly designing the filters in the synthesis tree.

If the transform implemented is a unitary transform, that is, $\mathbf{T}^T \mathbf{T} = \mathbf{I}$, where \mathbf{I} is the identity matrix, then the analysis filters and the synthesis filter are identical within a time reversal and a Perfect Reconstruction (PR) system is achieved [48]. Perfect reconstruction ensures that, in the absence of any subband processing, the output of the filter bank in Figure 2.1 will be a delayed copy of the input or $\hat{r}(n) = r(n - n')$ where n' is a positive integer. Since the filters are identical within a time reversal, the relationship between the analysis and synthesis filters becomes

$$G_m(z) = z^{-N} H_m(z^{-1}) \quad (2.5)$$

where z^{-N} is needed for causality.

Now consider the spreading sequence \mathbf{t}_m produced by the synthesis tree or, equivalently, by Equation 2.4. If this spreading sequence is processed by the analysis bank and the filter bank has the perfect reconstruction property, then the output of each decimator will be zero except for that which corresponds to the m th subband. The value of this subband will equal one. This operation is equivalent to

$$\mathbf{y}_m = \mathbf{T}^T \mathbf{t}_m \quad (2.6)$$

where \mathbf{y}_m is a vector which represents the output of the analysis bank. The operation in Equation 2.6 corresponds to correlating \mathbf{t}_m with each possible spreading code. The output vector \mathbf{y}_m , therefore, will be a unit vector with the m th element equal to one. This is the same vector which produced the spreading code via the synthesis bank.

The analysis filter bank, therefore, provides one method of demodulating a received spreading sequence. In practice, however, this is computationally redundant since the only subband output of interest is that associated with $H_m(z)$ and a traditional correlator receiver as discussed in Section 1.1 is preferred.

2.2 Matrix Representation of Multirate Filter Banks

Since it is the unitary solution to the filter bank design which is of interest, it is necessary to develop the conditions on the filters which will result in a perfect reconstruction system where the analysis filters are time reversed copies of the synthesis filters. In order to look at these conditions effectively, it is necessary to introduce matrix representation of the filter banks. Two different representations will be introduced. The *polyphase* representation looks at the filter bank properties in the z -domain, while the time domain representation extends the transforms given by Equations 2.4 and 2.6. The conditions for a perfect reconstruction filter bank are given for both the polyphase and the time-domain matrix forms.

2.2.1 Polyphase Matrix Representation

Consider a decimation filter $H_m(z)$ in the filter bank in Figure 2.1. If the downsampling is by a factor of N , an efficient description of the decimation is given by its *polyphase decomposition* [6]

$$H_m(z) = \sum_{n=0}^{N-1} H_{m,n}(z^N) z^{-n} \quad (2.7)$$

$$H_{m,n}(z^N) = \sum_{i=0}^{\infty} h_{m,n+iN} z^{-iN} \quad (2.8)$$

where $h_{m,n+iN}$ is the $(n + iN - 1)$ th element of the impulse response of $H_m(z)$ and the $H_{m,n}(z^N)$ terms are called the *polyphase components* of $H_m(z)$. The polyphase decomposition is useful since all terms of the same phase (modulo N) are grouped together in the polyphase components given by Equation 2.8. Substitution of these polyphase components into Equation 2.7 verifies the validity of the decomposition.

The entire system of decimators in Figure 2.1 can be represented by a polyphase component matrix which has the form [47]

$$\mathbf{H}_p(z) = \begin{bmatrix} H_{0,0}(z) & H_{0,1}(z) & \cdots & H_{0,N-1}(z) \\ H_{1,0}(z) & H_{1,1}(z) & \cdots & H_{1,N-1}(z) \\ \vdots & \vdots & \ddots & \vdots \\ H_{M-1,0}(z) & H_{M-1,1}(z) & \cdots & H_{M-1,N-1}(z) \end{bmatrix} \quad (2.9)$$

where each of the elements are directly derived from the polyphase components of Equation 2.8. Each element in this matrix therefore corresponds to the output of a one filter at a particular phase. For example, suppose a unit impulse is processed by the analysis bank. The output of the decimators is represented by a column of the polyphase matrix. The column is determined by the relative phase of the impulse with the downsampling operation.

A similar formulation exists for the synthesis filter bank. If the M filters in the synthesis filter bank are represented by $G_m(z)$ then the polyphase matrix becomes

$$\mathbf{G}_p(z) = \begin{bmatrix} G_{0,N-1}(z) & G_{0,N-2}(z) & \cdots & G_{0,0}(z) \\ G_{1,N-1}(z) & G_{1,N-2}(z) & \cdots & G_{1,0}(z) \\ \vdots & \vdots & \ddots & \vdots \\ G_{M-1,N-1}(z) & G_{M-1,N-2}(z) & \cdots & G_{M-1,0}(z) \end{bmatrix} \quad (2.10)$$

where $G_{m,n}$ are the polyphase components which are defined in a similar fashion as the $H_{m,n}$.

Recall that the solution of interest is PR system with FIR filters where the analysis filters are time reversed copies of the synthesis filters. For this type of system, the analysis polyphase matrix must satisfy [47]

$$[\mathbf{H}_p(z^{-1})]^T \mathbf{H}_p(z) = \mathbf{I} \quad (2.11)$$

where \mathbf{I} is the identity matrix. The synthesis filters then become time reversed copies of the analysis filters so that

$$\mathbf{G}_p(z) = z^{-l} \mathbf{H}_p(z^{-1}) \quad (2.12)$$

where z^{-l} is needed to ensure the synthesis filters are causal.

2.2.2 Time-Domain Matrix Representation

The time domain operation of the filter bank can be described by extending the matrix in Equation 2.6 to a block-circulant matrix. This is done so that processing on input vectors longer than M can be represented. For the analysis bank, the block-circulant matrix becomes [48]

$$\mathbf{T}_a = \begin{bmatrix} \ddots & \ddots & \ddots & \ddots & & & \\ & \mathbf{D}_0 & \mathbf{D}_1 & \cdots & \mathbf{D}_{K-1} & & \\ & & \mathbf{D}_0 & \mathbf{D}_1 & \cdots & \mathbf{D}_{K-1} & \\ & & & \mathbf{D}_0 & \mathbf{D}_1 & \cdots & \mathbf{D}_{K-1} \\ & & & & \ddots & \ddots & \ddots & \ddots \end{bmatrix} \quad (2.13)$$

with zeros being inserted into any blank entries. Each of the rows in the matrix contain the coefficients of the analysis bank filters and can be formed by partitioning the matrix of Equation 2.6 as

$$\mathbf{T}^T = [\mathbf{D}_0 \quad \mathbf{D}_1 \quad \cdots \quad \mathbf{D}_{K-1}]. \quad (2.14)$$

The number of columns in each of the \mathbf{D}_k sub-matrices is equal to the decimation factor N and the number of rows is equal to the number of subbands M .

In a similar fashion, the synthesis filter bank has a time-domain representation of

$$\mathbf{T}_s = \begin{bmatrix} \ddots & \ddots & \ddots & \ddots & & & \\ & \mathbf{B}_{K-1}^T & \cdots & \mathbf{B}_1^T & \mathbf{B}_0^T & & \\ & & \mathbf{B}_{K-1}^T & \cdots & \mathbf{B}_1^T & \mathbf{B}_0^T & \\ & & & \mathbf{B}_{K-1}^T & \cdots & \mathbf{B}_1^T & \mathbf{B}_0^T \\ & & & & \ddots & \ddots & \ddots & \ddots \end{bmatrix} \quad (2.15)$$

and, once again, zeros are inserted into the blank entries. This time, each of the submatrices, \mathbf{B}_k are of size M by N and are constructed from the matrix transform of Equation 2.4 by

$$\mathbf{T} = \begin{bmatrix} \mathbf{B}_0^T \\ \mathbf{B}_1^T \\ \vdots \\ \mathbf{B}_{K-1}^T \end{bmatrix}. \quad (2.16)$$

Each of the two transformation equations can now be extended. In general, if \mathbf{x} is a column vector of input data, then the output of the analysis bank, \mathbf{y} , is generated by

$$\mathbf{y} = \mathbf{T}_a \mathbf{x}. \quad (2.17)$$

The output vector consists of output from each of the subbands time-multiplexed into a single vector. Likewise, the synthesis bank is mathematically represented by

$$\mathbf{x} = \mathbf{T}_s \mathbf{y}. \quad (2.18)$$

The final relationship to be established is that between the polyphase matrices of Equations 2.9 and 2.10 and the time domain matrices of Equation 2.13 and 2.15. To accomplish this, the polyphase matrices are factored as polynomials with matrix coefficients so that [48]

$$\mathbf{H}_p(z) = \sum_{k=0}^{K-1} \mathbf{H}_{pk} z^{-k} \quad (2.19)$$

$$\mathbf{G}_p(z) = \sum_{k=0}^{K-1} \mathbf{G}_{pk} z^{-k}. \quad (2.20)$$

The relationship between the time-domain and the polyphase form now becomes

$$\mathbf{D}_{K-k-1} = \mathbf{H}_{pk} \mathbf{J} \quad (2.21)$$

$$\mathbf{B}_k = \mathbf{G}_{pk} \mathbf{J} \quad (2.22)$$

where \mathbf{J} is the antidiagonal matrix and is necessary to time reverse the filter coefficients such that convolution (as opposed to correlation) takes place.

As previously mentioned, the solution of interest is a unitary solution¹ where the amount of downsampling is equal to the number of subbands, also known as *maximal*

¹Notice that the unitary matrix will not be square. See Appendix A

decimation [45]. It was already stated that, under these conditions, the polyphase matrix must satisfy

$$\left[\mathbf{H}_p(z^{-1})\right]^T \mathbf{H}_p(z) = \mathbf{I}. \quad (2.23)$$

It can be shown that the time-domain solution to this is [48]

$$\mathbf{T}_a^T \mathbf{T}_a = \mathbf{I}. \quad (2.24)$$

In order to achieve the above condition, the matrices in \mathbf{T}_a must satisfy

$$\sum_{i=0}^{K-1} \mathbf{D}_{i+k}^T \mathbf{D}_i = 0, \quad k = 1, \dots, K-1. \quad (2.25)$$

The synthesis filters can now be a time reversed copy of the analysis filters so that

$$\mathbf{B}_k = \mathbf{D}_{K-k-1}. \quad (2.26)$$

This, in turn, will lead to a unitary transformation matrix to be used in Equations 2.4 and 2.6 which can then be utilized to generate the spreading codes.

2.3 The Two-Channel Subband Filter Bank

The simplest multirate subband tree is the two-channel subband filter bank shown in Figure 2.2. The two-channel filter bank is used due to the simplicity of the filter design. Additionally, more complex structures can be developed from the two-channel bank without the rigors of a direct m -band solution.

The two filters, $H_0(z)$ and $H_1(z)$ are often Quadrature Mirror Filters (QMF). The term Quadrature Mirror stems from the frequency responses of the filters. If $H_0(z)$ is a lowpass filter, then $H_1(z)$ will be a highpass filter whose frequency response is generated by mirroring the response of $H_0(z)$ about the frequency $\pi/2$ as shown in Figure 2.3. If the FIR filter $H_0(z)$ is known, then its QMF counterpart, $H_1(z)$, can easily be generated by [6]

$$H_1(z) = z^{-(N-1)} H_0(-z^{-1}) \quad (2.27)$$

where N is the filter order of $H_0(z)$.

The perfect reconstruction conditions given above can now be applied to the two-channel filter bank. Since there are only two subbands and the downsampling is by a factor of two, each of the polyphase matrices given by Equations 2.9 and 2.10 are of dimension two by two. Additionally, each of the factors of the matrix polynomials of

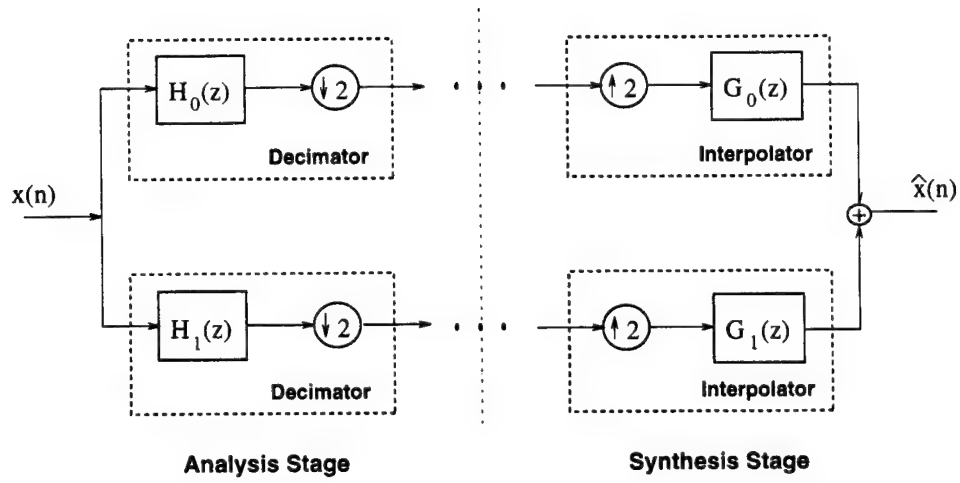


Figure 2.2: Two-Channel Subband Filter Bank

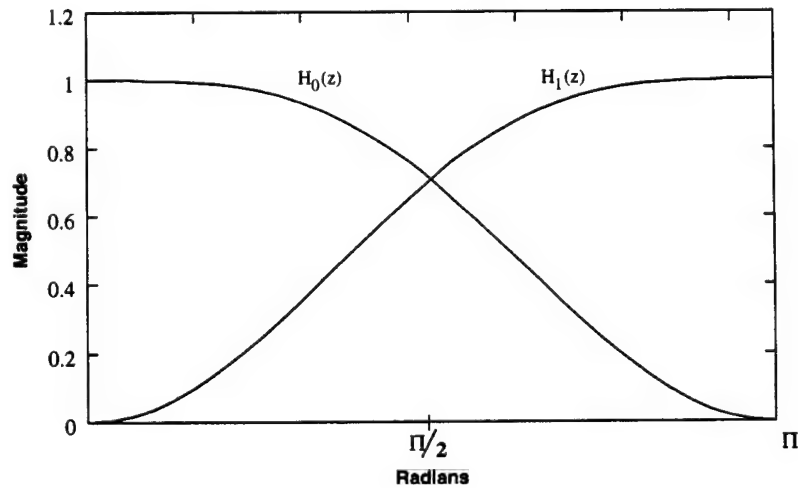


Figure 2.3: Quadrature Mirror Filter Frequency Responses

Equations 2.19 and 2.20 are also two by two as are the submatrices \mathbf{D}_k and \mathbf{B}_k . The number of these matrices, K , is determined by the filter length of $H_0(z)$ and $H_1(z)$ so that

$$K = \frac{N}{2} \quad (2.28)$$

where N is the FIR filter length. Using Equation 2.21 gives

$$\begin{bmatrix} \mathbf{D}_0 & \mathbf{D}_1 & \cdots & \mathbf{D}_K \end{bmatrix} = \begin{bmatrix} h_{0,N-1} & h_{0,N-2} & \cdots & h_{0,0} \\ h_{1,N-1} & h_{1,N-2} & \cdots & h_{1,0} \end{bmatrix} \quad (2.29)$$

where $h_{0,n}$ and $h_{1,n}$ are the n th components of the impulse responses of $H_0(z)$ and $H_1(z)$ respectively. Finally, applying Equation 2.25 gives the perfect reconstruction condition for $H_0(z)$ as [38]

$$\sum_{k=0}^{N-1} h_{0,k} h_{0,k+2n} = \delta_n \quad \forall n \geq 0 \quad (2.30)$$

where δ_n is the unit impulse function. Since $H_0(z)$ and $H_1(z)$ are quadrature mirror filters it is easy to show that the above condition will hold for the high pass filter as well. Once $H_0(z)$ is designed, $H_1(z)$ is determined by Equation 2.27. Since a unitary solution is being developed, the synthesis filters are simply the time reversed copies of the analysis filters. Therefore, for a two-channel PR-QMF subband filter bank, the following conditions must be met

$$H_1(z) = z^{-(N-1)} H_0(-z^{-1}) \quad (2.31)$$

$$G_0(z) = -H_1(-z) \quad (2.32)$$

$$G_1(z) = H_0(-z) \quad (2.33)$$

$$\sum_{k=0}^{N-1} h_{0,k} h_{0,k+2n} = \delta_n \quad \forall n \geq 0. \quad (2.34)$$

Two things should be noted here. The first is that only one of the four filters shown in Figure 2.2 needs to be designed. Once the design of $H_0(z)$ is complete, the other three filters follow directly from the above equations. The second note is that the design of $H_0(z)$ is itself limited. For an N tap FIR filter, there are $N/2$ conditions which the tap weights must satisfy for perfect reconstruction to occur. The remaining $N/2$ degrees of freedom are available to design the filter to fit the particular application.

2.3.1 Subband Tree Structures

The model discussed above is for a simple two channel subband filter bank. This simple model, however, can be used as the building block for larger structures which will decompose the input into multiple subbands and emulate the m -band tree shown in Figure 2.1. Although it is possible to design perfect reconstruction m -band filter banks directly [47] [39], it is often sufficient and simpler to use the two-band case as the building block for a hierarchical tree structure which achieves an m -band split.

The m -band structure employed in this thesis is known as the *full binary tree* and is shown in Figure 2.4 [45]. If $H_0(z)$ and $H_1(z)$ are ideal low and high pass filters

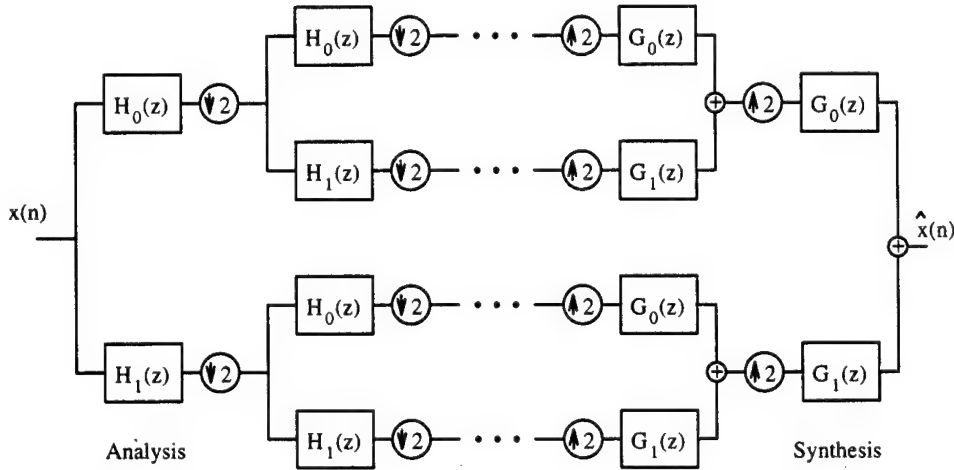


Figure 2.4: Full Binary Tree Structure

respectively, then the full binary tree structure will decompose the input signal into frequency bands which are of equal width and equally spaced as shown in Figure 2.5. A second popular tree structure, the *Dyadic Tree*, is shown in Figure 2.6 [45]. For clarity, only the analysis section of the filter bank is depicted. Recently, the dyadic tree has gained popularity due to its close connection with the Discrete Wavelet Transform (DWT) [27]. Unlike the full binary tree, each successive stage in the dyadic tree divides only the low frequency portion of the spectrum as shown in Figure 2.7. For this reason it is also known as an *Octave Band* subband tree. By decomposing only the lowest frequencies of the input signal, some time resolution of $x(n)$ is gained at the expense of frequency resolution at the upper bands.

The actual frequency response of a subband in an m -band tree can be calculated by determining the response of the *product filter* for that subband. The product filter is calculated by using the *noble identities* shown in Figure 2.8 which allow for the inter-

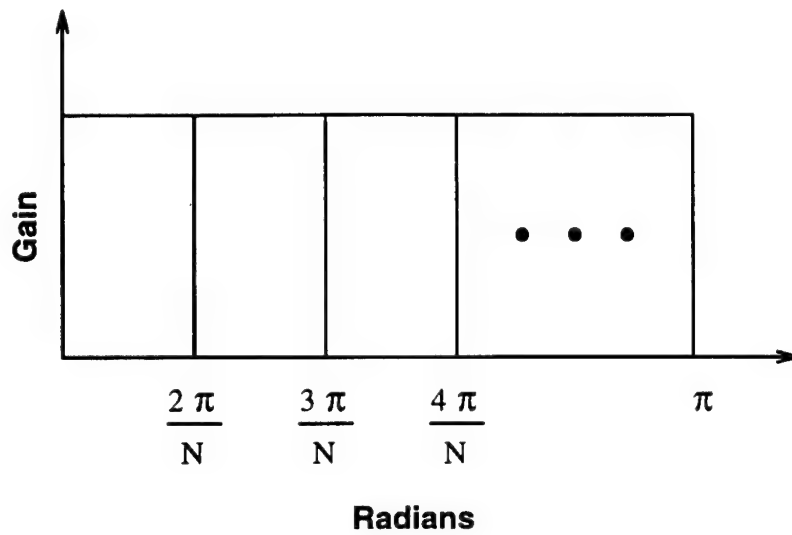


Figure 2.5: Normalized Frequency Response of an Ideal L-Stage Full Binary Tree

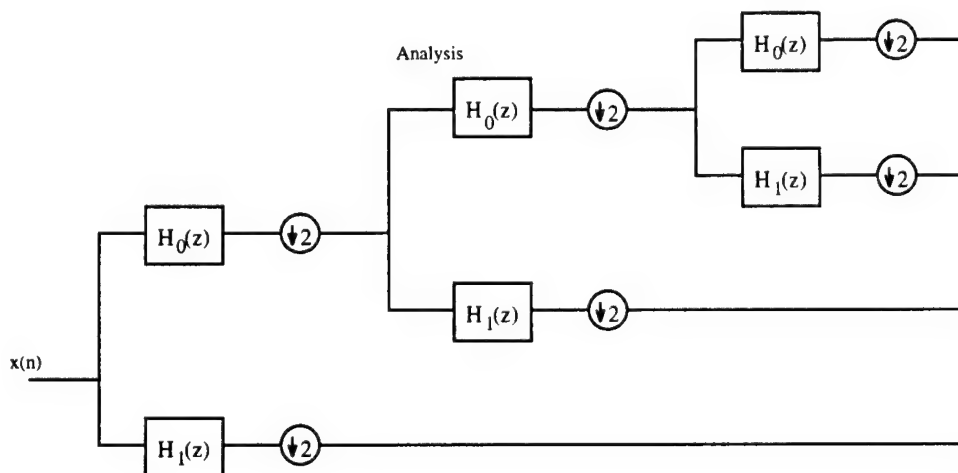


Figure 2.6: Dyadic Tree Structure

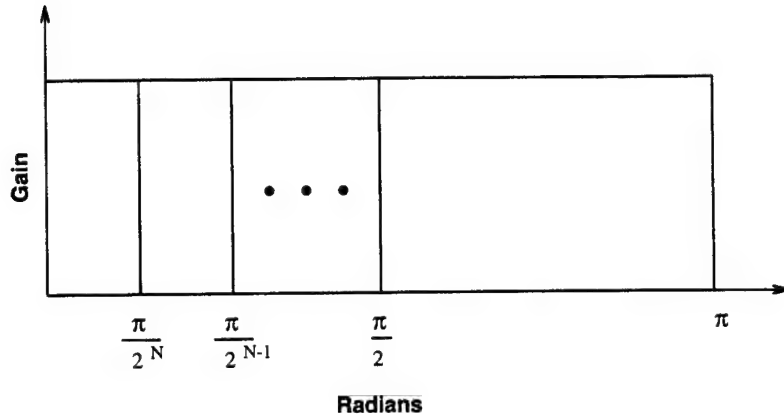


Figure 2.7: Normalized Frequency Response of an Ideal L-Stage Dyadic Subband Tree

changing of a filtering and downsampling operation [45]. Implementing these identities

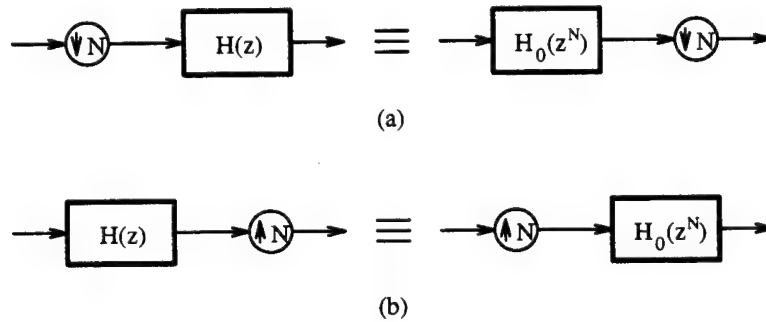


Figure 2.8: The *Noble Identities* for Decimation and Interpolation

in the four-band full binary tree of Figure 2.4 gives the equivalent structure shown in Figure 2.9 which involves only a single decimation/interpolation along each branch. This idea can easily be extended to larger tree structures. For example, consider a full binary tree with L levels. The product filter for the subband along the branch which contains all of the $H_0(z)$ filters is

$$\tilde{H}_0(z) = \prod_{l=0}^L H_0(z^{2^l}). \quad (2.35)$$

The frequency response of $\tilde{H}_0(z)$ is the frequency response of the subband. The 2^l term appears in the right hand side of the equation because the downsampling, which occurs in each decimator, must be accounted for using a noble identity. A similar formulation can be made for any other branch of a subband tree structure.

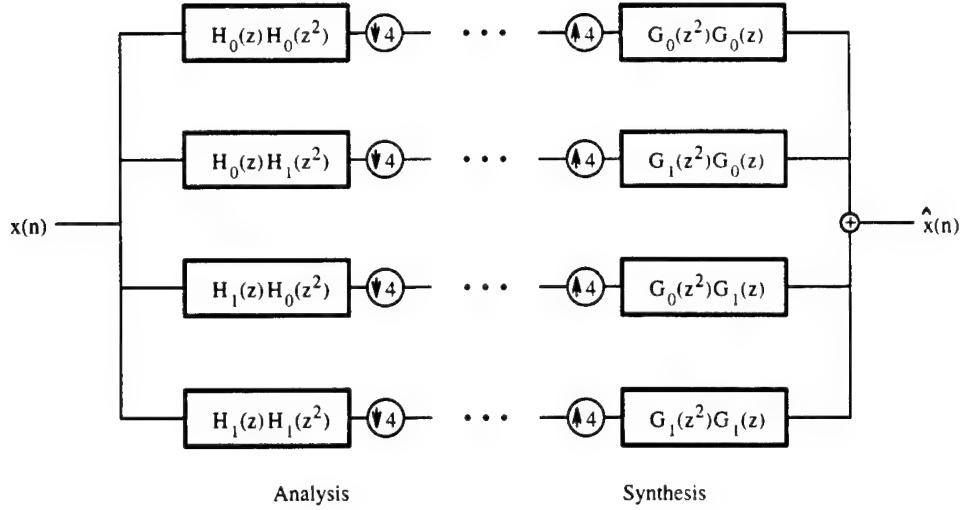


Figure 2.9: Four Band Tree Using Product Filters

2.4 Progressive Optimality and Filter Bank Design

It has been shown that recursively using the same set of QMF filters in the design of hierarchical subband structures does not necessarily produce an optimal tree [43]. Additionally, the task of determining the cross correlations and other properties between all subband outputs quickly becomes computationally complex. Therefore, a technique known as Progressive Optimality will be used [42]. The method of progressive optimality states that, at each node in the tree, a new set of filters should be designed which specifically incorporate the criteria at that particular stage. For example, each tree construction will start with the design of QMF pair $A_1(z)$ and $A'_1(z)$, shown in Figure 2.10. The design problem will be applied using the two subbands associated with $A_1(z)$ and

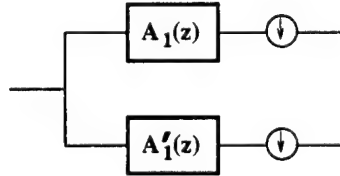


Figure 2.10: Progressively Optimized Filter Banks - Level 1

$A'_1(z)$. Once this initial filter design is complete, the design focus shifts to the QMF pair occurring after the $A_1(z)$ branch as shown in Figure 2.11. The design performed at this node will only consider the subbands associated with the new QMF pair, $B_1(z)$

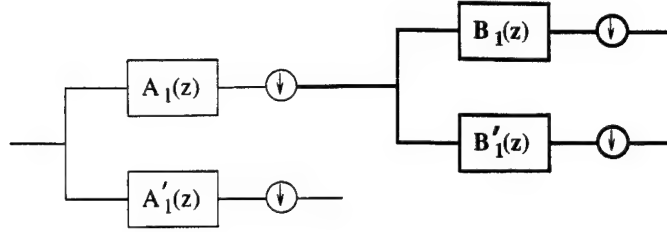


Figure 2.11: Progressively Optimized Filter Banks - Level 2A

and $B'_1(z)$, cascaded with the $A_1(z)$ decimator. Subbands from the lower half of the tree are ignored. Once this second set of filters is complete, the lower QMF pair, shown highlighted in Figure 2.12, is then designed while ignoring the subbands from the upper half of the tree. This process continues until the entire tree is completed.

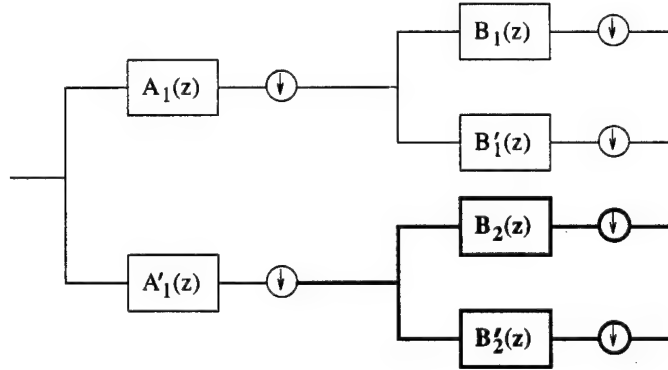


Figure 2.12: Progressively Optimized Filter Banks - Level 2B

2.5 Subband Tree Applications

The original motivation for the development of the subband tree structures came from the field of source coding for audio and video signals. By using the proper filters, the energy from a source can be isolated to a few subbands, thereby allowing a more efficient bit allocation scheme and larger coding gains [50]. Since any linear transform can be realized by an m -band tree structure, the use of multirate trees has quickly pervaded many other areas of signal processing research such as feature extraction [8], interference suppression [28], and transmultiplexer design [46] to name a few.

Recently, it was shown that the popular *Discrete Wavelet Transform* can be implemented as a Dyadic subband tree [7, 27]. This connection between wavelets and subband tree applications has generated a large amount of interest in time-frequency decompositions and research in the area has extended to many different applications [24].

As will be shown, the transform implemented by an analysis bank employing perfect reconstruction quadrature mirror filters forms an orthonormal basis. This motivates the use of the tree structures for communications. By using the basis functions as the spreading codes, an N -dimensional orthogonal signaling set can be realized. Proper choice of the filter coefficients can then tailor the waveforms to suit a particular communications channel.

2.6 Properties of PR-QMF Based Spreading Codes

Two important properties which must be studied for the PR-QMF based spreading codes are the cross correlation between the codes and the autocorrelation of the codes. To this end, the time-domain matrix introduced in Section 2.2.2 will be partitioned and the resulting matrices utilized to construct the codes generated by the hierarchical full binary tree structure of Section 2.3.1. Once representations of these codes are developed, the properties mentioned above will be described in equation form for use in the filter coefficient design problem.

2.6.1 Generation of the PR-QMF Based Spreading Codes

Consider the full binary tree structure shown in Figure 2.4. If the filters along the branch leading to a particular subband are known, the product filter for that branch can be calculated as specified in Section 2.3.1. By taking the inverse z -transform of that product filter, the spreading code associated with that subband will be generated. An alternative method is to use the time domain matrix notation introduced earlier. This approach has the advantage that the spreading codes are represented directly in terms of the filter coefficients and no intermediate transforms are required.

Consider the time-domain matrix representation for the two-band filter bank shown in Figure 2.2. The matrix equation for the filter bank operation was given in Equation 2.17 as

$$\mathbf{y} = \mathbf{T}_a \mathbf{x} \quad (2.36)$$

where \mathbf{x} is a column vector of infinite length which represents the input data. The output vector \mathbf{y} consists of multiplexed output from each of the subbands. For a filter

bank using maximal decimation, the amount of downsampling is equal to the number of subbands and the input and output vectors are of equal length. For the two-channel case, therefore, every other element of the output vector \mathbf{y} contains a sample from $H_0(z)$ while the remaining interleaved samples are from $H_1(z)$.

For the representation of spreading codes it is desirable to represent each subband independently. Therefore, the time-domain matrix \mathbf{T}_a will be partitioned into two different matrices each of which will represent one branch of decimation. Let \mathbf{H}_0 be a matrix which contains every other row of \mathbf{T}_a , that is, \mathbf{H}_0 is a matrix containing the filter coefficients of $H_0(z)$ and has the form

$$\mathbf{H}_0 = \begin{bmatrix} & & & & & & \\ & & & & & & \\ & & \ddots & & & & \\ h_{0,N-1} & h_{0,N-2} & \cdots & h_{0,0} & & & \\ & h_{0,N-1} & h_{0,N-2} & \cdots & h_{0,0} & & \\ & & h_{0,N-1} & h_{0,N-2} & \cdots & h_{0,0} & \\ & & & h_{0,N-1} & h_{0,N-2} & \cdots & h_{0,0} \\ & & & & \ddots & & \end{bmatrix} \quad (2.37)$$

where $h_{0,n}$ are the elements of the impulse response of \mathbf{H}_0 . The remaining rows of \mathbf{T}_a are used to construct \mathbf{H}_1 which has a similar form.

Likewise, if $G_0(z)$ is used in an interpolator, the matrix operator for its representation is generated by partitioning \mathbf{T}_s and has the form

$$\mathbf{G}_0^T = \begin{bmatrix} & & & & & & \\ & & & & & & \\ & & \ddots & & & & \\ g_{0,N-1} & g_{0,N-2} & \cdots & g_{0,0} & & & \\ & g_{0,N-1} & g_{0,N-2} & \cdots & g_{0,0} & & \\ & & g_{0,N-1} & g_{0,N-2} & \cdots & g_{0,0} & \\ & & & g_{0,N-1} & g_{0,N-2} & \cdots & g_{0,0} \\ & & & & \ddots & & \end{bmatrix}. \quad (2.38)$$

Both of the above matrices are unbounded and given for the unrealistic case of infinite length input vectors. To account for the edge effects, present when using finite length vector inputs, the matrix operators will be modified to a circulant form. For a decimator using $H_0(z)$, the modified matrix operator is

$$\mathbf{H}_0 = \begin{bmatrix} h_{0,N-1} & h_{0,N-2} & \cdots & h_{0,0} & & & \\ & h_{0,N-1} & h_{0,N-2} & \cdots & h_{0,0} & & \\ & & \vdots & & & & \\ h_{0,N-3} & \cdots & h_{0,0} & & h_{0,N-1} & h_{0,N-2} \end{bmatrix}. \quad (2.39)$$

The expression for the input/output relationships for the decimators are now

$$\mathbf{y}_0 = \mathbf{H}_0 \mathbf{x} \quad (2.40)$$

$$\mathbf{y}_1 = \mathbf{H}_1 \mathbf{x} \quad (2.41)$$

The actual size of the matrix is dependent upon the length of the input vector. Notice that there are twice as many columns as there are rows. Therefore, the output vector \mathbf{y}_0 will contain exactly one half as many elements as the input vector, \mathbf{x} , thereby maintaining consistency with the idea of downsampling a signal by two. A similar formulation can

be made for an interpolator. In this case, the relationships become

$$\mathbf{x}_0 = \mathbf{G}_0 \mathbf{y} \quad (2.42)$$

$$\mathbf{x}_1 = \mathbf{G}_1 \mathbf{y} \quad (2.43)$$

Notice that the output vectors from these operations, \mathbf{x}_0 and \mathbf{x}_1 will contain twice as many elements as the input vector. Unless otherwise specified, operator matrices in this thesis refer to the modified operators for finite length data vectors.

Since the operator matrices introduced above are partitions of the time-domain matrices \mathbf{T}_a and \mathbf{T}_s , the perfect reconstruction conditions are still valid. Specifically, if the perfect reconstruction conditions are satisfied then

$$\mathbf{H}_0^T \mathbf{H}_0 = \mathbf{I} \quad (2.44)$$

$$\mathbf{H}_1^T \mathbf{H}_1 = \mathbf{I}. \quad (2.45)$$

Since the synthesis filters are time reversed copies of the analysis filters, similar results are obtained for \mathbf{G}_0 and \mathbf{G}_1 . Finally, since $H_0(z)$ and $H_1(z)$ are quadrature mirror filters, it follows that

$$\mathbf{H}_0^T \mathbf{H}_1 = 0. \quad (2.46)$$

Using the operator matrices defined above, the spreading codes can be generated directly and without using product filters and the z -transform. Let \mathbf{A} be an operator matrix for the decimation process associated with an N tap FIR filter $A(z)$. The matrix for the corresponding interpolation associated with the reconstruction filter in the synthesis bank is, therefore, the transpose of \mathbf{A} . Let the column vector \mathbf{x} be the input vector to the synthesis bank whose first element is a one with all others being zero. If $A(z)$ is used in the simple two band structure of Figure 2.2, then the corresponding spreading code generated by the synthesis bank is [19]

$$\mathbf{c} = \mathbf{A}^T \mathbf{x}. \quad (2.47)$$

In general, for a tree of depth L , the spreading code along a branch with filters $A_1(z)$, $A_2(z)$, \dots , $A_L(z)$, and $A_1(z)$ as the first stage filter is

$$\mathbf{c} = \left[\prod_{l=1}^L (\mathbf{A}_l)^T \right] \mathbf{x} \quad (2.48)$$

where the matrices \mathbf{A}_1 to \mathbf{A}_L are the decimation matrices, each of appropriate dimension, and the product is carried out in ascending order as follows

$$\prod_{l=1}^L (\mathbf{A}_l)^T = (\mathbf{A}_1)^T (\mathbf{A}_2)^T \dots (\mathbf{A}_L)^T. \quad (2.49)$$

By using Equation 2.48 to represent a particular spreading code, the properties of the codes can be directly formulated in terms of the operator matrices. This allows a direct connection between the spreading code properties and the filter coefficients used in the subband tree.

Equation 2.48 can also be used to determine the length of a spreading code. If only a single stage with an N tap filter is used, the spreading code length will be equal to the number of taps in the filter. The operator matrix for that stage will have $N/2$ rows and N columns. Each subsequent stage in the filter bank will double the length of the spreading code (there is an upsampling by two) and the operator matrix for that stage will have twice as many rows and columns as the previous stage. Therefore, for a filter bank with L stages using N tap filters, the length of the spreading code is

$$l = N \cdot 2^{L-1} \quad (2.50)$$

For example, a four stage tree using four tap filters will result in codes of length 32.

2.6.2 Orthogonality Between Spreading Codes

As mentioned in Section 1.2 performance in a multiuser channel is highly dependent upon the cross correlations between spreading codes. These cross correlations can now be calculated using the matrix expression of Equation 2.48 for a spreading code generated by a PR-QMF filter bank. Recall from Section 1.5.1 that calculations must be made for both a synchronous and an asynchronous communications system. Additionally, for the asynchronous system, there are two different polarity cases to consider.

The Synchronous Case

Consider two arbitrary codes, \mathbf{c}_b and \mathbf{c}_c , generated from a tree of depth L . If the two branches which generate these codes diverge in the tree at level M , then the branches have $M - 1$ common filters. At level M , each branch contains one filter from a QMF pair. Beyond level M , the filters along each branch differ. Let the operator matrices for the first $M - 1$ filters be represented by $\mathbf{A}_1 \dots \mathbf{A}_{M-1}$ as shown in Figure 2.13. The QMF pair at level M will be denoted by matrix operators \mathbf{A}_M and \mathbf{A}'_M . Finally, let $\mathbf{B}_{M+1} \dots \mathbf{B}_L$ and $\mathbf{C}_{M+1} \dots \mathbf{C}_L$ represent the operators for the differing filters of codes \mathbf{c}_b and \mathbf{c}_c , respectively. The two codes can now be represented by

$$\mathbf{c}_b = \left[\prod_{i=1}^{M-1} (\mathbf{A}_i)^T \right] [\mathbf{A}_M^T] \left[\prod_{j=M+1}^L (\mathbf{B}_j)^T \right] \mathbf{x} \quad (2.51)$$

$$\mathbf{c}_c = \left[\prod_{i=1}^{M-1} (\mathbf{A}_i)^T \right] [\mathbf{A}'_M^T] \left[\prod_{j=M+1}^L (\mathbf{C}_j)^T \right] \mathbf{x}. \quad (2.52)$$

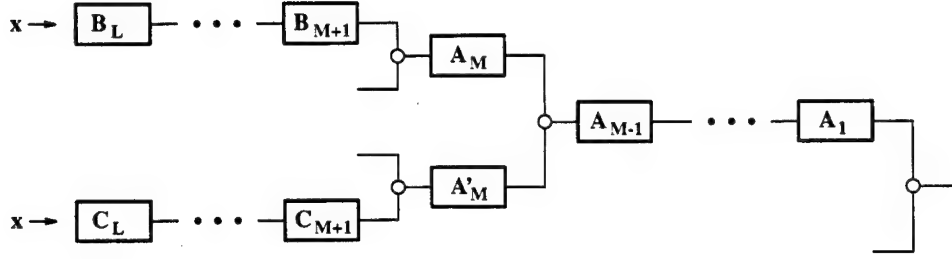


Figure 2.13: Spreading Code Branches

The cross correlation between these two codes is

$$\begin{aligned}
 r &= \mathbf{c}_b^T \mathbf{c}_c \\
 &= ([\prod_{i=1}^{M-1} (\mathbf{A}_i)^T][\mathbf{A}_M^T][\prod_{j=M+1}^L (\mathbf{B}_j)^T]\mathbf{x})^T \\
 &\quad ([\prod_{i=1}^{M-1} (\mathbf{A}_i)^T][\mathbf{A}'_M^T][\prod_{j=M+1}^L (\mathbf{C}_j)^T]\mathbf{x}) \\
 &= \mathbf{x}^T [\prod_{j=L}^{M+1} (\mathbf{B}_j)][\mathbf{A}_M][\prod_{i=M-1}^1 (\mathbf{A}_i)] \\
 &\quad [\prod_{i=1}^{M-1} (\mathbf{A}_i)^T][\mathbf{A}'_M^T][\prod_{j=M+1}^L (\mathbf{C}_j)^T]\mathbf{x} \\
 &= \mathbf{x}^T [\prod_{j=L}^{M+1} (\mathbf{B}_j)][\mathbf{A}_M][\mathbf{A}'_M^T][\prod_{j=M+1}^L (\mathbf{C}_j)^T]\mathbf{x} \\
 &= 0
 \end{aligned} \tag{2.53}$$

since $\mathbf{A}_i \mathbf{A}_i^T = \mathbf{I}$ due to the perfect reconstruction condition and $\mathbf{A}_M \mathbf{A}'_M^T = 0$ for any quadrature mirror filter pair. This result assures the orthogonality between any two spreading codes generated by the PR-QMF tree. This is consistent with the fact that the transformation generated by the PR-QMF synthesis tree is a unitary transformation. If each of the spreading codes are orthogonal to each other, then any off diagonal element of the multiplication of a matrix of these spreading codes by its transpose will be zero and this multiplication will result in the identity matrix.

The Asynchronous Case

When arbitrary delays are introduced, the cross correlations between user transmissions can no longer be guaranteed to be zero. Therefore, the polarity of the data bits being

modulated by the spreading codes becomes significant. As shown in Figure 1.6, there are two different polarity cases to consider.

For case one, all of the data bits are of positive polarity. Let the two codes be represented by column vectors \mathbf{c}_1 and \mathbf{c}_2 . For a given delay time of δ chips, the cross correlation between the two codes is

$$\rho_\delta = (\mathbf{c}_1)_\delta^T \mathbf{c}_2 \quad (2.54)$$

where $(\mathbf{c}_1)_\delta$ is a circular shift down of the vector \mathbf{c}_1 by δ positions. In a similar fashion, the cross correlations for case two, where a polarity change occurs, can be represented by

$$\rho_\delta^- = (\mathbf{c}_1)_\delta^T \mathbf{K}_\delta \mathbf{c}_2 \quad (2.55)$$

where \mathbf{K}_δ a diagonal matrix whose first δ diagonal elements are negative one and the remaining elements are positive one.

Now consider a node in a subband tree which occurs at stage L . Let the filters along the branch leading to that node be designated by $A_1(z), A_2(z), \dots, A_{L-1}(z)$ and the let the final QMF pair be designated as $A_L(z)$ and $A'_L(z)$. The codes generated by these two branches are

$$\mathbf{c} = \left[\prod_{l=1}^{L-1} (\mathbf{A}_l)^T \right] \mathbf{A}_L^T \mathbf{x} \quad (2.56)$$

$$\mathbf{c}' = \left[\prod_{l=1}^{L-1} (\mathbf{A}_l)^T \right] \mathbf{A}'_L^T \mathbf{x}. \quad (2.57)$$

To obtain the cross correlations, the circular shift $(\mathbf{c})_\delta$ must be generated. In matrix notation this becomes [19]

$$(\mathbf{c})_\delta = (\mathbf{A}_1)_\delta^T \left[\prod_{l=2}^{L-1} (\mathbf{A}_l)^T \right] \mathbf{A}_L^T \mathbf{x} \quad (2.58)$$

where $(\mathbf{A}_1)_\delta$ is a circular shift down by δ rows. For a given delay of δ chips, the cross correlation between the two codes under polarity case one is

$$\begin{aligned} \rho_\delta &= (\mathbf{c}_1)_\delta^T \mathbf{c}_2 \quad (2.59) \\ &= ((\mathbf{A}_1)_\delta^T \left[\prod_{l=2}^{L-1} (\mathbf{A}_l)^T \right] \mathbf{A}_L^T \mathbf{x})^T (\mathbf{A}_1^T \left[\prod_{l=2}^{L-1} (\mathbf{A}_l)^T \right] \mathbf{A}'_L^T \mathbf{x}) \\ &= \mathbf{x}^T \mathbf{A}_L \left[\prod_{l=L-1}^2 (\mathbf{A}_l) \right] [(\mathbf{A}_1)_\delta \mathbf{A}_1^T] \left[\prod_{l=2}^{L-1} (\mathbf{A}_l)^T \right] \mathbf{A}'_L^T \mathbf{x} \\ &= \mathbf{a}_L^T \mathbf{P}^T \mathbf{Q}_\delta \mathbf{P} \mathbf{a}'_L \end{aligned}$$

where \mathbf{a}_L and \mathbf{a}'_L are column vectors containing the filter coefficients of $A_L(z)$ and $A'_L(z)$ respectively and

$$\mathbf{P} = [\prod_{l=2}^{L-1} (\mathbf{A}_l)^T]. \quad (2.60)$$

Both the coefficient vectors and the the matrix \mathbf{P} are not dependent on the shift δ . The shift is represented by

$$\mathbf{Q}_\delta = (\mathbf{A}_1)_\delta \mathbf{A}_1^T. \quad (2.61)$$

A similar formulation can be made for ρ_δ^- , however, in this case let

$$\mathbf{Q}_\delta^- = (\mathbf{A}_1)_\delta \mathbf{K}_\delta \mathbf{A}_1^T \quad (2.62)$$

so that

$$\rho_\delta^- = \mathbf{a}_L^T \mathbf{P}^T \mathbf{Q}_\delta^- \mathbf{P} \mathbf{a}'_L. \quad (2.63)$$

Equations 2.60 and 2.63, therefore, represent the cross correlations between the spreading codes directly in terms of the operator matrices. Notice that, if $\delta = 0$, then $\mathbf{K}_\delta = \mathbf{I}$ and $\mathbf{P}^T \mathbf{P} = \mathbf{I}$. Since, for a QMF pair, $\mathbf{a}_l^T \mathbf{a}'_l = 0$, the cross correlation between the codes is zero and they are orthogonal for both polarity cases. This can be seen as a special case of Equation 2.53 where $M = L$.

2.6.3 Autocorrelation Properties of PR-QMF Spreading Codes

Another important property which must be considered is the autocorrelation of the spreading code. The autocorrelation directly effects the receiver synchronization performance as well as the performance of the system in the presence of multipath interference.

Consider a code generated by one branch of a PR-QMF tree of depth L . Let the filters along that branch be designated by $A_1(z), A_2(z), \dots, A_L(z)$. The autocorrelation of the code with a delay of zero is

$$\begin{aligned} \xi_0 &= ([\prod_{l=1}^L (\mathbf{A}_l)^T] \mathbf{x})^T ([\prod_{l=1}^L (\mathbf{A}_l)^T] \mathbf{x}) \\ &= \mathbf{x}^T [\prod_{l=L}^1 (\mathbf{A}_l)] [\prod_{l=1}^L (\mathbf{A}_l)^T] \mathbf{x} \\ &= 1 \end{aligned} \quad (2.64)$$

due to Equations 2.44 and 2.45. If, as in the asynchronous cross correlation case, delays of the codes are taken into account, then there are, once again, the two polarity cases

of Figure 1.6. This time, however, the interfering data bits are using the same code as the signal of interest. The remainder of the autocorrelation sequence can therefore be represented by [20]

$$\begin{aligned}
\xi_\delta &= ((\mathbf{A}_1)_\delta^T [\prod_{l=2}^{L-1} (\mathbf{A}_l)^T] \mathbf{A}_L^T \mathbf{x})^T (\mathbf{A}_1^T [\prod_{l=2}^{L-1} (\mathbf{A}_l)^T] \mathbf{A}_L^T \mathbf{x}) \\
&= \mathbf{x}^T \mathbf{A}_L [\prod_{l=L-1}^2 (\mathbf{A}_l)] [(\mathbf{A}_1)_\delta \mathbf{A}_1^T] [\prod_{l=2}^{L-1} (\mathbf{A}_l)^T] \mathbf{A}_L^T \mathbf{x} \\
&= \mathbf{a}_L^T \mathbf{P}^T \mathbf{Q}_\delta \mathbf{P} \mathbf{a}_L
\end{aligned} \tag{2.65}$$

where \mathbf{P} and \mathbf{Q} are defined as in Section 2.6.2 and \mathbf{a}_L is a column vector of the $A_L(z)$ filter coefficients.

For case 2, a similar formulation can be made giving

$$\xi_\delta^- = \mathbf{a}_L^T \mathbf{P}^T \mathbf{Q}_\delta^- \mathbf{P} \mathbf{a}_L \tag{2.66}$$

where, again, \mathbf{Q}_δ^- is defined by Equation 2.62.

Both the autocorrelations and the cross correlations of the spreading codes have now been formulated directly in terms of the filter coefficients. As expected, for the synchronous system, the cross correlations were identically zero and the autocorrelations were normalized to unity. For the asynchronous system, however, this was not the case since it is impossible for finite length codes to be completely orthogonal over all time shifts and all polarity cases.

Chapter 3

Optimized Filter Design for PR-QMF Based Spreading Codes

Since the spreading codes are simply the impulse responses of the PR-QMF subband synthesis stage, the coefficients used in the filters which comprise the subband tree clearly have a direct influence over the resulting properties of the codes. As shown earlier, for any two channel PR-QMF subband tree only one of the four filters needs to be designed. Furthermore, the freedom in the design of that filter is restricted by the perfect reconstruction conditions. However, for an N -tap FIR filter, there still remain $N/2$ degrees of freedom which can be used for design purposes.

When imposing the additional design criteria such that the filters, and therefore the resulting spreading codes, have desirable properties, the number of conditions on the tap weights increases so that the problem becomes over constrained, i.e. the desired properties cannot be achieved while still maintaining perfect reconstruction. Therefore, the coefficient search will be set up as a multivariable optimization problem in which the filter tap weights are the variables of optimization [3]. The properties which the spreading codes should obey will be represented as an objective function to be minimized and the optimization will be constrained by the perfect reconstruction conditions. The solution to the constrained optimization search will be used as the tap weights in the filter being designed.

In Chapter 2 a formulation of the PR-QMF based codes was developed directly in terms of the coefficients of the filters in the subband tree. Additionally, several properties of the codes were developed using these code representations. The task remaining, therefore, is to formulate the objective functions which utilize these expressions such that, when employed in the multivariable optimization, spreading codes will be designed with the desired properties.

In this chapter, objective functions will be developed for several different types of interference channels. The simplest type of interference is that which can be modeled by a stationary random process. This type of model is well suited for a variety of interference sources such as narrowband jamming. In addition to stationary interference, the two interference sources discussed in Sections 1.2 and 1.3, namely multiuser and multipath interference, will be considered. An objective function will then be developed for a multiuser channel where there is partial synchronization between the users. Finally, an objective function will be presented for a channel which contains interference from multiple sources.

3.1 Optimized Filter Design for Anti-Jam Communications

One of the most common types of interference encountered in communications is stationary interference. Examples of stationary interference sources are intentional jamming by hostile forces, unintentional interference caused by known or unknown RF transmitters, and electromagnetic interference. Additionally, there are some channels where the available spectrum is shared by both narrowband and spread spectrum signals. In many of these situations, the interference can be measured and recorded, thereby providing the spread spectrum system some *a priori* knowledge of the interference source. Under such situations, it is desired to develop spreading codes such that the interference will have little impact on the spread spectrum system.

To communicate successfully in the presence of a stationary interference source, the energy from the interference should be isolated from the energy of the signal. In the context of the system under consideration, it is desired that the interference energy be isolated, as much as possible, to a few subbands. The codes associated with those subbands will not be used as spreading codes. The remaining subbands will have very little interference energy in them and, therefore, the corresponding codes will be unaffected by the interference and suitable for use in the system. An ideal example of this is shown in Figure 3.1. In this simple four-band system, the analysis bank is being used to demodulate the received signal as described in Section 2.1. If all of the interference energy is isolated to the subband using $H_4(z)$, while the spreading code was generated using $H_2(z)$, then the interference will have no impact upon the decision of the spreading code polarity and the bit decision. Similarly, codes generated by the subbands using $H_0(z)$ or $H_3(z)$ could also be used without interference from the jammer.

In order to design the filters such that the interference energy is isolated to a small number of subbands, some *a priori* knowledge about the interference source is required. Specifically, we assume that the interference is stationary and the autocorrelation ma-

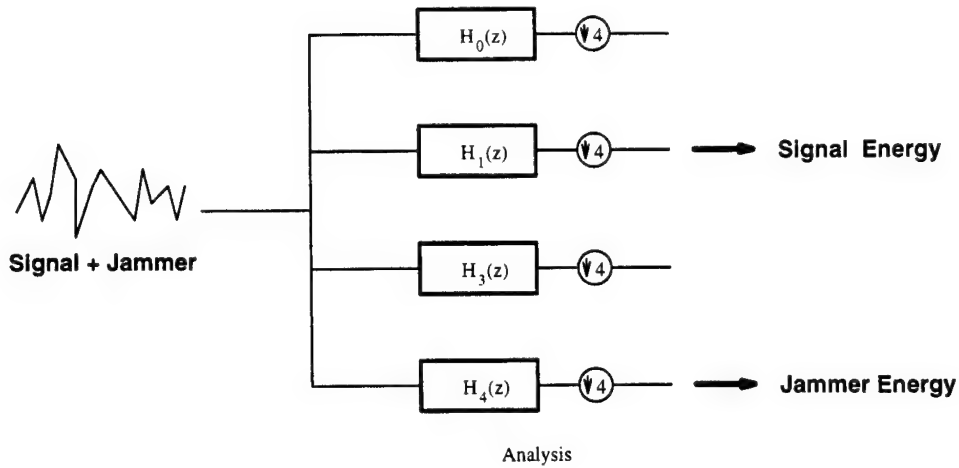


Figure 3.1: Demodulation of a Signal Plus Interference

trix is known. A measure known as *energy compaction* can then be applied to the problem [22]. Energy compaction is the ability of a filter to isolate the energy of a given signal. Let \mathbf{x} and \mathbf{y} be the infinite length input and output vectors, respectively, for a filter $A(z)$. The autocorrelation matrix for the output of the filter can be calculated as follows [45]

$$\begin{aligned} \mathbf{y} &= \mathbf{A}\mathbf{x} \\ E[\mathbf{y}\mathbf{y}^T] &= E[\mathbf{A}\mathbf{x}\mathbf{x}^T\mathbf{A}^T] \\ \mathbf{R}_{\mathbf{y}\mathbf{y}} &= \mathbf{A}\mathbf{R}_{\mathbf{x}\mathbf{x}}\mathbf{A}^T \end{aligned} \tag{3.1}$$

where $\mathbf{R}_{\mathbf{x}\mathbf{x}}$ and $\mathbf{R}_{\mathbf{y}\mathbf{y}}$ are the autocorrelation matrices of \mathbf{x} and \mathbf{y} , respectively, and \mathbf{A} is an infinite length operator matrix for the filter $A(z)$. The energy of the output will be greatest when the diagonal elements of $\mathbf{R}_{\mathbf{y}\mathbf{y}}$ are maximized. Each of these identical elements are given by

$$[\mathbf{R}_{\mathbf{y}\mathbf{y}}]_{k,k} = \sigma_y^2 = \mathbf{a}^T \mathbf{R}_{\mathbf{x}\mathbf{x}} \mathbf{a} \tag{3.2}$$

where $[\cdot]_{i,j}$ represents the i th row and j th column of the matrix inside the bracket and \mathbf{a} is a column vector of the filter coefficients.

This last expression provides a measure of the energy compaction of a filter to a particular input. For any QMF pair being designed, one filter from the pair will maximize this measure. The complementary filter in the QMF pair will therefore minimize the measure. For example, if the interference source contains primarily low frequency energy, a filter which compacts this energy will be a lowpass filter. The QMF counterpart will therefore be a highpass filter and, thus, will attenuate most of the interference energy.

The optimization problem for a channel impaired by stationary interference can now be given as

$$F_{AJ} = \min \{-\mathbf{a}^T \mathbf{R}_{xx} \mathbf{a}\} \quad (3.3)$$

subject to the perfect reconstruction conditions,

$$\sum_{k=0}^{N-1} a_k a_{k+2n} = \delta_n \quad \forall n \geq 0 \quad (3.4)$$

where a_k are the filter coefficients, \mathbf{R}_{xx} is the autocorrelation matrix of the interference, and δ_n is the unit impulse function. The change of sign in the objective function is included to allow a minimization to be performed. The constraints are the perfect reconstruction conditions for a two-channel PR-QMF filter bank given by Equation 2.34.

If progressive optimality is to be used in the filter bank design, a new set of filters must be designed at each node. In the original development of the progressively optimal design technique, the product filters for each branch were calculated as described in Section 2.3.1. The optimization was then performed on these product filters [42]. In this application, it is computationally simpler to calculate the new statistics of the interfering source after it has been decimated. For example, consider the design of $A_1(z)$ as shown in Figure 3.2a. It is assumed that $A_0(z)$ has already been designed and the autocorrelation function of the interference source, \mathbf{R}_{xx} , is known. Let \mathbf{y}' be the filter output of $A_0(z)$ prior to the downsampler, and let \mathbf{y} be the output after the first downsampling of two. Finally, let L_n be a linear operator which represents the discrete time filtering operation of $A_0(z)$. The autocorrelation matrix coefficients of \mathbf{y}' are given by [40]

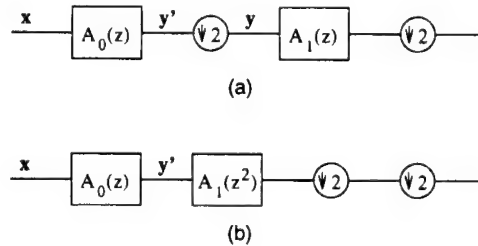


Figure 3.2: Interchange of a Filter and Downsampler

$$[\mathbf{R}_{y'y'}]_{m,n} = L_m \{ L_n \{ [\mathbf{R}_{xx}]_{m,n} \} \} \quad (3.5)$$

where m and n are the discrete time indexes of operation. Now, let $A_1(z)$, the filter to be designed, have an impulse response vector \mathbf{a}_1 . Using the *noble identity* for a decimator, shown in Figure 2.8a, the order of the filter and the downsampler can be interchanged

in the tree such that $A_1(z)$ will operate directly on $\mathbf{R}_{\mathbf{y}'\mathbf{y}'}$ as shown in Figure 3.2b. The identity gives the z -transform of the new filter as $A_1(z^2)$. If energy compaction is again used as the optimization criteria, the new objective function becomes

$$F_{AJ} = \min \left\{ -\mathbf{a}_1^T \mathbf{R}'_{\mathbf{y}'\mathbf{y}'} \mathbf{a}_1 \right\} \quad (3.6)$$

where $\mathbf{R}'_{\mathbf{y}'\mathbf{y}'}$ is an autocorrelation matrix constructed from the autocorrelation sequence of \mathbf{y}' downsampled by a factor of two [18]. This process continues until the spreading codes are of the desired length.

Once the entire tree is complete, the codes suitable for use in the system must be selected. This selection is most easily done by calculating the cross correlation of each generated code with the anticipated interference and selecting those codes most orthogonal to the interference source. This set then provides a “pool” of codes which the transmitter can use by either selecting one to use for every bit, or by hopping among the valid codes according to some predetermined sequence. Although the latter is more complex, especially from a receiver synchronization point of view, an advantage occurs in the spectral flatness of the resulting transmission [18].

3.2 Optimization Functions for the Multiuser Channel

The optimization problem for the stationary interference channel formulated above is relatively simple and straightforward. It does however, provide a clear illustration of the subband tree design method; that is, formulate an objective function for the interference, determine the effects of decimation on the interference source or objective function, and design the subband tree using progressive optimality.

The objective function for the multiuser channel is both theoretically and computationally more complex. It is dependent upon both the expected number of users in the channel and the anticipated signal to noise ratio. In many practical applications, however, both of these values are known to the system designer. Therefore, use of these quantities to design the codes is not unreasonable. Finally, it will be shown that in the most important case, a channel with a large number of users, the two quantities are not needed.

The BER for a multiuser channel is directly related to the cross correlations between the users and, therefore, the set of spreading codes being utilized. As shown in Section 2.6.2 this cross correlation is identically zero for the synchronous case. For the asynchronous case, however, this is not so and all relative time delays between all generated codes must be considered. Additionally, for the partial synchronization case, only certain time delays need to be considered. For an arbitrary full subband tree of depth L this quickly becomes computationally complex and unmanageable. Therefore,

once again, the tree will be progressively optimized and only one set of two codes will be considered at any one time. For example, consider the ideal case of two codes which are *completely orthogonal*; that is, their cross correlation is zero for all polarities and all relative time delays between the two codes. These codes must, therefore, be disjoint in the frequency domain. Any further linear processing by the decimators will not cause the signals to spectrally overlap and, therefore, all codes generated by subsequent operations on them will be completely orthogonal as well.

3.2.1 The Two User Channel

Although it is clearly not a realistic and practical scenario, an objective function will first be developed for a system in which there are only two users transmitting at any particular time. This two user case will illustrate the process whereby the BER is determined as a function of the cross correlations. Once that is established and the objective function developed, a channel with multiple users will be considered.

If there are only two users in the channel, then one user will be transmitting the signal of interest and the second user will be an interference source. Assume that both users are transmitting with equal power and the thermal (AWGN) noise in the channel has a variance of σ_η^2 . Also, assume that both the users and the noise are independent. If the receiver for the signal of interest is using the correlator receiver discussed in Section 1.1, the decision variable (after the correlation) can be modeled as [29]

$$r = \pm s + \eta + \rho_\delta \quad (3.7)$$

where s is due to the signal, η is a random component due to AWGN, and ρ_δ is due to the interference from the other user (i.e. the cross correlation between the two codes) and is dependent upon the relative delay δ between the two codes. The calculation of this quantity, ρ_δ , for two codes associated with a given QMF pair was given in Section 2.6.2.

Assume that a +1 is transmitted such that the polarity of s is positive. The BER can now be calculated conditioned on a specific delay δ . First the conditional expectation is taken giving

$$\begin{aligned} \mu_{r|\delta,+1} &\triangleq E[s + \eta + \rho_\delta] \\ &= s + \rho_\delta \end{aligned} \quad (3.8)$$

since the noise is a zero mean process and, given a fixed δ , the other two quantities are deterministic. The deterministic nature of these two variables also affects the second moment of the decision variable. Since the noise is the only random quantity it follows that [28]

$$\begin{aligned} \sigma_{r|\delta,+1}^2 &\triangleq E[(s + \eta + \rho_\delta)^2] - \mu_{r|\delta,+1}^2 \\ &= \sigma_\eta^2. \end{aligned} \quad (3.9)$$

The conditional BER can now be calculated as [29]

$$\begin{aligned} P_{e|\delta,+1} &= Q\left(\frac{\mu_{r|\delta}}{\sigma_{r|\delta}}\right) \\ &= Q\left(\frac{s + \rho_\delta}{\sigma_\eta}\right) \end{aligned} \quad (3.10)$$

where

$$Q(x) = \frac{1}{\sqrt{2\pi}} \int_x^\infty e^{-(y^2/2)} dy \quad (3.11)$$

is the Gaussian tail probability commonly referred to as the *Q-function*.

The unconditional BER can be calculated by assuming each delay is equally likely. Additionally, due to the different bit polarity possibilities discussed in Section 1.5.1, for every positive offset from the signal mean s (i.e. a positive value of the cross correlation), there is a corresponding negative offset as well. Therefore, the unconditional BER is

$$P_e = \sum_\delta \frac{1}{N} \left[Q\left(\frac{s + \rho_\delta}{\sigma_\eta}\right) + Q\left(\frac{s - \rho_\delta}{\sigma_\eta}\right) \right] \quad (3.12)$$

where N is the total number of possible delays. Since an identical result would occur for a -1 being transmitted, the conditioning upon the data bit polarity can be removed.

For the two user channel, this probability is the quantity which should be minimized. The objective function for the two user channel therefore becomes

$$F_{MU} = \min \left\{ \sum_\delta \frac{1}{N} \left[Q\left(\frac{s + \rho_\delta}{\sigma_\eta}\right) + Q\left(\frac{s - \rho_\delta}{\sigma_\eta}\right) \right] \right\} \quad (3.13)$$

or

$$F_{MU} = \min \left\{ \sum_\delta \left[Q\left(\frac{s + \rho_\delta}{\sigma_\eta}\right) + Q\left(\frac{s - \rho_\delta}{\sigma_\eta}\right) \right] \right\} \quad (3.14)$$

since the $1/N$ term is just a scaling factor and will not affect the minimization. Once the signal power and the signal to noise ratio is fixed, the value of the above function is determined solely by the cross correlation values which are directly related to filter coefficients.

3.2.2 Channels With Few Users

The simple two-user case discussed above showed the connection between the cross correlation values between two codes and the performance of the codes in terms of the bit

error rate. In the two-user model a conditional BER was calculated from a given test statistic of the received signal. This test statistic included an offset, ρ_δ , which is based upon the relative delay between the two users. The unconditional BER was then calculated by summing up all of these possibilities dividing by the total number of delays. Although this same principle could be applied to a channel with more than one user, the computational effort increases exponentially with the number of users. Therefore, for a channel with more than one user, the *distribution* of all possible cross correlations will be considered and the unconditional probability of error will be calculated based upon that distribution.

Consider a channel with N users as shown in Figure 3.3 where N is a relatively small number. Assume that all users are transmitting with equal power. If the signal of interest is being transmitted by one of the users, then there are $N - 1$ signals which will cause interference. Once again there will be an offset to the mean of the signal of interest at the output of the correlator similar to that represented by Equation 3.8. This offset, however, is now caused by a combination of all possible cross correlations of every code with the signal of interest. All of these possible cross correlations will form some sort of distribution. By calculating all of these possibilities and then forming a histogram, an approximation to this distribution can be found.

Once this histogram is known, the procedure and functions developed in Section 3.2.1 can be used with two modifications. First, instead of using the offset, ρ_δ , caused by an individual user cross correlation, the center of each histogram bin, ρ_i , should be used for the calculation of the conditional BER. Secondly, since each possible offset is no longer equally likely, the probabilities cannot be ignored in the objective function. Instead, the unconditional BER must be calculated using the probability of each offset giving

$$F_{MU} = \min \left\{ \sum_i P_i \left[Q \left(\frac{s - \rho_i}{\sigma_n} \right) \right] \right\} \quad (3.15)$$

where P_i is the probability associated with each histogram bin centered at ρ_i . Notice that since the histograms are symmetrical (due to the different polarity cases), only one Q -function is needed.

If progressive optimality is used to design the tree, only two codes can be under consideration at any one time and a histogram representing the cross correlation distribution of all codes cannot be generated. Therefore, an approximation to the histogram must be constructed using only the two available codes. This can be done by treating the cross correlations between two codes as a random variable. For example, consider the channel shown in Figure 3.3 with $N = 3$. In this case there are two users adding interference into the channel. Let the cross correlation between the signal of interest and the first interferer be a random variable denoted by ρ_{I_1} and for the second interferer, ρ_{I_2} . Since the interference is added in the channel, the aggregate interference is formed by adding the two random variables. The distribution of the aggregate interference is

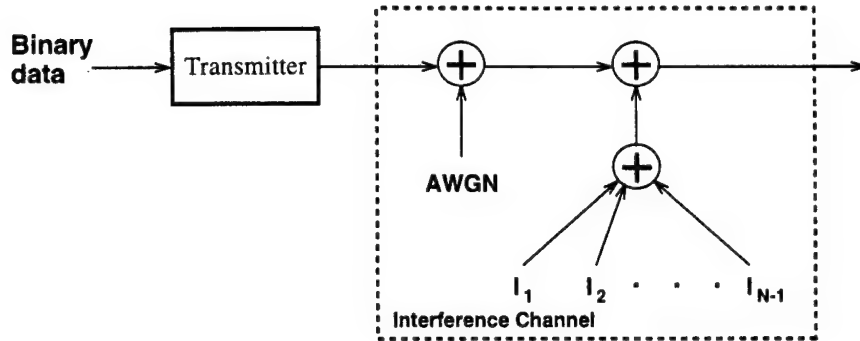


Figure 3.3: Interference Channel With N Users

therefore determined by convolving the distributions of ρ_{I_1} and ρ_{I_2} [40]. This can be extended beyond the case of two interferers by performing more convolutions using each interference distribution.

For progressively optimized codes, however, there is only one distribution available since only two codes are being considered at one time. Therefore, the composite histogram, representing the distribution of the sum off all user interference, can be approximated by convolving the available distribution with itself the appropriate number of times. For example, if the channel is expected to have four interferers, the histogram should be convolved with itself four times. The optimization can then proceed as discussed above.

3.2.3 Channels With Many Users

For even a modest number of users, the method described above for calculating the objective function quickly exceeds current processing capabilities. For a large number of users, a different objective function must be found which will still accurately “weight” the cross correlation values in accordance with how they effect the BER.

Fortunately, the problem where there are a large number of users in the channel is actually the simplest case to design for. The objective function can be obtained by extending the arguments from Section 3.2.2 to a limiting case. The model for this is also shown in Figure 3.3. The random variable representing the composite interference signal is the sum of each individual interference source which are themselves zero mean random variables. By using arguments from the Central Limit Theorem [10], this sum converges to a zero mean Gaussian distribution. If this second source of interference in the channel of Figure 3.3 is Gaussian distributed, it is easy to show that the BER is minimized when the variance of the distribution is minimized. Furthermore, the variance of this

Gaussian distribution is smallest when the variances of the contributing distributions are minimized [52].

Once again, if progressive optimization is used, only one set of cross correlation values are available and only one distribution is available. Therefore, the objective will be to minimize the variance of this distribution which, in turn, will minimize the variance of the resulting Gaussian distribution. In terms of the cross correlations the objective function becomes

$$F_{MU} = \min \left\{ \sum_{\delta} [(\rho_{\delta})^2 + (\rho_{\delta}^-)^2] \right\} \quad (3.16)$$

where ρ_{δ} is calculated in accordance with Section 2.6.2.

Figure 3.4 compares the function developed above with that of Equation 3.14 for two different SNRs. The functions are normalized over the range of ρ_{δ} so a comparison

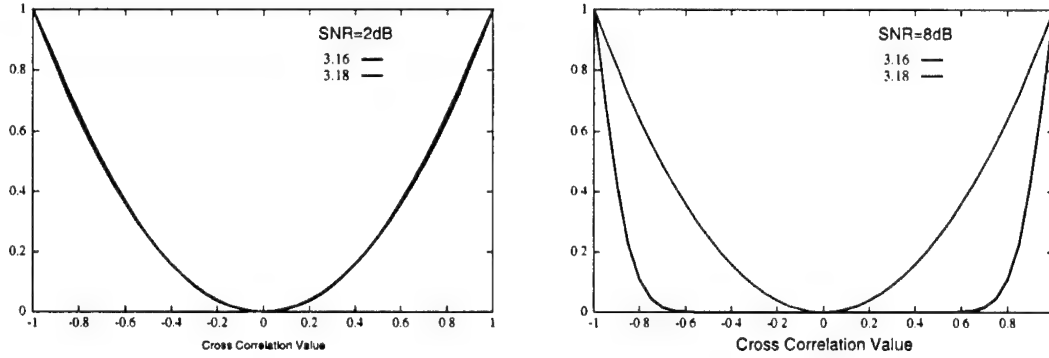


Figure 3.4: Comparison of Gaussian Approximation Objective Function Argument

can be made. As the additive channel noise (both from thermal noise and interference) increases the approximation of Equation 3.16 tends towards the ideal.

3.3 Multiuser Channel With Coarse Synchronization

In many communication systems, synchronization between the users is achieved through the use of a beacon or timing signal transmitted by a base station. For example, consider the mobile to base transmissions as shown in Figure 3.5. Previously, it was assumed that an asynchronous system occurred because of both transmit clock differential and variances in the propagation paths. Suppose, however, that the base station is transmitting

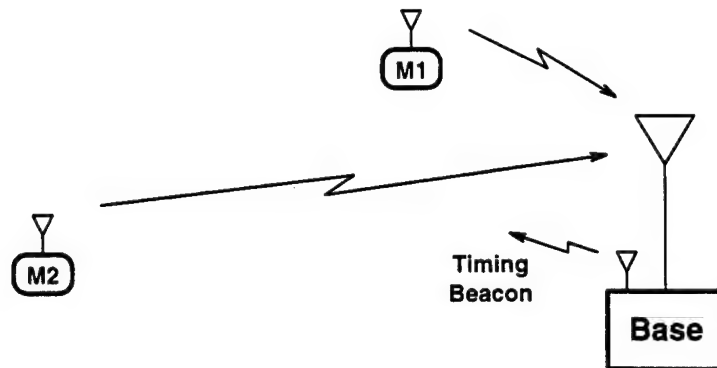


Figure 3.5: Mobile to Base Communications System

a timing signal which each mobile unit can use to synchronize their respective transmit clocks. The only cause for different delay times, therefore, would be the different propagation paths between the users and the base station.

The *microcell* [41] trend in cellular communications has the effect of shortening this distance and thus the delay times as well. Originally proposed to increase capacity in a PCS environment, the microcell architecture limits the physical size of a cell. Under these conditions, partial synchronization between the users is possible and there are some delay times which need not be considered in the objective function.

3.3.1 Alternate Representation of Spreading Code Shifts

Although the formulation of this objective function would seem to be a straightforward extension of the previous section, the use of progressive optimality in a hierarchical tree structure prevents this. Previously, the goal was to produce codes which were completely orthogonal over all time shifts. Linear processing by subsequent decimation did not negate any orthogonality which was already attained between two codes and, therefore, the progressively optimal approach worked. In this case, however, the codes are not completely orthogonal. It must therefore be determined how the final objective, i.e. codes with low cross correlations over a subset of all possible time shifts, affects the design of filters in the earlier stages of the tree.

In order to “backtrack” the objective through the tree, the expressions for a circular shift of a code must be redefined in a more complex format. This is best seen by first looking at an example prior to giving the formula for the general case. Consider a code generated by a full binary subband tree structure with three levels and eight tap filters

in each decimator. Equation 2.48 gives the equation for this code as

$$\mathbf{c} = \mathbf{A}_1^T \mathbf{A}_2^T \mathbf{A}_3^T \mathbf{x} \quad (3.17)$$

where \mathbf{x} is a unit vector and \mathbf{A}_l is an operator matrix representing a decimation using the filter $A_l(z)$. In this case $A_1(z)$ is used in the first split in the subband tree. To represent a circular shift of the code Equation 2.58 is used so that

$$(\mathbf{c})_\delta = (\mathbf{A}_1)_\delta^T \mathbf{A}_2^T \mathbf{A}_3^T \mathbf{x} \quad (3.18)$$

where $(\cdot)_\delta$ is a circular shift of the vector or matrix.

An alternative and more complex method of representing the circular shift involves performing a shift on more than one matrix or vector in the right hand side of Equation 3.18. For the code under consideration, this alternative method has the form

$$(\mathbf{c})_\delta = (\mathbf{A}_1)_{\delta_1}^T (\mathbf{A}_2)_{\delta_2}^T (\mathbf{A}_3)_{\delta_3}^T (\mathbf{x})_{\delta_x}^T \quad (3.19)$$

Each of the matrix shift indicators, δ_1 , δ_2 , and δ_3 , can take on a value of either zero or one. The values allowable for δ_x is dependent upon the filter length. In this example since each of the filters are of length eight, the matrix \mathbf{A}_3 has eight rows and four columns. The vector \mathbf{x} , therefore, must be of length four and the shift indicator, δ_x , can take on values of zero, one, two, or three.

The effect on each of the shift indicators on δ is as follows. If δ_1 is a one then \mathbf{c} will be circularly shifted by one position. If δ_2 is a one then \mathbf{c} will be circularly shifted by two positions. Finally, if δ_3 is a one then \mathbf{c} will be circularly shifted by four positions. For the unit vector shift, δ_x , number of shifted positions of the spreading code is equal to $8 \cdot \delta_x$. Other shift values for $(\mathbf{c})_\delta$ are generated by combining different values of the shift indicators on the right hand side of Equation 3.19. For example, if a shift of 19 is desired, the indicators would be $\delta_1 = 1$, $\delta_2 = 0$, $\delta_3 = 1$, and $\delta_x = 2$. Notice that the maximum shift which can be indicated is when $\delta_1 = \delta_2 = \delta_3 = 1$ and $\delta_x = 3$. In this case δ will equal 31. Since a code generated by a three stage full binary tree using eight tap filters is of length 32, it is possible to specify every shift using the above notation. Notice that although it is possible for each δ_i to take on values other than zero or one, those two values are the only ones necessary to represent each possible shift.

Now consider the general case of a code generated by a full binary tree with L stages and N -tap filters in each decimator. Let the filters along the branch generating the code be $A_1(z), A_2(z), \dots, A_L(z)$ with $A_1(z)$ occurring in the first split. A shift of δ positions of the code \mathbf{c} can be represented by

$$(\mathbf{c})_\delta = \left[\prod_{l=1}^L (\mathbf{A}_l)_{\delta_l}^T \right] (\mathbf{x})_{\delta_x}. \quad (3.20)$$

The shift indicators are chosen so that

$$\delta = \delta_x 2^L + \sum_{l=1}^L \delta_l 2^{l-1}. \quad (3.21)$$

The allowable values for the shift indicators are

$$\delta_l \in \{0, 1\} \quad (3.22)$$

$$\delta_x \in \{0, 1, 2, \dots, \frac{N}{2}\}. \quad (3.23)$$

Although this formulation is much more complex than that given by Equation 2.58 it is necessary to consider how a given shift of a code will effect every filter in the branch generating that code.

3.3.2 Objective Functions for Coarse Synchronization

First Stage Optimization

Now that the new representation of a circularly shifted code has been developed, it can be combined with the expression for the cross correlations of the codes. The first case which will be considered is the design of the QMF pair which occurs at the first split in a hierarchical subband tree structure as shown in Figure 3.6. Equations 2.54 and 2.55

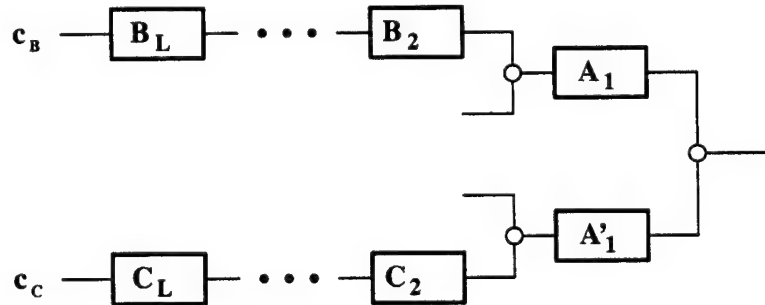


Figure 3.6: Branch Split at Stage 1

in Section 2.6.2 gave the cross correlation between two spreading codes as

$$\rho_\delta = (\mathbf{c}_c)_\delta^T \mathbf{c}_b \quad (3.24)$$

for polarity case one of Figure 1.6 and

$$\rho_\delta^- = (\mathbf{c}_b)_\delta^T \mathbf{K}_\delta \mathbf{c}_c \quad (3.25)$$

for polarity case two. Recall that \mathbf{K}_δ is a diagonal matrix whose first δ diagonal elements are negative one and the remaining elements are positive one.

Consider the cross correlations between two codes generated by the branches shown in Figure 3.6. For polarity case one substitution of Equation 3.20 into Equation 3.24 gives

$$\begin{aligned}\rho_\delta &= \left((\mathbf{A}_1)_{\delta_1}^T \left[\prod_{l=2}^L (\mathbf{C}_l)_{\delta_l}^T \right] (\mathbf{x})_{\delta_x} \right)^T \left((\mathbf{A}'_1)^T \left[\prod_{l=2}^L (\mathbf{B}_l)^T \right] \mathbf{x} \right) \\ &= (\mathbf{x})_{\delta_x}^T \left[\prod_{l=L}^2 (\mathbf{C}_l)_{\delta_l} \right] (\mathbf{A}_1)_{\delta_1} (\mathbf{A}'_1)^T \left[\prod_{l=2}^L (\mathbf{B}_l)^T \right] \mathbf{x}.\end{aligned}\quad (3.26)$$

For polarity case two, a similar result is attained by substitution of Equation 3.20 into Equation 3.25

$$\begin{aligned}\rho_\delta &= \left((\mathbf{A}_1)_{\delta_1}^T \left[\prod_{l=2}^L (\mathbf{C}_l)_{\delta_l}^T \right] (\mathbf{x})_{\delta_x} \right)^T \mathbf{K}_\delta \left((\mathbf{A}'_1)^T \left[\prod_{l=2}^L (\mathbf{B}_l)^T \right] \mathbf{x} \right) \\ &= (\mathbf{x})_{\delta_x}^T \left[\prod_{l=L}^2 (\mathbf{C}_l)_{\delta_l} \right] (\mathbf{A}_1)_{\delta_1} \mathbf{K}_\delta (\mathbf{A}'_1)^T \left[\prod_{l=2}^L (\mathbf{B}_l)^T \right] \mathbf{x}\end{aligned}\quad (3.27)$$

The filter coefficients for $A_1(z)$ are contained in the two terms in the middle of the above equations

$$\mathbf{V}_\delta = (\mathbf{A}_1)_{\delta_1} \mathbf{A}'_1{}^T \quad (3.28)$$

$$\mathbf{V}_\delta^- = (\mathbf{A}_1)_{\delta_1} \mathbf{K}_\delta \mathbf{A}'_1{}^T \quad (3.29)$$

As discussed above, the shift indicator can be only a zero or a one. Since the operator matrices are generated from a QMF pair, the result for $\delta_1 = 0$ is $\mathbf{V}_\delta = \mathbf{V}_\delta^- = 0$. For $\delta_1 = 1$, the multiplications result in matrices which are dependent upon δ .

Since every element in the matrices \mathbf{V}_δ and \mathbf{V}_δ^- contributes to the cross correlation values, these are the terms which should be minimized. For computational simplicity, the objective will be to minimize the squares of the elements. The objective function thus becomes

$$F_{CS} = \min \left\{ \sum_{\delta} \sum_i \sum_j \left([\mathbf{V}_\delta]_{i,j}^2 + [\mathbf{V}_\delta^-]_{i,j}^2 \right) \right\} \quad (3.30)$$

where $[\cdot]_{i,j}$ represents the i th row and the j th column of the matrix inside the brackets. The outer summation should only be performed over the shifts δ which are of interest.

Once again, the resulting objective function is very computationally intensive and unrealistic given current processing capabilities. For this reason, approximations are

made by not including every element of \mathbf{V}_δ^- . Due to the structure of the operator matrices, \mathbf{V}_δ is a circulant matrix. Additionally, an analysis of \mathbf{V}_δ^- shows that nearly every row is identical to, within a circular shift, or an additive inverse of, the same row which comprises \mathbf{V}_δ . Therefore, an objective function which approximates the one given by Equation 3.30, yet is able to be implemented, is

$$F_{CS} = \min \{ \mathbf{v} \mathbf{v}^T \} \quad (3.31)$$

where \mathbf{v} is a vector which represents the row that can be used to construct \mathbf{V}_δ . Using this approximation, some of the rows unique to \mathbf{V}_δ^- are not being considered. Generation of the vector \mathbf{v} is easily accomplished by using Equation 3.28, with $\delta_1 = 1$ and then extracting the first row of \mathbf{V}_δ .

Subsequent Stage Optimizations

The optimization for subsequent stages becomes even more complex than the first stage optimization discussed above. Things are again simplified, however, by not considering the matrices generated under polarity case two and using only Equation 3.24. Again, although this is only an approximation, it allows for optimization function which can be calculated using current processing capabilities.

Consider the design of a filter at stage M as shown in Figure 2.13 which is reproduced as Figure 3.7 for convenience. It has already been shown that the two codes generated

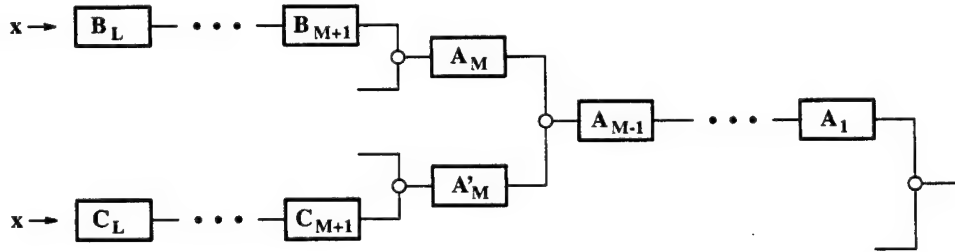


Figure 3.7: Spreading Code Branches

by the two different subbands depicted in the figure can be represented by

$$\mathbf{c}_b = \left[\prod_{i=1}^{M-1} (\mathbf{A}_i)^T \right] \mathbf{A}_M^T \left[\prod_{j=M+1}^L (\mathbf{B}_j)^T \right] \mathbf{x} \quad (3.32)$$

and

$$\mathbf{c}_c = \left[\prod_{i=1}^{M-1} (\mathbf{A}_i)^T \right] \mathbf{A}_M'^T \left[\prod_{j=M+1}^L (\mathbf{C}_j)^T \right] \mathbf{x}. \quad (3.33)$$

Using both of these expressions in Equation 3.24 along with Equation 3.20 gives

$$\begin{aligned}\rho_\delta &= \left(\left[\prod_{i=1}^{M-1} (\mathbf{A}_i)_{\delta_i}^T \right] (\mathbf{A}_M)_{\delta_M}^T \left[\prod_{j=M+1}^L (\mathbf{B}_j)_{\delta_j}^T \right] (\mathbf{x})_{\delta_x} \right)^T \\ &\quad \left(\left[\prod_{i=1}^{M-1} (\mathbf{A}_i)^T \right] \mathbf{A}_M'^T \left[\prod_{j=M+1}^L (\mathbf{C}_j)^T \right] \mathbf{x} \right) \\ &= (\mathbf{x})_{\delta_x}^T \left[\prod_{j=L}^{M+1} (\mathbf{B}_j)_{\delta_j} \right] (\mathbf{A}_M)_{\delta_M} \mathbf{W}_\delta \mathbf{A}_M'^T \left[\prod_{j=M+1}^L (\mathbf{C}_j)^T \right] \mathbf{x}\end{aligned}\quad (3.34)$$

where

$$\mathbf{W}_\delta = \left[\prod_{m=M-1}^1 (\mathbf{A}_m)_{\delta_m} \right] \left[\prod_{m=1}^{M-1} (\mathbf{A}_m)^T \right] \quad (3.35)$$

and represents the filters in Figure 3.7 which have already been designed. Once again, it is the middle of Equation 3.34 which is of interest since that contains the filter coefficients to be optimized. Therefore, let

$$\mathbf{V}_\delta = (\mathbf{A}_M)_{\delta_M} \mathbf{W}_\delta \mathbf{A}_M'^T \quad (3.36)$$

As in the previous section, for any particular δ , the rows of \mathbf{V}_δ are identical except for a circular shift. Let \mathbf{v}_δ be a row from \mathbf{V}_δ . Since the shift indicators on the right hand side of the above equation can take on only one of two values and since there are M of these indicators, there are 2^M different possibilities for \mathbf{v}_δ . The objective function then becomes

$$F_{CS} = \min \left\{ \sum_{\delta} \mathbf{v}_\delta \mathbf{v}_\delta^T \right\} \quad (3.37)$$

which again provides an approximation which can be implemented.

Final Stage Optimization

At the L th stage of the subband tree, shown in Figure 3.8, each of the filters along the branch except for the final QMF pair will already have been designed. Equation 3.34 then becomes

$$\rho_\delta = (\mathbf{x})_{\delta_x}^T (\mathbf{A}_L)_{\delta_L} \left[\prod_{l=L-1}^1 (\mathbf{A}_l)_{\delta_l} \right] \left[\prod_{l=1}^{L-1} (\mathbf{A}_l)^T \right] \mathbf{A}_L'^T \mathbf{x} \quad (3.38)$$

$$= (\mathbf{x})_{\delta_x}^T (\mathbf{A}_L)_{\delta_L} \left[\prod_{l=L-1}^2 (\mathbf{A}_l)_{\delta_l} \right] (\mathbf{A}_1)_{\delta_1} \mathbf{A}_1'^T \left[\prod_{l=2}^{L-1} (\mathbf{A}_l)^T \right] \mathbf{A}_L'^T \mathbf{x} \quad (3.39)$$

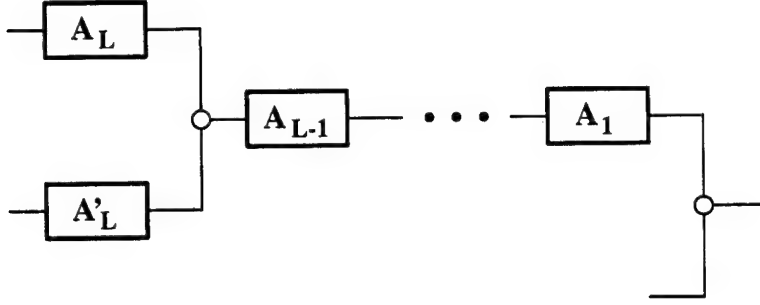


Figure 3.8: Final Stage Split

$$= \mathbf{x}^T \mathbf{A}_L \left[\prod_{l=L-1}^2 (\mathbf{A}_l) \right] (\mathbf{A}_1)_\delta \mathbf{A}'_1{}^T \left[\prod_{l=2}^{L-1} (\mathbf{A}_l)^T \right] \mathbf{A}'_L{}^T \mathbf{x} \quad (3.40)$$

$$= \mathbf{A}_L^T \mathbf{P}^T \mathbf{Q}_\delta \mathbf{P} \mathbf{a}'_L \quad (3.41)$$

where

$$\mathbf{P} = \left[\prod_{l=2}^{L-1} (\mathbf{A}_l)^T \right]. \quad (3.42)$$

and

$$\mathbf{Q}_\delta = (\mathbf{A}_1)_\delta \mathbf{A}'_1{}^T. \quad (3.43)$$

This expression is identical to Equation 2.60 from Section 2.6.2. Since this is the simpler form of the cross correlation and is easier to calculate, all of the methods of Section 3.2 can be used. The difference is that only the relevant shifts of δ should be considered in the objective function.

3.4 Optimized Filter Design for Multipath Channels

As discussed in Section 1.3, a spread spectrum system is often used to combat the fading which occurs in a multipath channel. In particular, if the bandwidth of the spread signal is much larger than the coherence bandwidth of the multipath interference, frequency selective fading occurs and communications may still be possible since only a portion of the signal will be affected. It is desirable, therefore, that a spreading code, and thus the resulting transmitted signal, be spectrally flat within the assigned bandwidth, thereby producing a broadband signal.

A property of a spreading code which can be used for this measure is the autocorrelation function of the signal. This is possible since the Fourier Transform directly relates the Power Spectral Density (PSD) of the signal with its autocorrelation [40]. Ideally, the PSD of the transmitted signal should be flat. Therefore, the autocorrelation of the spreading sequence should be an impulse.

Another approach to the problem is from a time-domain point of view. Each of the multipath components arriving at the receiver will be a delayed version of the transmitted signal (along with some attenuation and a phase shift). If each of these delayed components is uncorrelated with the desired signal, then no interference will be encountered. Therefore, the ideal autocorrelation sequence for a signal in a multipath channel would be an impulse response.

A second reason why it is desirable for a spreading code to exhibit an impulse function for its autocorrelation sequence is that it becomes easier for the receiver to achieve synchronization. As discussed in Section 1.1, a spread spectrum receiver must either synchronize the spreading code in phase to the received signal or sample the sliding correlator output at the appropriate time. It can be shown that a spreading sequence whose autocorrelation is nearly an impulse function will decrease the probability that the receiver will synchronize incorrectly or begin sampling at the wrong time [9].

Let, ξ_δ and ξ_δ^- , be the autocorrelation values of the spreading sequence with a delay of δ for the two polarity cases shown in Figure 1.6. The calculation of these quantities in terms of the filter coefficients used in the subband tree was given in Section 2.6.3. From the perfect reconstruction condition given in Equation 2.34, it is known that

$$\xi_0 = 1 \quad (3.44)$$

$$\xi_0^- = 1. \quad (3.45)$$

For all other values of δ , the autocorrelation should be driven towards zero. Again, for simplicity, a quadratic measure will be used so the objective function becomes

$$F_{MP} = \min \left\{ \sum_{\delta=1}^{N-1} [(\xi_\delta)^2 + (\xi_\delta^-)^2] \right\}. \quad (3.46)$$

As with the other objectives, this minimization should be constrained by the perfect reconstruction conditions.

3.5 Optimized Filter Design for Composite Channels

It is a rare situation when the communications system engineer is presented with a channel in which only one type of interference occurs. Often, two or more of the interference

sources discussed in this chapter are present. In this case, an objective function must be generated which incorporates all the interference types which are present. There is, however, no one set of filter coefficients which will generate a set of codes ideal for every set of channel conditions. Therefore, the designer must first analyze the channel and the expected channel conditions to determine the priority or weight which each objective function should be given. For example, if little or no narrowband interference is expected then the weight which that objective function receives in the optimization problem should be small.

Once the relative weights are determined, the composite optimization problem can be formulated as

$$F_C = \alpha F_{AJ} + \beta F_{MU} + \gamma F_{MP} + \cdots \quad (3.47)$$

subject to

$$\sum_{k=0}^{N-1} a_k a_{k+2n} = \delta_n \quad \forall n \geq 0$$

where the different objective functions are denoted by F_{AJ} , F_{MU} , and F_{MP} and α , β , and γ are the relative weights assigned to the different objectives. As in each of the earlier sections, progressive optimality should be incorporated in the filter bank design.

3.6 Objective Functions for Other Interference Sources

In this section, objective functions were developed for several different types of commonly encountered interference sources for which a spread spectrum system is employed to combat. The general method for the subband tree design was also demonstrated. First, formulate the objective for the spreading codes. Next, determine the effects of the decimation/interpolation upon the spreading code objectives. Finally, design the subband tree structure using a progressively optimal approach.

This method of designing spreading codes can be extended to all applications where spread spectrum signals are used such as LPI/D or high resolution ranging applications. Additionally, objective functions can be developed for applications where spreading codes are not normally utilized. Examples of these are non-linear channels [32] and OFDM applications.

Chapter 4

Performance Analysis and Results

Once the subband filter bank, and therefore the resulting spreading codes, are designed, it is desirable to know the performance of the codes when employed in the various interference channels. To this end, an analytical expression and algorithm will be developed so that the BER and other results can be calculated given the spreading codes and the expected type of interference. Similar to the approach utilized for the designing of the codes in Section 3.2 the decision variable generated in the receiver (after correlation) will be used to generate statistics from which a conditional BER can be calculated. This conditional BER can then be employed, along with the appropriately generated probabilities, to arrive at an unconditional BER for the set of codes.

Finally, in order to test the merits of the newly developed spreading codes, several example subband trees were generated using the objectives and constraints of Chapter 3. The codes were then extracted from the trees as described in Chapter 2 and compared to m -sequences and Gold codes in the narrowband interference and the multiuser channel, respectively. Additionally, the properties of the codes, as they relate to the objective functions, are also examined.

Each of the optimizations performed in this section were accomplished using the Matlab Optimization Toolbox [14]. The algorithm employed by this toolbox for a constrained optimization is the Sequential Quadratic Programming method. Since there is no guarantee that a global minimum will be reached it, was suggested to start the optimization from different starting points [14]. In each of the design problems, the optimization was performed with at least 100 different starting vectors whose elements were randomly chosen from a uniform distribution ranging from minus one to one.

4.1 Performance in the Presence of Stationary Interference

The first channel considered in Chapter 3 was the simple case of a channel which, in addition to the ever present AWGN, contains a stationary interference source. Codes were then designed which were uncorrelated with the interference so that the decision variable at the output of the correlator would be unaffected by the interference source. To analyze the performance of these codes, the statistics of this correlator output will be used to determine the effectiveness of this method.

4.1.1 Analysis

Consider a set of N codes developed from a PR-QMF subband tree. Out of this set of N codes, assume that M of the codes are selected for use in the system in accordance with Section 3.1; that is, it was determined that M of the codes are sufficiently uncorrelated with the anticipated interference such that they can be successfully used in the system. Finally, assume the transmitter is hopping over all of the usable codes such that the probability of using any one of the M codes is equal.

The interference in this analysis will be modeled as a single tone jammer of a given frequency, ω , and a given phase, θ . The receiver will be modeled as one of the structures discussed in Section 1.1 where the received signal is processed by a correlator receiver. No other processing of the received signal (i.e. equalization, excision, etc.) is assumed. If a signal corrupted by AWGN and interference is input to the receiver, the decision variable at the correlator output can be represented by

$$r = s + \rho_{m,\omega,\theta} + \eta \quad (4.1)$$

where η is the thermal noise component, with zero mean and variance of σ_η^2 , and ρ is correlation between the spreading sequence and the interference with frequency ω and phase θ . The subscript m in the correlation term indicates that the correlation is calculated for only one of the M possible spreading codes. The signal component is represented by s and, without loss of generality, is assumed to be of positive polarity.

Similar to the method used in Section 3.2.1, a conditional BER can be determined from the above decision variable. First, the mean of r is calculated by

$$\begin{aligned} \mu_{r|m,\omega,\theta} &\triangleq E[s + \rho_{m,\omega,\theta} + \eta] \\ &= s + \rho_{m,\omega,\theta} \end{aligned} \quad (4.2)$$

since η is a zero mean process and, given a particular spreading code, interference frequency, and phase, the other two quantities are deterministic. Additionally, because

everything but the noise is deterministic, the variance of r is the variance of the noise so that

$$\begin{aligned}\sigma_{r|m,\omega,\theta}^2 &\triangleq E[(s + \rho_{m,\omega,\theta} + \eta)^2] - \mu_{r|m,\omega,\theta}^2 \\ \sigma_{r|m,\omega,\theta}^2 &= \sigma_\eta^2.\end{aligned}\quad (4.3)$$

where the noise variance is denoted by σ_η^2 . The conditional BER therefore becomes [29]

$$\begin{aligned}P_{e|m,\omega,\theta} &= Q\left(\frac{\mu_{r|m,\omega,\theta}}{\sigma_{r|m,\omega,\theta}}\right) \\ &= Q\left(\frac{s + \rho_{m,\omega,\theta}}{\sigma_\eta}\right)\end{aligned}\quad (4.4)$$

where $Q(\alpha)$ is the Q -function defined by Equation 3.11.

The unconditional BER for a given spreading code can now be calculated by integrating over the range of anticipated jammer frequencies and all possible phases (assuming phase and frequency are independent and uniformly distributed) so that

$$P_{e|m} = \frac{1}{2\pi\Delta_\omega\theta} \int_\Omega \int_{-\pi}^\pi Q\left(\frac{s + \rho_{m,\omega,\theta}}{\sigma_\eta}\right) d\theta d\omega \quad (4.5)$$

where Δ_ω is the range of jammer frequencies. The integral over Ω indicates that the integration should take place over all jammer frequencies.

Since all M codes are equally likely, the unconditional BER is the average of the BERs conditioned upon the spreading codes. This gives the final expression for the BER as

$$\begin{aligned}P_e &= \frac{1}{M} \sum_m P_{e|m} \\ &= \frac{1}{2M\pi\Delta_\omega\theta} \sum_m \int_\Omega \int_{-\pi}^\pi Q\left(\frac{s + \rho_{m,\omega,\theta}}{\sigma_\eta}\right) d\theta d\omega.\end{aligned}\quad (4.6)$$

The above result can easily be modified to account for different interference scenarios. For example, suppose that each jammer frequency is not equally likely (note that phase will almost always be uniformly distributed). The term $\frac{1}{\Delta_\omega}$ would then be replaced by a probability measure of that frequency $p_\omega(\omega)$. Since this is a frequency dependent term, it must be brought inside the integral so that

$$P_e = \frac{1}{2M\pi\theta} \sum_m \int_\Omega \int_{-\pi}^\pi p_\omega(\omega) Q\left(\frac{s + \rho_{m,\omega,\theta}}{\sigma_\eta}\right) d\theta d\omega. \quad (4.7)$$

4.1.2 Results

In Section 3.1 the objective function for filter design was developed for a channel characterized by narrowband interference. The objective function was based upon the energy compaction criteria where some knowledge of the expected interference was given. The optimization problem was formulated as

$$F_{AJ} = \min \{ -\mathbf{a}^T \mathbf{R}_{xx} \mathbf{a} \} \quad (4.8)$$

subject to

$$\sum_{k=0}^{N-1} a_k a_{k+2n} = \delta_n \quad \forall n \geq 0$$

where a_k are the filter coefficients, \mathbf{a} is a column vector of these coefficients, \mathbf{R}_{xx} is the autocorrelation matrix of the interference, and δ_n is the unit impulse function.

This optimization problem was utilized to design a full binary subband tree of 5 stages using 4-tap FIR filters, resulting in spreading codes of length 64. The interference source for which the codes were optimized was a set of single tone jammers whose normalized range spanned $\omega = [\frac{\pi}{8}, \frac{\pi}{4}]$. Each jammer in this range was considered to be equally likely and the power of the interference was assumed to be independent of frequency and phase. After each stage was designed, a new autocorrelation function for the decimated interference was calculated as described in Section 3.1 so that the progressively optimal approach could be used.

After three stages of the tree, product filters were calculated according to Section 2.3.1. The frequency responses of the product filters, and therefore the corresponding subbands, are shown in Figure 4.1. For reference, the range of jammers considered is drawn in the figures as a rectangular box. It can be seen from the figures that after three stages of decimation, a significant amount of jammer energy is isolated to a few subbands while other subbands contain only trace amounts of energy.

By continuing the tree construction to five stages, 64 possible spreading codes, each of length 64, were developed. Out of these 64 possible codes, only 32 codes are unique. The remaining codes are time shifted versions of the others. This is due to the construction process of the codes. Each subband in the tree is able to produce one unique spreading codes. A five stage full binary tree, therefore, can produce 32 different codes. Since four tap filters are being used, an operator matrix for a decimator at level five will be of size two by four. The unit vector in Equation 2.48, therefore, is of length two.

Of the set of codes generated by the tree, it was determined that 24 of the 32 codes were sufficiently uncorrelated with the range of expected interference energy and, therefore, were suitable for use in the system. The results for a single tone jammer were calculated in accordance with Section 4.1.1 and are shown in Figure 4.2. The power of

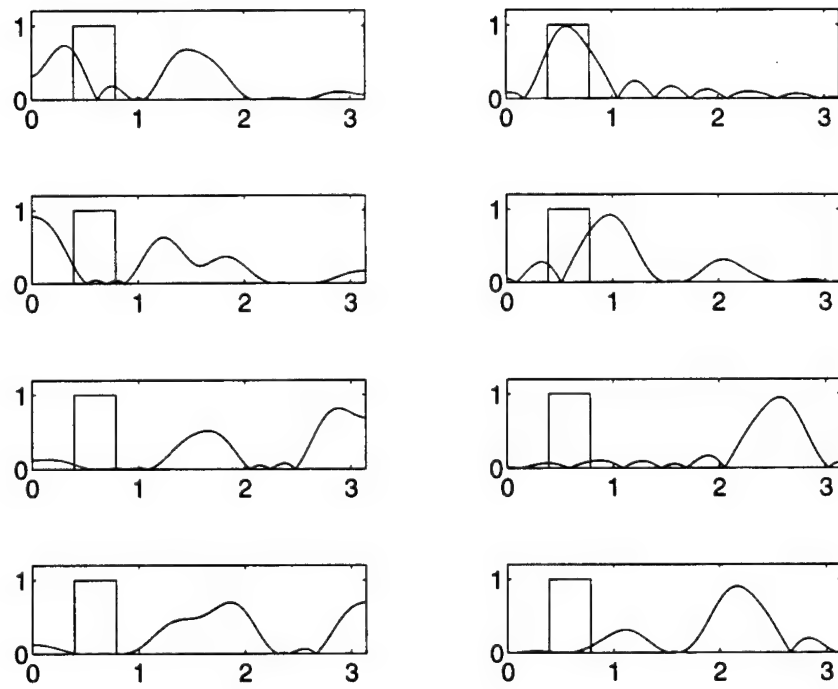


Figure 4.1: Magnitude Responses of the 3rd Stage Subbands

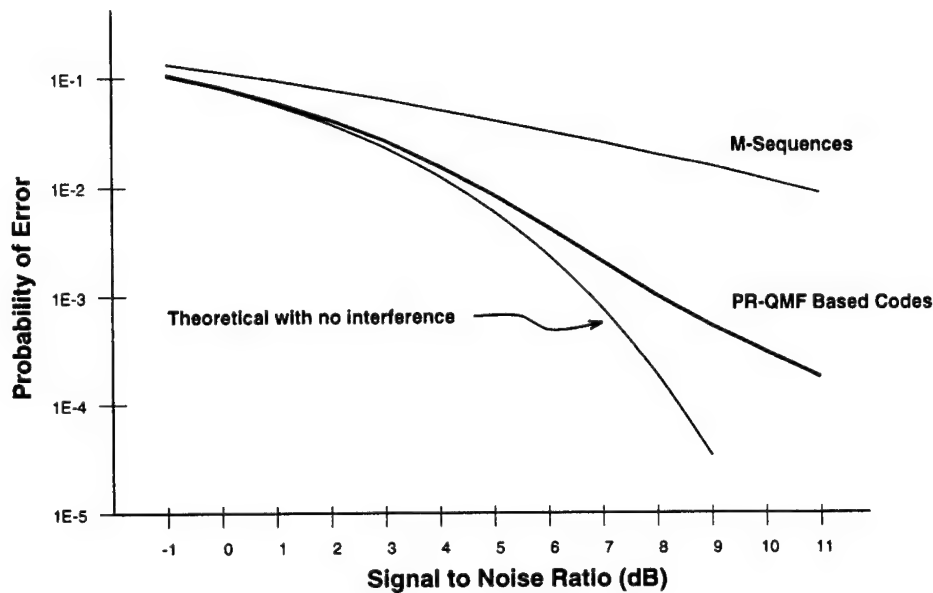


Figure 4.2: Performance Against 10dB Jamming

the jammer tested is 10dB and refers to the power of the jammer divided by the power of the signal. The range of interference tested is the entire frequency range for which the tree was designed. For reference, similar calculations were performed for a DSSS system using *m*-sequences. The *m*-sequence tested was 63 chips long. As can be seen from the figure, the PR-QMF Based Spreading Codes show significant improvement over the *m*-sequences. This, however, is not surprising since some *a priori* knowledge about the interference was available when designing the system.

Additional insight can be gained by looking at the normalized frequency spectrum of the signal being transmitted over the channel. This was generated by a computer simulation of the DSSS system shown in Figure 1.1 using the newly developed codes. The set of 24 codes used to generate the curve in Figure 4.2 were randomly chosen, one code per bit, for use as the sequence to spread the random bit stream. The frequency spectrum of the transmitter output was then taken and normalized. The result is shown in Figure 4.3. Notice that there exists a null in the spectrum in the range of frequencies of the interference. It is this null which accounts for the improved performance shown in Figure 4.2.

As outlined above, only the portion of the codes generated which are least correlated with the interference are used. It follows, therefore, that if improved performance is desired, fewer codes should be included in the pool of usable codes. In other words, keep eliminating codes from the pool until the desired level of performance is attained. The

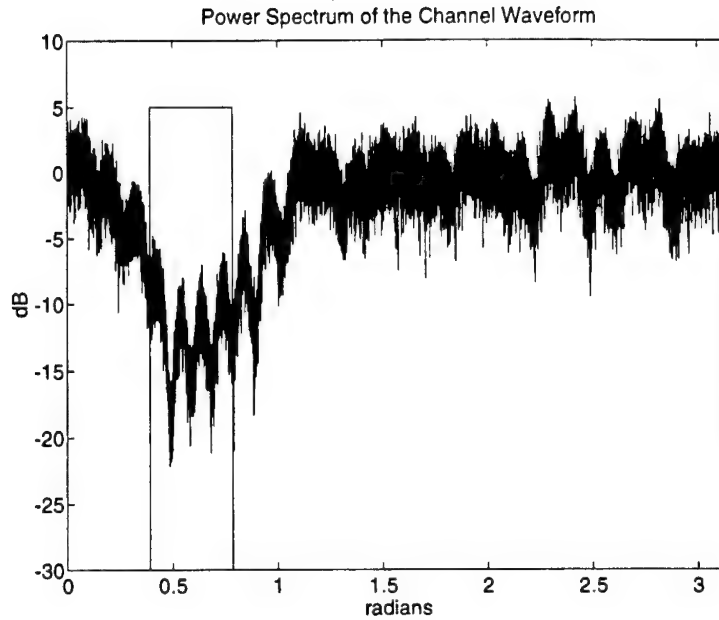


Figure 4.3: Frequency Spectrum of the PR-QMF Based System

results of doing this for a 15dB single tone jammer are shown in Figure 4.4. Note that the jammer power is 5dB more than that for the earlier results. In reducing the number of usable codes from 24 to 20, the codes which were most correlated with the interference were removed. The price paid for the improved performance is that of spectral flatness of the transmitted signal. Since fewer codes are used, all subband frequencies are not present in signal. Although the depth of the null shown in Figure 4.3 would be greater, the width of the null would increase as well.

Finally, in order to verify the analytical results developed in Section 4.1.1 a computer model of the system shown in Figure 1.1 was constructed. A Monte Carlo simulation was then used to determine the performance in the presence of AWGN and a jammer with a randomly chosen phase. The spreading codes were generated prior to the start of the simulation and a table look-up was used to reference them. For each simulation point, a minimum of 200 errors were counted before calculation of the BER. Results were generated using a code pool of 24 codes and a channel with a 10dB single tone jammer transmitting at a frequency of 7 cycles per data bit or a normalized frequency of $7\pi/32$. Figure 4.5 shows the simulation results plotted along with the results calculated analytically for a jammer at that frequency. The close agreement between the two results helps verify the analytical method of calculating the BER.

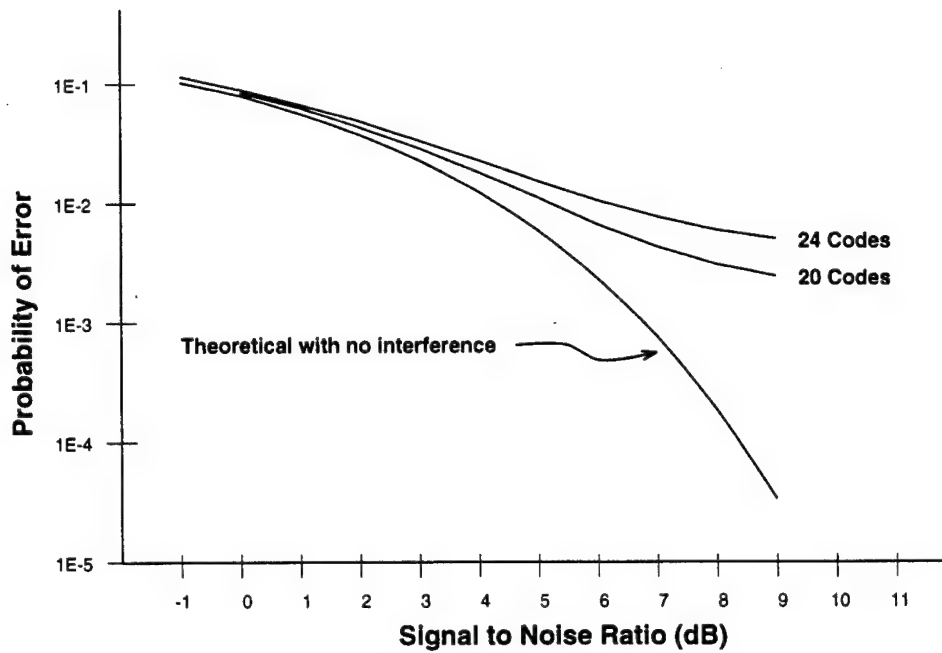


Figure 4.4: Results Using a Reduced Code Pool, JSR=15dB

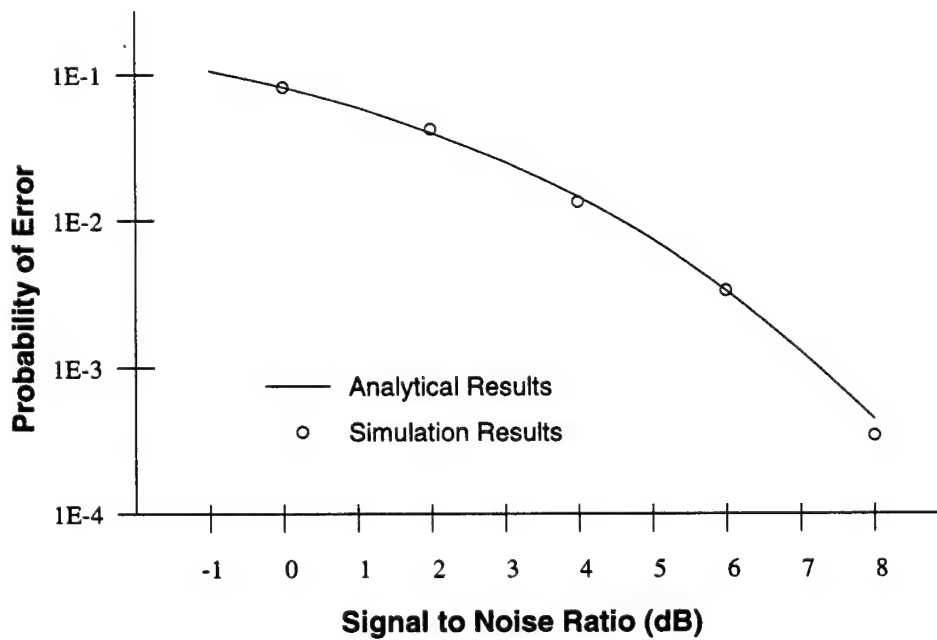


Figure 4.5: Results for a Single Tone Jammer, $\omega=0.687$, JSR=10dB

4.2 Multiuser Channel

4.2.1 Analysis

Conditional BER For the Multiuser Channel

Similar to the analysis developed above for the stationary interference channel, the BER for the multiuser channel can be calculated by first generating a conditional BER expression and then removing the conditioning through either an integration or, in the case of the multiuser channel, a summation. To calculate the conditional BER, a test statistic from the correlator output will again be utilized.

Consider a set of codes generated from a PR-QMF subband tree. If the full binary tree is being used then each of the codes will have identical length and the number of codes generated, N , will be equal to the number of subbands

$$N = 2^L \quad (4.9)$$

where L is the depth of the tree. Assume that the codes are to be used in a channel in which M users are transmitting at any one time and each user is assigned only one of the N codes which is used such that the entire code modulates a single data bit at a time. After correlation in the receiver, the decision variable presented to the threshold device can be represented by

$$r = s_i + \rho_{i,1,\delta_1} + \rho_{i,2,\delta_2} + \cdots + \rho_{i,M-1,\delta_{M-1}} + \eta \quad (4.10)$$

where s_i is the signal of interest, ρ_{i,m,δ_m} is the correlation between the spreading codes of user m and the signal of interest, and η is the channel noise with variance σ_η^2 . The third index, δ_m , in the cross correlation terms signifies that the cross correlation is dependent upon the delay time of interfering signal. Since the receiver is assumed to be synchronized on the signal of interest, the delay time for s_i is always zero. As in Section 4.1.1, the conditional BER is calculated as

$$\begin{aligned} P_{e|i,\chi,\delta_1,\dots,\delta_{M-1}} &= Q\left(\frac{\mu_{r|i,\chi,\delta_1,\dots,\delta_{M-1}}}{\sigma_{r|i,\chi,\delta_1,\dots,\delta_{M-1}}}\right) \\ &= Q\left(\frac{s_i + \rho_{i,1,\delta_1} + \cdots + \rho_{i,M-1,\delta_{M-1}}}{\sigma_\eta}\right) \end{aligned} \quad (4.11)$$

where the numerator and denominator of the Q -function were calculated using methods similar to Equations 4.2 and 4.3. The conditioning upon χ in the left hand side of Equation 4.12 represents the particular set of M codes which are using the channel out of a total number of N available codes.

Calculating the Unconditional BER

The expression given in Equation 4.12 can now be used to calculate the unconditional BER by summing over all possibilities, each weighted by the appropriate probabilities, so that

$$P_e = \sum_{i=1}^N \sum_{\chi} \sum_{\delta_1} \sum_{\delta_2} \cdots \sum_{\delta_{M-1}} p_i p_{\chi} p_{\delta_1|\chi} p_{\delta_2|\chi} \cdots p_{\delta_{M-1}|\chi} P_{e|i,\chi,\delta_1,\dots,\delta_{M-1}} \quad (4.12)$$

where $p_{\delta_m|\chi}$ is the probability that code m of the set of codes contained in χ has a delay of δ_m . The summation over χ indicates that all subsets of M codes out of N possibilities must be considered. Finally, the summation over i indicates that calculations over each of the N codes must be performed.

The first set of summations considered are the innermost summations which are dependent upon the relative delays associated with a particular code in χ and the code used by the signal of interest. Since summing over all delay possibilities is intensive, a histogram can be used to represent the distribution of cross correlation values between codes i and m as shown in Figure 4.6. In the histogram, a particular cross correlation

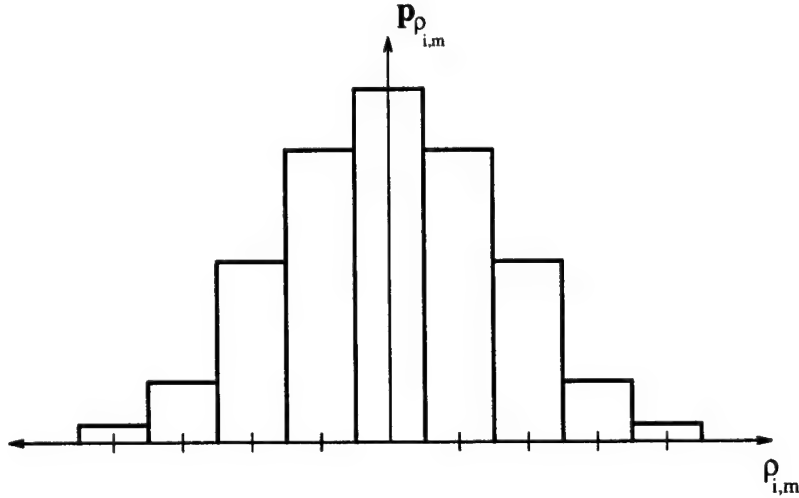


Figure 4.6: Sample Histogram of Cross Correlation Values

value between code i and code m is represented by $\rho_{i,m}$. The probability of this value occurring is $p_{\rho_{i,m}}$. By summing over all of these appropriately weighted relative delays, an expression for the BER conditioned upon s_i and χ can be formulated as

$$P_{e|i,\chi} = \sum_{\rho_{i,1}} \sum_{\rho_{i,2}} \cdots \sum_{\rho_{i,M-1}} p_{\rho_{i,1}} p_{\rho_{i,2}} \cdots p_{\rho_{i,M-1}} P_{e|i,\chi,\rho_{i,1},\dots,\rho_{i,M-1}} \quad (4.13)$$

where the summations over the histogram bin values are performed for every code contained in χ .

An alternative and more efficient method is to treat each of the cross correlations between code i and code m as a random variable whose distribution is approximated by the histogram discussed above. Since from Equation 4.10 each of these random variables is added in the channel, their sum can be represented by a single random variable whose distribution is the convolution of each of the individual distributions. Once again, a histogram can be used to approximate this distribution. Let the bin centers of this histogram be denoted by $\rho_{i,\chi}$ since the histogram is constructed using every code in χ . The probability of each of these bin centers can be represented by $p_{\rho_{i,\chi}}$. Equation 4.13 can now be formulated as

$$P_{e|i,\chi} = \sum_{\rho_{i,\chi}} p_{\rho_{i,\chi}} P_{e|i,\chi,\rho_{i,\chi}} \quad (4.14)$$

where

$$P_{e|i,\chi,\rho_{i,\chi}} = Q\left(\frac{s_i + \rho_{i,\chi}}{\sigma_\eta}\right) \quad (4.15)$$

Since the above equation involves only one summation, the number of calculations do not increase exponentially as M increases.

The next conditioning to consider is the conditioning based on the set of codes contained in χ . If there is a total of N codes available and M users are in the channel (including user s_i), then there are

$$C_\chi = \frac{(N-1)!}{(M-1)!(N-M)!} \quad (4.16)$$

possible code combinations. If all of these combinations are equally likely then probability of any particular set of codes being used by the interfering users is

$$p_\chi = \frac{1}{C_\chi}. \quad (4.17)$$

Finally, if there is an equal possibility that any one code will be used for the signal of interest then

$$p_i = \frac{1}{N}. \quad (4.18)$$

By combining Equations 4.12, 4.14, 4.17, and 4.18 the final expression for the unconditional BER for the multiuser channel can be written as

$$P_e = \frac{1}{NC_\chi} \sum_{i=1}^N \sum_{\chi} P_{e|i,\chi}. \quad (4.19)$$

As with the stationary interference analysis model of Section 4.1.1, the result given in Equation 4.19 can be modified and used to calculate other results of interest about a multiuser system.

Calculation of Other Multiuser Results

As stated in Section 1.2 the goal of a multiuser system is to maximize the number of users while maintaining acceptable performance, which in this case, is measured by the BER. It is therefore desirable to calculate the BER as a function of the number of users such that some measure of the capacity of the channel is attained. In this case, capacity refers to the number of users which can share the same time frequency space using a CDMA system. To calculate the capacity, the signal to thermal noise ratio in Equation 4.15 is fixed and the BER is calculated for different values of M .

A second modification which can be incorporated into Equation 4.19 is to include the effects of imperfect power control. This is also known as the *near-far problem* since it occurs when one transmitter is in close proximity to the receiver while the other is far away[23]. If both are using equal power, the signal from the near transmitter will arrive at the receiver with a much higher signal level than the far transmitter.

In an FDMA or TDMA system, the users attain a high degree of orthogonality due to the guard zones which are placed between the user transmissions and, therefore, these two multiuser systems are unaffected by imperfect power control. In a CDMA system, however, orthogonality is achieved by the low cross correlations between the codes. Since these cross correlations can never be zero, poor power control can seriously degrade system performance [5].

In a cellular system, perfect power control, can theoretically be achieved by the use of a pilot signal of known power transmitted by the base station [12]. Each of the mobile units receiving the pilot can determine the power level of the pilot and then inversely adjust their transmitted power accordingly. In a practical situation, however, field trials have shown that this method can achieve only a certain amount of accuracy [49].

In the above model for determining multiuser performance it was assumed that the signal received from each user had identical power. To modify this for the case of imperfect power control discussed above, the cross correlation values in Equation 4.10 must be changed to reflect the different received signal levels. For example, if user m has a received signal level which is larger than the level of the signal of interest, the cross correlation value, ρ_{i,m,δ_m} , would increase. The conditional BER in Equation 4.12 must also reflect this. Therefore, when calculating the unconditional BER, additional integrals must be performed to account for the probabilities of each interfering user having a power different from the normalized power used in Equation 4.10.

Let $P_{e|i,\chi,g_1,\dots,g_{M-1}}$ be the BER conditioned upon a given user, i , a given set of interfering codes, χ , and a set of gains, g_1, \dots, g_{M-1} , which represent the imperfections of the power control loop described above. The cross correlations in Equation 4.10 are each multiplied by these gains and $P_{e|i,\chi,g_1,\dots,g_{M-1}}$ can be calculated in the same manner

as Equation 4.14. The next step is to remove the conditioning on the gain factors by integrating so that

$$P_{e|i,X} = \int_{G_1} \int_{G_2} \cdots \int_{G_{M-1}} p_{g_1} p_{g_2} \cdots p_{g_{M-1}} P_{e|i,X,g_1,\dots,g_{M-1}} dg_1 dg_2 \cdots dg_{M-1} \quad (4.20)$$

where G_m is the range of the possible gains and p_{g_m} is the probability distribution of the gains. The remainder of the BER calculation remains unchanged.

The final modification to the analysis of Section 4.2.1 which will be discussed is the case of coarse synchronization discussed in Section 3.3. In this case, the modification is straightforward and consists of only conditioning on and summing over the delay times of interest. Alternatively, for the values of δ_m which are known not to occur, the value of $p_{\delta_2|X}$ in Equation 4.12 can simply be set to zero. If the histogram approach of Equation 4.13 or 4.14 is used, then the generation of the histograms should not include data points generated by time shifts which cannot occur.

4.2.2 Multiuser/Multipath Interference Results

In this section, a number of different subband trees are designed in order to demonstrate the results of developing and using the PR-QMF based codes in a communications system. In addition to the BER results derived from the analysis given above, a number of other aspects, such as the frequency response of the codes, will be examined. Also, since the objective functions are based upon the cross correlation between the codes, these will also be examined to determine how well the objectives are met. Comparisons will be made to the Gold codes since these are the most commonly used set of codes in currently fielded CDMA systems [54].

It should be noted that the title of this section includes both multiuser and multipath interference and that results from using both objectives are examined. Subband trees are designed using both the multiuser and multipath criteria by utilizing the composite interference objective function given in Section 3.5. This is done since, as will be shown, the two objectives and the corresponding results are both closely linked to the concepts about multiuser communications discussed in Section 1.2.

In general, the multivariable optimization problem considered in this section is to minimize

$$F_C = \alpha F_{MU} + \beta F_{MP} \quad (4.21)$$

subject to

$$\sum_{k=0}^{N-1} h_k h_{k+2n} = \delta_n \quad \forall n \geq 0 \quad (4.22)$$

where h_k are the filter coefficients being designed. The function F_{MP} is the multipath objective function given by Equation 3.46. The multiuser objective function, F_{MU} , is either the objective function for which all delays, δ_m , are possible (Section 3.2) or the situation in which partial synchronization between the users is achieved (Section 3.3). Due to processing limitations, the simplified approximations to the objectives will be used in each case.

As mentioned in Section 3.5, α and β are weighting factors which determine the importance of the multiuser and multipath objectives in the overall minimization. Since it is the resulting arguments of the minimization which are of interest, the actual values of α and β are not important. Instead, it is the ratio of the two weighting factors which will influence the optimization result. Therefore, for each of the designs in this section, the multipath weighting factor in Equation 4.21 is always taken to be

$$\beta = 1 - \alpha \quad (4.23)$$

and only α needs to be specified. As always, the filter banks are designed using the concept of progressive optimality.

Two Special Cases

There are two special cases of the subband filter bank design problem which deserve special attention. In the first case, the weighting is chosen as $\alpha = 1$ and the multipath objective criteria are completely ignored as the subband tree is constructed. Under these conditions, a three stage full binary subband tree was designed which contained eight tap filters at each stage. This design process resulted in a set of eight spreading codes each of length 32. The users in the channel were assumed to be operating asynchronously so the multiuser objective function of Section 3.2 was used.

After completion of the tree, the codes were constructed and their frequency response was calculated. The normalized frequency response of the eight codes are shown in Figure 4.7. Notice that each of the codes is narrowband and that the set of responses resembles the channels in an FDMA system. This result is due the construction of the objective function which contained only a multiuser objective. The goal of the multiuser optimization was to construct codes which are completely orthogonal. As discussed in Section 1.2, this orthogonality can be achieved in two ways 1) time domain orthogonality (TDMA) or 2) frequency domain orthogonality (FDMA). During the construction of the objective function, however, any possible orthogonality in the time domain was eliminated by considering all relative delays between the two codes under construction. Therefore, any orthogonality achieved by the optimization must occur in the frequency domain. This factor resulted in the generation of narrowband codes and, therefore, an FDMA-like system. If this approach is taken to the limiting case of a direct m -

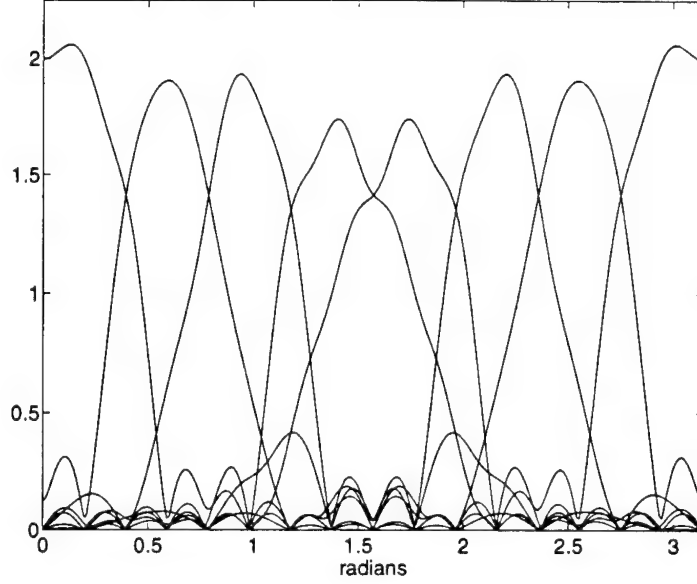


Figure 4.7: Frequency Response of Multiuser Codes

band design with infinite length filters, a pure FDMA unitary transformation matrix, as discussed in Section 1.5, would result.

The second interesting case to consider is the pure multipath objective or when $\alpha = 0$. In this case, cross correlations between the codes are not considered in the objective function and the first stage optimization becomes

$$F_{MP} = \min \left\{ \sum_{\delta=1}^{N-1} [(\xi_{\delta})^2 + (\xi_{\delta}^-)^2] \right\} \quad (4.24)$$

where ξ_{δ} and ξ_{δ}^- are the autocorrelation functions developed in Section 2.6.3. Unlike the optimizations considered up to this point, this constrained minimization has an exact solution where the objective function achieves its minimum value of $F_{MP} = 0$ when the filter coefficients are

$$\mathbf{h}_1 = [1 \ 0 \ 0 \ \dots \ 0]^T \quad (4.25)$$

and

$$\mathbf{h}_2 = [0 \ 0 \ \dots \ 0 \ 1]^T \quad (4.26)$$

where \mathbf{h}_1 and \mathbf{h}_2 are vectors containing the coefficients of the QMF pair at the first split. Furthermore, this solution exactly satisfies the perfect reconstruction constraint of

Equation 4.22. The optimal solution, therefore, is to modulate the data by an impulse function thereby attaining the desired result of a wideband transmitted signal. If the impulses are ideal, then each delayed version of the signal appearing at the receiver will be completely uncorrelated with the received signal and the effect multipath interference will be negated.

If this design were continued such that a full binary tree is constructed, the resulting spreading codes would be a series of impulses, each occurring at a different time interval. This, however, is a TDMA system discussed in Section 1.2. Once again, the ideal case can be attained by directly constructing an m -band tree. Instead of having infinite length filters as the FDMA model, the filter length must equal the number of subbands (or decimation factor) since this is the minimum filter length such that an orthogonal transformation results. The solution again becomes a series of time space impulses and the transformation matrix becomes the identity matrix of pure TDMA discussed in Section 1.5. Although such a system might work well for the multipath channel, it is easy to see that it is virtually useless for the asynchronous multiuser channel where the start time of the user transmissions are completely unregulated.

Cross Correlation Analysis

The objective function for the multiuser channel attempts to drive the cross correlation between each of the codes to zero. As a simple example of how well this objective was met, two sample codes were extracted from the multiuser tree designed in the previous section. The cross correlations between these two codes were calculated for all possible time shifts and are plotted in Figure 4.8a. For comparison purposes, the same calculation and plot was performed on two different 31 chip Gold codes and two different PR-QMF based codes using Daubechies' four tap filter coefficients for an orthonormal wavelet basis [7]. The plots are shown in Figures 4.8b and 4.8c respectively. It is easy to see from the figure that the two optimized codes clearly have a lower cross correlations values than the other two sets and should perform much better in a multiuser environment.

This same calculation was then performed between all different possible pairs of the optimized PR-QMF based codes; that is, the cross correlations were calculated for every combination of two codes and over every possible delay value. A histogram was then generated from the resulting cross correlation values and is plotted in Figure 4.9a. Again, for comparison purposes, a similar plot is provided for length 31 Gold codes and is shown in Figure 4.9b. Since the Gold codes are binary valued sequences, the cross correlations between two codes take on a finite set of values. These discrete values are shown as spikes in the figure as opposed to histogram bins.

There are several things which should be noted here. The most obvious is the variance of the cross correlations for the PR-QMF Based Codes is much smaller than that for the

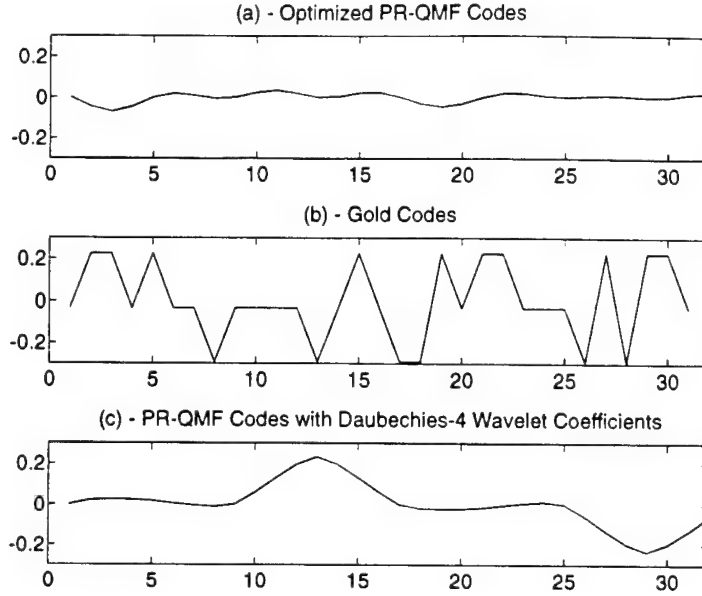


Figure 4.8: Cross Correlation Values of Sample Codes

Gold Codes. In fact a calculation of the sample variance for the two sets of codes shows that the variance of the Gold Codes is between two and three times that of the PR-QMF Based Codes. This is not surprising since the objective function was to minimize the variance of the cross correlations between two spreading codes generated by a QMF pair. It can be seen from the figure, however, that there are several cross correlations which are much larger than desired (i.e. $|\rho| > 0.5$). These are due to the progressively optimal approach and edge effects. For example, the finite length filters cannot produce completely orthogonal codes at the early stages. This non-orthogonality then manifests itself through high cross correlation results during the later stages of the tree. Finally, in Section 1.4 it was stated that there are only three possible cross correlation values for any two Gold codes. This, however, is true only for polarity case one of Section 1.5.1 where the bit polarity of the interference does not change. If the case where one of the data bits changes polarity is considered (Figure 1.6b), then several other cross correlation values will be produced as reflected in the above plot.

BER Analysis

The most important measure of performance is the bit error rate achieved when using the codes in a channel characterized by multiuser interference. Therefore, BER results

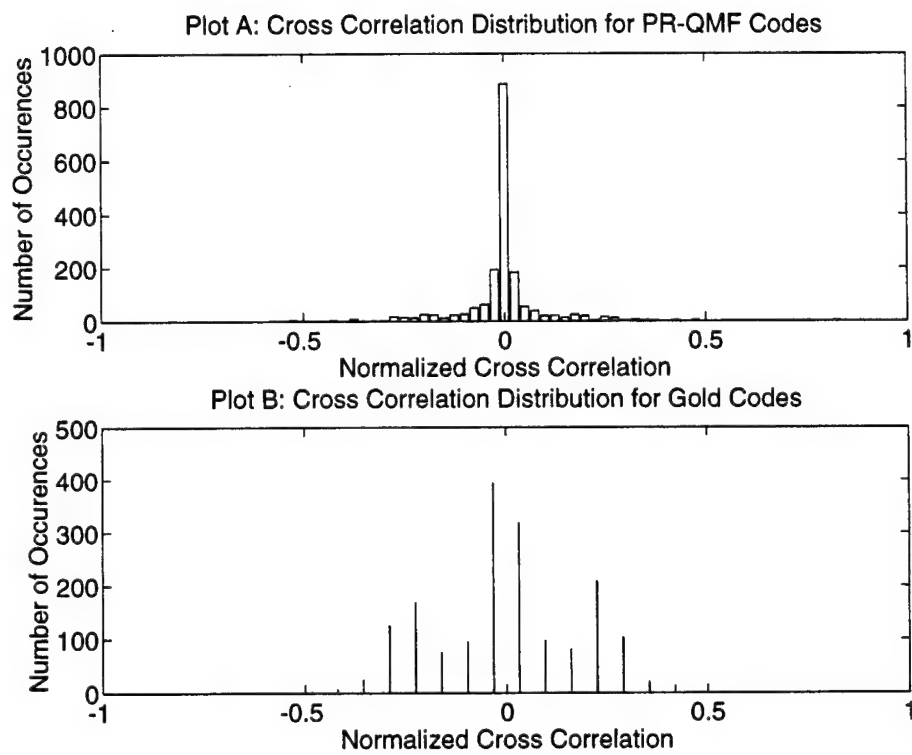


Figure 4.9: Histograms of Cross Correlation Values

were generated using the PR-QMF based codes which were optimized with the multiuser objective. The first BER curve, shown in Figure 4.10, compares the results using the analytical expressions derived in Sections 4.2.1 and 4.2.1 with the results of using the codes in a computer simulation of a multiuser spread spectrum system. The channel was

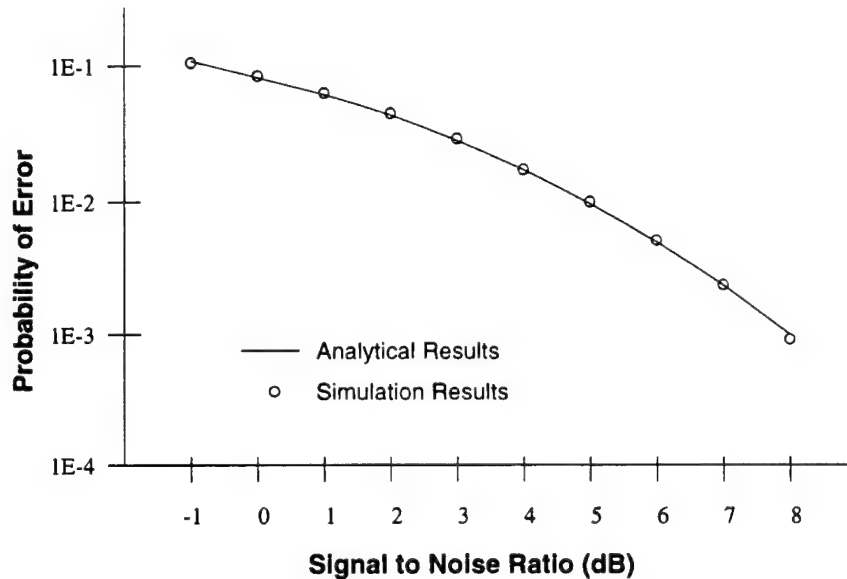


Figure 4.10: Multiuser Computer Simulation Results

assumed to have four users (three interferers) each operating asynchronously with perfect power control. The simulations used several different sets of codes randomly chosen from the eight codes available. The delay times were also randomly chosen and equiprobable. The results of all simulations were averaged to generate the data in the curve. The analytical methods of BER calculation outlined in section 4.2 was then performed using the same subset of codes and delay times. The curves show good agreement between the two different methods which, as with the single tone jammer channel, serve to verify the analytical development.

The unconditional BER was then calculated using the analytical method and the optimized multiuser PR-QMF based codes. Once again, the results were generated for a four user channel with perfect power control. In this case, however, every possible code combination and all possible delay times were taken into account when removing the conditioning. The curve is shown in Figure 4.11. Again, for comparison purposes, identical calculations were performed for 31 chip Gold codes and the results are plotted on the same graph. The lower most curve in the figure is the theoretical curve for BPSK and represents what would be achieved if no multiuser interference was present. It can be seen that the PR-QMF based codes provide about 2 dB better performance than similar

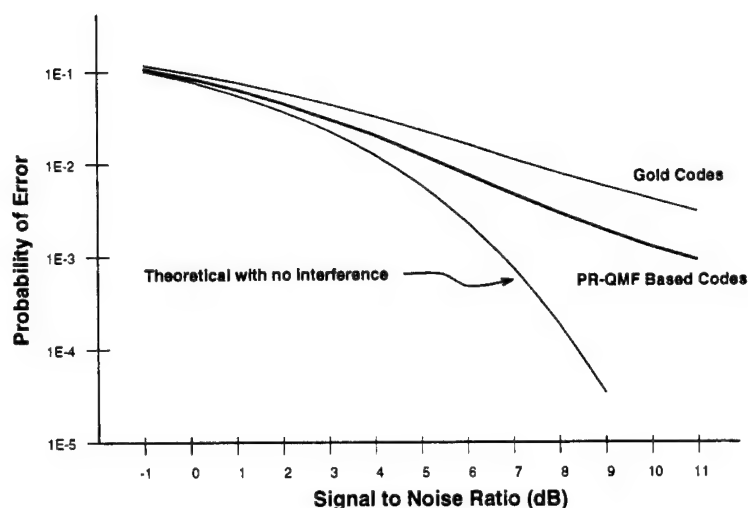


Figure 4.11: Multiuser BER Results

length Gold Codes, however, this improvement is gained at the expense of emulating an FDMA system, thus sacrificing some of the other desirable features of a spread spectrum system.

Spreading Codes for Composite Objective Functions

The two different filter banks designed above and the succeeding analysis demonstrate the two extremes of multiuser communications. It also shows the duality between multipath and multiuser communications and the connection to the duality of the TDMA and FDMA systems discussed in Section 1.2. Each of these two different techniques, TDMA and FDMA, can thus be considered a special case of a CDMA. The PR-QMF based codes using a full binary tree and the objective function of Equation 4.21 can approximate these two special cases by choosing α to be either a zero or a one. By choosing other values of α , the filter banks represent a whole class of codes of varying spread and of different performance characteristics when employed in a multiuser channel.

Several filter banks were thus designed for various values of α and the spreading codes were extracted accordingly. For each case, a three stage full binary tree with eight tap filters was constructed so that length 32 spreading codes were generated. Following the methods of Section 4.2.1, the capacity of the system, in terms of the number of users supported, was then calculated. The results for different code sets, along with that for 31 chip Gold codes, are shown in Figure 4.12. Once again, perfect power control is assumed. The energy per bit to the thermal noise power spectral density is 13dB so that

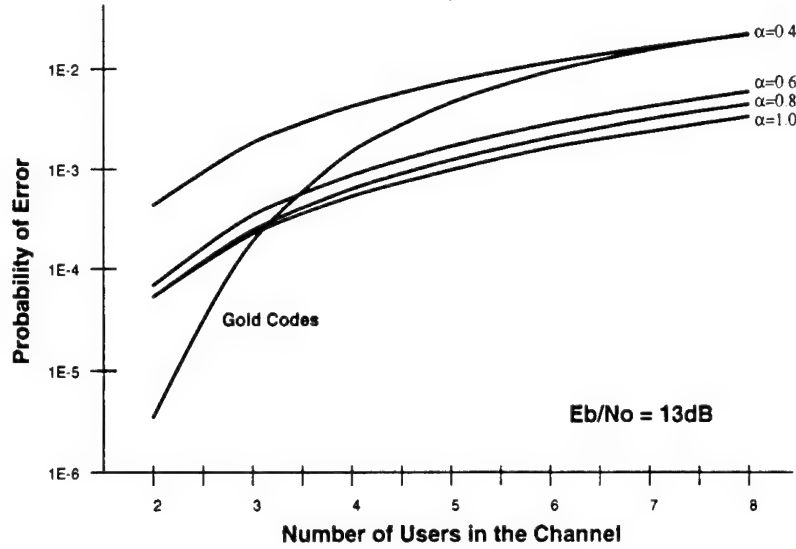


Figure 4.12: Capacity for Various Weighting Factors

the channel with only one user would achieve a BER of $P_e = 1.3 \times 10^{-10}$. This figure is well beyond the target BER for proper vocoder performance of $P_e = 1 \times 10^{-3}$ [12].

As expected, as the multiuser objective is decreased, the multiuser performance of the PR-QMF based codes degrades accordingly. At the target rate of $P_e = 1 \times 10^{-3}$, the Gold codes are capable of supporting at most three users in the channel at one time. The PR-QMF codes based mostly on multiuser interference, however, were able to support more than that. The codes for $\alpha = 6$ and $\alpha = 8$ each could support four users while the codes based only upon multiuser interference could support five users at a time. This shows that even in the somewhat trivial case of short code lengths, the PR-QMF codes show increased capacity.

Notice, that for two or three users, the Gold codes equal or outperform the optimized codes. This is due to the outliers in the PR-QMF cross correlation histogram of Figure 4.9. Since the BER is averaged over all possibilities, these few cross correlation terms significantly degrade the performance. This degradation, however, is not of much concern since the optimized codes were designed for a channel with eight different users. Had only two codes been desired, a single stage tree using 32 tap filters would have been designed and performance with only two users would improve significantly.

Finally, some subjective comparisons can be made about the frequency responses of the different codes. The frequency responses of sample codes from two different filter bank designs are shown in Figure 4.13. Both of the codes were generated by the same subband of the two different subband trees. The effect of decreasing α is clearly seen

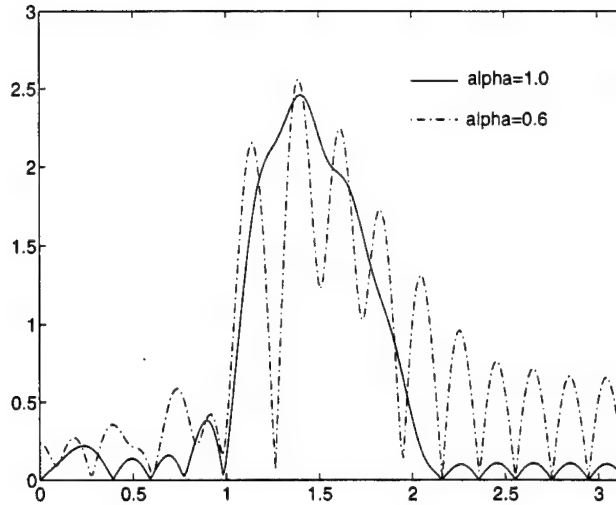


Figure 4.13: Sample Frequency Responses, $\alpha = 1.0$ and $\alpha = 0.6$

since the code generated by the tree with $\alpha = 0.6$ contains much more “out of band” energy than the code designed solely for multiuser interference. In figure 4.14 a similar comparison is made, however, the second code is taken from a subband tree designed for primarily multipath interference. Notice that the code is now very wideband and that any frequency localization of the subband is completely lost. As shown in Figure 4.12, however, the performance of these codes in a multiuser channel is decidedly worse than the other PR-QMF based codes, as well as, the performance of the Gold codes.

Effects of Inaccurate Power Control

In each of the above results, it was assumed that the users were operating with perfect power control so that the received signal level at the base station would be identical for each code. As mentioned in Section 4.2.1 perfect power control is difficult to achieve in a practical situation and power variations can degrade the performance of a CDMA system. As shown in Figure 4.9, the cross correlations of the PR-QMF based codes are generally smaller in magnitude than those for the Gold codes. It is therefore suspected that, although some impairment would exist, the effect will not be as great as for the Gold codes.

To verify this, capacity results were generated for a system where the users display inaccurate power control. The gain factors, g_m , and their corresponding probabilities,

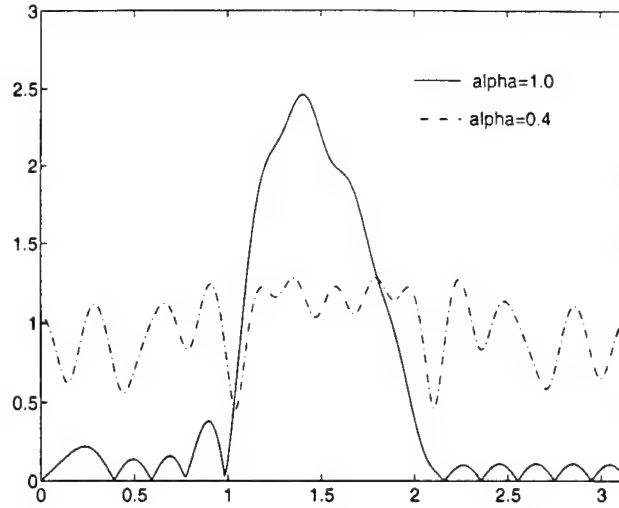


Figure 4.14: Sample Frequency Responses, $\alpha = 1.0$ and $\alpha = 0.4$

p_{gm} , were taken from experimental results of implementing, in a city cellular environment, a power control system similar to that described above [49]. Three different gain factor were used, -2dB, 0dB, and +2dB, with their respective probabilities of occurrence being 0.112, 0.702, and 0.186. Each code set was weighted by the gain factors prior to calculating the BER. Every possible combination was considered. A weighted BER, using the appropriate probabilities, was then calculated. The results for the multiuser based codes are shown in Figure 4.15. As expected, the lack of perfect power control shows a slight degradation in the PR-QMF based system performance.

Codes with Partial Synchronization

The final set of subband trees which were designed are for a system where, through the use of a timing signal or beacon, some synchronization between the users is attained. Unlike the subband trees designed earlier, the trees designed in this section consist of a full binary tree with five stages and eight tap filters at each stage. This design resulted in 32 spreading codes each of length 128. The larger tree was chosen for two reasons. The first reason was to verify that the progressively optimality and PR-QMF method of generating codes could successfully be extended beyond the academic cases to codes of practical length. Current effective spreading margins of proposed spread spectrum systems (both cellular and otherwise) are on the order of 128 chips per data bit and above [25, 23].

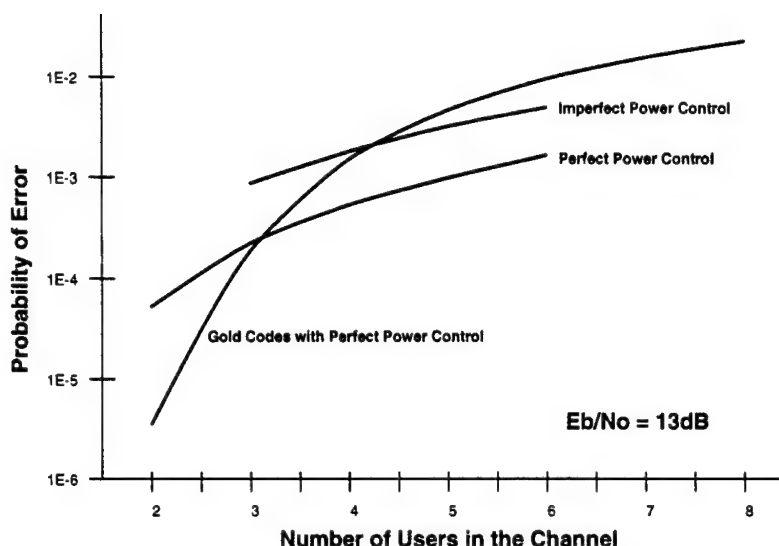


Figure 4.15: Capacity Inaccurate Power Control

A second reason for the longer codes is so a practical system with partial synchronization can be modeled. Assume that maximum distance between the transmitters and the base station receiver is three kilometers. If a timing beacon is transmitted from the base station, the maximum round trip delay time is six kilometers divided by the speed of light or 20 microseconds. If the vocoder operates at 9.6 kilobits per second and each data bit is spread by a code of length 128, then the chip duration is 813.8 nanoseconds and the delay times can vary over only the first 25 values of the spreading code. For example, suppose that the user transmitting the signal of interest is co-located with the base station and the interfering user is located three kilometers away. The differential delay between the start of each users bit interval will be twenty microseconds or 25 chips. Due to physical symmetry (i.e. the two mobile units swap positions), there is uncertainty over the last 25 chips as well. For simplicity, assume every possible delay in the ± 25 chip range is equally likely.

Under these conditions, a five stage tree was constructed as described in Section 3.3 using a weighting factor of $\alpha = 0.7$. After extracting the codes from the tree, the cross correlations between all of the codes were calculated. A histogram of these cross correlations are shown in Figure 4.16. The lower histogram is the same calculation for 127 chip Gold codes. Once again, the histogram for the PR-QMF based codes shows a much narrower spread than that of the Gold codes. Note that only the cross correlations possible in the above scenario were calculated and plotted. Cross correlations not included in the minimization were ignored. A cursory look at these "unimportant" values showed many which were well above the values shown in the figure ($|\rho_{\delta_m}| > .75$).

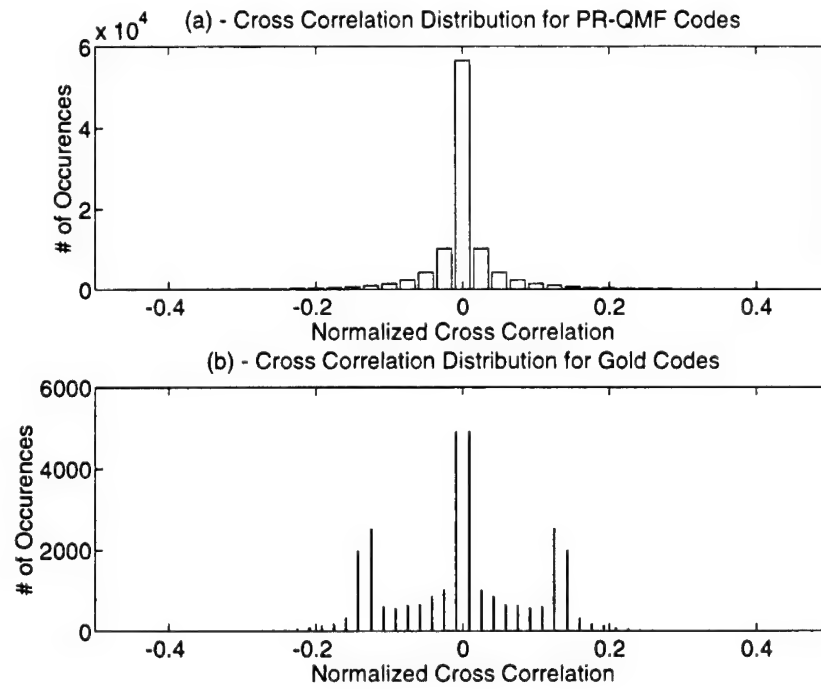


Figure 4.16: Cross Correlation Results for Codes With Partial Synchronization

After extracting the codes from the tree, the capacity was calculated and is plotted in Figure 4.17. The same calculations were again performed for 127 chip Gold codes.

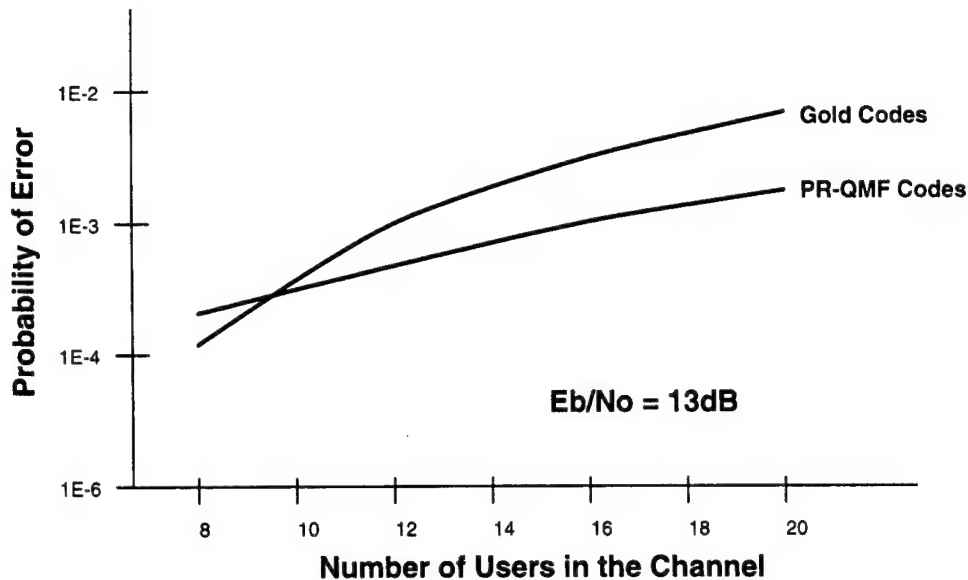


Figure 4.17: Capacity Results for Codes With Partial Synchronization

The improvement attained by the PR-QMF based codes demonstrates both the validity of the partial synchronization objective function, as well as, the ability of the PR-QMF based technique to extend to longer length spreading codes.

One final interesting result is the frequency response of two codes which were optimized for partial synchronization. The response of two codes generated by two adjacent subbands (one from each decimator of a QMF pair) are plotted in Figure 4.18. Notice that the frequency response of the two codes almost completely overlap. The cross correlations of interest, however, are still small in magnitude. These cross correlations can be seen in Figure 4.19. The cross correlation values are plotted versus the delay between the two codes. Although some of these values are considerably large, the values over the range of interest, the first 25 and the last 25, were successfully minimized. This demonstrates the ability of two or more codes to attain low cross correlation properties using both time domain and frequency orthogonality.

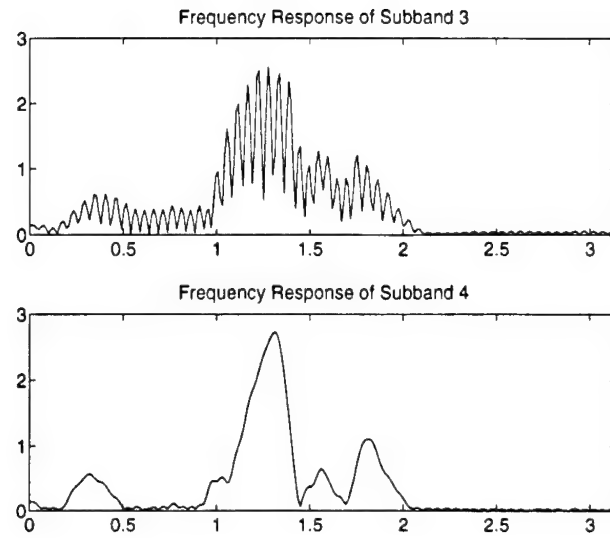


Figure 4.18: Frequency Response of Codes With Partial Synchronization

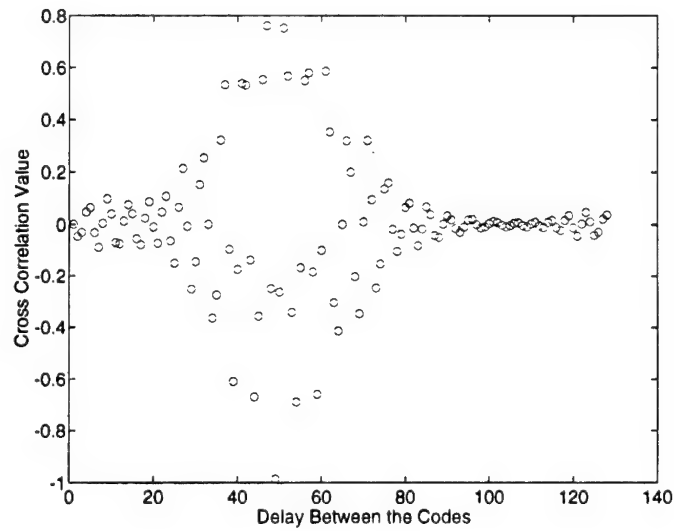


Figure 4.19: Cross Correlations of Two Codes Designed For Partial Synchronization

Chapter 5

Conclusions

5.1 Summary of Work

An original class of spreading codes based upon multirate subband filter banks has been introduced and developed in this thesis. Unlike maximal length sequences, this new set of codes is not limited to having binary valued chips. Instead, the elements of the sequences are determined by an optimization process which emphasizes certain desirable code properties.

It was shown that a set of spreading codes could be modeled as a linear transformation on a unit vector and that the design of a particular set of spreading codes is directly related to the design of that transformation. It also was shown that some other areas of spreading code design research [31, 11] are encompassed by this problem and that subsequent transformations of the signal set do not replace the problem of properly designing the transformation matrix. The design of this transformation matrix, therefore, is actually the more general problem since the other methods can be represented as a factorization of this matrix.

It was next shown that these linear transformations can be modeled using a multirate subband filter bank and that a linear transformation design can be replaced by the corresponding filter bank design. Although the use of multirate filter bank to perform a linear transformation is a common technique, using the resulting transformation to form a set of spreading codes is a new concept.

Other areas of research are actively involved in using a wavelet basis to construct communications waveforms [26]. The work performed in this thesis extends and generalizes this concept in several ways. Many of the conditions and restrictions imposed by a wavelet basis were removed in the design of the filters. Conditions such as regularity

were not included in the design process. More importantly, progressive optimality was employed in the filter bank design instead of the simpler method of reiterating the same filter throughout the subband tree. Finally, the more general and interesting cases of the asynchronous channel and the partially synchronous channel were explored.

The use of a multivariable optimization problem to design subband trees was extended to the communications problem in this thesis. A general methodology was given for the design process and objective functions were developed for several channels of interest to the mobile communications problem. It was shown that the method could extend beyond the academic cases to spreading codes of practical length. Other work has already utilized these concepts for a different communication channel [32].

In addition to the design methodology, an analytical method of BER analysis was developed in this thesis. For the stationary interference channel, the interference was modeled as single-tone interference. First, a conditional BER was calculated for a specific frequency and phase of the tone. This was then removed through an integration over all phases and over the frequencies of interest. For the multiuser channel, a similar method was used. First a conditional BER was calculated and then, using one of several methods to decrease the computational load, the conditioning was removed. An expression was given so the capacity and other results of interest could be attained. The validity of the analytical BER analysis was verified by comparison with computer simulation of the systems.

5.2 Conclusions

The design of several example filter banks show some interesting and important results. For a channel characterized by stationary interference, the PR-QMF based codes performed significantly better than maximal length sequences. This is due to channel information being incorporated into the design of the codes.

When designing for an asynchronous multiuser system, the optimal design becomes an FDMA like system with the ideal extension to an m -band structure becoming pure FDMA. The dual problem is when a system is designed for purely multipath interference. In this case the full binary tree resembles a TDMA system and the ideal m -band structure becomes pure TDMA. Both of these systems are approximated by the full binary subband tree structures examined in this thesis. Furthermore, by choosing various weighting factors, an entire class of CDMA codes can be developed from the subband tree structure. It was shown that when the multiuser objective was heavily weighted the codes outperform (in terms of BER and capacity) the Gold codes.

The last filter bank studied was for a system where the users acquire partial synchro-

nization. In this situation, some orthogonality can be attained in the time domain. A look at the frequency response of the codes shows that two codes can spectrally overlap, yet still retain the required orthogonality over the time shifts of interest. Additionally, the longer length codes showed that the PR-QMF based method, coupled with progressive optimality, can be successfully extended to codes of practical length.

5.3 Future Directions

The work accomplished in this thesis has laid the groundwork for the design of communication signals using the multirate filter bank approach. This is more flexible than previous heuristic methods and is more general than other active areas of research which limit the underlying basis used to construct the codes. Additionally, unlike other design methods, the more interesting and complex problem of the asynchronous communications channel is addressed.

Continuation of this work can extend in several areas. Objective functions can be developed for other types of interference sources such as pulsed interference or non-linear interference [32]. Additionally, more work can be done to further refine the objective function for the multipath interference so that the objective can represent more specific multipath channels. Finally, using techniques suggested in this thesis, filter design for an OFDM or multitone channel can be accomplished. It may be possible to match the channel more accurately with a fewer number of carriers if the filters are designed specifically for the channel characteristics.

Further study is also needed to determine some of the practical aspects of implementing the waveforms. Some amount of quantization of the code values will be required and the effect of this quantization must be studied. Additionally, a linear mapping to a carrier was assumed in this thesis. Further work can be done to provide an extension to a non-linear mapping such as phase modulation.

Another obvious extension of this work is to consider objectives and constraints for a direct m -band design. If the limiting cases are included, these designs should provide exact reproductions of the TDMA and FDMA systems. Possibilities include the use of both real and complex modulated filter bank structures [44].

The design for users with partial synchronization also shows a great deal of promise. As computing power increases, many of the compromises which were necessarily made in the objective functions can be removed. By combining this with a possible direct m -band design considerable gains may be attainable by the resulting spreading codes. Additionally, as processing capability increases, longer codes may be synthesized which will allow for new applications.

Chapter 6

Bibliography

Bibliography

- [1] A. Akansu and R. Haddad. *Multiresolution Signal Decomposition*. Academic Press, Inc., 1992.
- [2] M. Bellanger and J. Daguet. TDM-FDM transmultiplexer: Digital polyphase and FFT. *IEEE Transactions on Communications*, 22(9), September 1974.
- [3] H. Caglar, Y.Liu, and A. Akansu. Optimal PR-QMF design for subband image coding. *Journal of Visual Communication and Image Representation*, 4(3):242–253, September 1993.
- [4] J. Cardall and R. Cnossen. Civil application of differential GPS. In *The Proceedings of the International Telemetry Conference*, 1981.
- [5] D. Cox. Wireless network access for personal communications. *IEEE Communications Magazine*, 30(12), December 1992.
- [6] R. Crochiere and L. Rabiner. *Multirate Digital Signal Processing*. Prentice Hall, Inc., 1983.
- [7] I. Daubechies. Orthonormal basis of compactly supported wavelets. *Communications on Pure and Applied Mathematics*, 41:909–996, November 1988.
- [8] A. Devaney and B. Hisconmez. Wavelet signal processing for radar target identification. In H. Szu, editor, *SPIE Proceedings - Wavelet Applications*, pages 389–399, 1994.
- [9] R. Dixon. *Spread Spectrum Systems With Commercial Applications*. John Wiley and Sons, Inc., 1994.
- [10] W. Feller. *An Introduction to Probability Thoery and Its Applications: Volume II*. John Wiley and Sons, Inc., 1966.
- [11] G. Fettweis, A. Bahai, and K. Anvari. On multi-carrier code division multiple access modem design. In *Proceeding of the IEEE 44th VTS Conference*, pages 914–917, May 1994.

- [12] K. Gilhousen, I. Jacobs, R. Padovani, A. Viterbi, L. Weaver, and C. Wheatley. On the capacity of a cellular CDMA system. *IEEE Transactions on Vehicular Technology*, pages 303–312, May 1991.
- [13] R. Gold. Optimal binary sequences for spread spectrum multiplexing. *IEEE Transactions on Information Theory*, pages 619–621, October 1967.
- [14] A. Grace. *Optimization Toolbox Users Guide*. The MathWorks, Inc., 1990.
- [15] T. Ha. *Digital Satellite Communications*. McGraw-Hill, Inc., 1990.
- [16] S. Haykin. *Digital Communications*. John Wiley and Sons, Inc., 1988.
- [17] J. Hershey, G. Saulnier, A. Hassan, and S. Hladik. Geometric harmonic modulation: A new spread spectrum genre. In *The Proceedings of the IEEE International Conference on Communications*, pages 1345–1349, 1995.
- [18] K. Hetling, G. Saulnier, and P. Das. Optimized filter design for PR-QMF based spread spectrum communications. In *The Proceedings of the IEEE International Conference on Communications*, pages 1350–1354, 1995.
- [19] K. Hetling, G. Saulnier, and P. Das. Optimized PR-QMF based codes for multiuser communications. In H. Szu, editor, *SPIE Proceedings - Wavelet Applications*, pages 248–259, 1995.
- [20] K. Hetling, G. Saulnier, and P. Das. PR-QMF based codes for multipath/multiuser communications. In *The Proceedings of the IEEE Global Telecommunications Conference*, 1995.
- [21] L. Hinderks. Digital Audio Broadcasting: Current status and future directions. In *The Proceedings of the NJIT Symposium on Applications of Subbands and Wavelets*, 1994.
- [22] N. Jayant and P. Noll. *Digital Coding of Waveforms*. Prentice-Hall, Inc., 1984.
- [23] R. Kohno, R. Meidan, and L. Milstein. Spread spectrum access methods for wireless communications. *IEEE Communications Magazine*, 33(1):58–67, January 1995.
- [24] J. Kovacevic and I. Daubechies. Scanning the special issue on wavelets. *Proceedings of the IEEE*, 84(4):507–509, April 1996.
- [25] V. Li and X. Qiu. Personal communication systems. *Proceedings of the IEEE*, 83(9), September 1995.
- [26] A. Lindsey and M Medley. Wavelets and communications - an overview. In H. Szu, editor, *SPIE Proceedings - Wavelet Applications*, pages 466–475, 1996.

- [27] S. Mallat. A theory for multiresolution signal decomposition: The wavelet representation. *IEEE Transactions on Pattern Analysis and Machine Intelligence*, 11(7), July 1989.
- [28] M. Medley, G. Saulnier, and P. Das. The application of wavelet-domain adaptive filtering to spread spectrum communications. In H. Szu, editor, *SPIE Proceedings - Wavelet Applications*, pages 233-247, 1995.
- [29] L. Milstein and P. Das. An analysis of a real-time transform domain filtering digital communication system - Part 1: Narrowband interference rejection. *IEEE Transactions on Communications*, 28(6), June 1980.
- [30] R. Orr, C. Pike, and M. Bates. Multiple access communications using wavelet technology. In H. Szu, editor, *SPIE Proceedings - Wavelet Applications*, pages 283-294, 1995.
- [31] R. Orr, C. Pike, and M. Lyall. Wavelet transform domain communication systems. In H. Szu, editor, *SPIE Proceedings - Wavelet Applications*, pages 271-281, 1995.
- [32] S. Ozen. A new spreading code design for multiple access satellite communication systems. Master's thesis, Rensselaer Polytechnic Institute, 1996.
- [33] R. Pickholtz, D. Schilling, and L. Milstein. Theory of spread spectrum communications. *IEEE Transactions on Communications*, 30(5), May 1982.
- [34] J. Proakis. *Digital Communications*. McGraw-Hill, Inc., 1989.
- [35] S. Sandberg, M. Tzannes, P. Heller, R. Orr, C. Pike, and M. Bates. A family of wavelet-related sequences as a basis for an LPI/D communications system prototype. In *Proceedings of the IEEE Military Communications Conference*, pages 537-542, October 1993.
- [36] D. Schilling, R. Pickholtz, and L. Milstein. Spread spectrum goes commercial. *IEEE Spectrum*, August 1990.
- [37] R. Scholtz. The origins of spread spectrum communications. *IEEE Transactions on Communications*, 30(5):822-853, May 1982.
- [38] M. Smith and T. Barnwell. A procedure for designing exact reconstruction filter banks for tree-structured subband coders. In *The Proceedings of the IEEE ICASSP*, 1984.
- [39] M. Smith and T. Barnwell. A new filter bank theory for time-frequency representation. *IEEE Transactions on ASSP*, 35(3), March 1987.
- [40] H. Stark and J. Woods. *Probability, Random Processes, and Estimation Theory for Engineers*. Prentice-Hall, Inc, 1986.

- [41] R. Steele and M. Nofal. Teletraffic performance of microcellular personal communication networks. *Proceedings of the Institute of Electrical Engineering*, 139(8), August 1992.
- [42] M. Tazebay and A. Akansu. Progressive optimality in hierarchical filter banks. In *The Proceedings of IEEE International Conference on Image Processing*, pages 825–829, 1994.
- [43] M. Tazebay and A. Akansu. Progressive optimization of time-frequency localization in subband trees. In *The Proceedings of the IEEE International Symposium on Time-Frequency and Time-Scale Analysis*, pages 128–131, 1994.
- [44] P. Vaidyanathan. Quadrature mirror filter banks, M-band extensions and perfect reconstruction techniques. *Signal Processing Magazine*, 4:4–20, July 1987.
- [45] P. Vaidyanathan. *Multirate Systems and Filter Banks*. Prentice-Hall, Inc, 1993.
- [46] M. Vetterli. Perfect transmultiplexers. In *The Proceedings of the IEEE International Conference on ASSP*, pages 2567–2570, 1986.
- [47] M. Vetterli. A theory of multirate filter banks. *IEEE Transactions on ASSP*, 35(3):356–372, March 1987.
- [48] M. Vetterli and D. LeGall. Perfect reconstruction FIR filter banks: Some properties and factorizations. *IEEE Transactions on ASSP*, 37(7):1059–1071, July 1989.
- [49] A. Viterbi and R. Padovani. Implications of mobile cellular CDMA. *IEEE Communications Magazine*, 30(1), December 1992.
- [50] J. Woods and S. O’Neil. Subband coding of images. *IEEE Transactions on ASSP*, 34(10), October 1986.
- [51] G. Wornell. Emerging applications of multirate signal processing and wavelets in digital communications. *Proceedings of the IEEE*, 84(4):586–603, April 1996.
- [52] J. Wozencraft and I Jacobs. *Principles of Communication Engineering*. Waveland Press, Inc., 1965.
- [53] L. Yu and J. Salt. An efficient and practical spreading function for direct sequence spread spectrum CDMA systems. In *The Proceedings of the IEEE International Conference on Communications*, pages 1355–1363, 1995.
- [54] R. Ziemer and R. Peterson. *Digital Communications and Spread Spectrum Systems*. Macmillan, Inc., 1985.

Appendix A

Matrix Notation and Operations

The representation of linear transforms, the perfect reconstruction conditions, and the properties of the PR-QMF based codes are all heavily dependent upon matrix notation to represent the various operations. In this chapter, therefore, some of the basic matrix notations and manipulations utilized in this thesis are reviewed.

A.1 Notation and Specialized Matrices

Unless otherwise stated, all vectors in this thesis are column vectors and are denoted by a lower case bold face letter such as \mathbf{x} . A matrix uses an upper case bold face letter such as \mathbf{X} . The transpose of a matrix or vector is denoted by \mathbf{X}^T . For any two matrices \mathbf{X} and \mathbf{Y}

$$(\mathbf{XY})^T = \mathbf{Y}^T \mathbf{X}^T. \quad (\text{A.1})$$

If a matrix is the function of another variable, for example z , then it is written as $\mathbf{X}(z)$.

There are several special vectors and matrices which need to be defined. The *identity* matrix is denoted by \mathbf{I} with its size determined from the context. The *antidiagonal* matrix, \mathbf{J} , is of the form

$$\mathbf{J} = \begin{bmatrix} 0 & 0 & 0 & \cdots & 0 & 0 & 1 \\ 0 & 0 & 0 & \cdots & 0 & 1 & 0 \\ \vdots & & & & \vdots & & \\ 0 & 1 & 0 & \cdots & 0 & 0 & 0 \\ 1 & 0 & 0 & \cdots & 0 & 0 & 0 \end{bmatrix}. \quad (\text{A.2})$$

The antidiagonal matrix is useful for reversing the columns of matrix. For example, let

$$\mathbf{X} = \begin{bmatrix} \mathbf{x}_1 & \mathbf{x}_2 & \cdots & \mathbf{x}_N \end{bmatrix} \quad (\text{A.3})$$

where the \mathbf{x}_n are column vectors. Multiplying by \mathbf{J} gives

$$\mathbf{XJ} = \begin{bmatrix} \mathbf{x}_N & \mathbf{x}_{N-1} & \cdots & \mathbf{x}_1 \end{bmatrix}. \quad (\text{A.4})$$

In this thesis, a *unit vector* is defined as a vector which contains all zeros except for a single element which is one. The non-zero element is indicated by a subscript. For example, the unit vector \mathbf{y}_3 is

$$\mathbf{y}_3 = \begin{bmatrix} 0 & 0 & 1 & 0 & \cdots & 0 \end{bmatrix}^T. \quad (\text{A.5})$$

The unit vector and its transpose are useful for extracting a column or row from a matrix. For example, multiplying \mathbf{X} from Equation A.3 by unit vector \mathbf{y}_i gives

$$\begin{aligned} \mathbf{z} &= \mathbf{Xy}_i \\ &= \begin{bmatrix} \mathbf{x}_1 & \mathbf{x}_2 & \cdots & \mathbf{x}_N \end{bmatrix} \mathbf{y}_i \\ &= \mathbf{x}_i. \end{aligned} \quad (\text{A.6})$$

Extraction of a row is accomplished by a premultiplication of the matrix with the transpose of a unit vector.

A matrix \mathbf{C} is called a *block-circulant* matrix if it has the form

$$\mathbf{C} = \begin{bmatrix} \mathbf{C}_1 & \mathbf{C}_2 & \mathbf{C}_3 & \cdots & \mathbf{C}_{N-2} & \mathbf{C}_{N-1} & \mathbf{C}_N \\ \mathbf{C}_N & \mathbf{C}_1 & \mathbf{C}_2 & \cdots & \mathbf{C}_{N-3} & \mathbf{C}_{N-2} & \mathbf{C}_{N-1} \\ \vdots & & & & & \vdots & \\ \mathbf{C}_3 & \mathbf{C}_4 & \mathbf{C}_5 & \cdots & \mathbf{C}_N & \mathbf{C}_1 & \mathbf{C}_2 \\ \mathbf{C}_2 & \mathbf{C}_3 & \mathbf{C}_4 & \cdots & \mathbf{C}_1 & \mathbf{C}_N & \mathbf{C}_1 \end{bmatrix} \quad (\text{A.7})$$

where the \mathbf{C}_n are themselves matrices. The simplest case occurs when each submatrix is a single element and the matrix is called a *circulant* matrix.

A matrix \mathbf{X} is called a *unitary* matrix if it satisfies

$$\mathbf{XX}^T = \mathbf{I}. \quad (\text{A.8})$$

Traditionally, \mathbf{X} is a square matrix, however, in the context of multirate subband systems, the definition is extended to include any matrix (square or otherwise) which fits the above definition. If the elements of a unitary matrix are functions of a variable, then the matrix is known as a *paraunitary* matrix.

A.2 Shift Operations on Vectors and Matrices

Let \mathbf{x} be a finite length column vector with N elements x_1 through x_N . A shift of \mathbf{x} is denoted by $(\mathbf{x})_\delta$ where delta is the number of shifted positions. The shift is a circular shift down so that

$$(\mathbf{x})_\delta = \begin{bmatrix} x_{N-\delta+1} & x_{N-\delta+2} & \cdots & x_N & x_1 & \cdots & x_{N-\delta} \end{bmatrix}^T. \quad (\text{A.9})$$

If \mathbf{X} is a matrix, then the shift is performed upon each column in \mathbf{X} so that

$$(\mathbf{X})_\delta = \begin{bmatrix} (\mathbf{x}_1)_\delta & (\mathbf{x}_2)_\delta & \cdots & (\mathbf{x}_N)_\delta \end{bmatrix}. \quad (\text{A.10})$$

If a shift and a transpose of a vector or matrix are both defined as in $(\mathbf{x})_\delta^T$ or $(\mathbf{X})_\delta^T$, then the shift is performed prior to the transpose.

Let \mathbf{Z} be a matrix resulting from the multiplication of two matrices \mathbf{X} and \mathbf{Y} . It is straightforward (yet tedious) to show that

$$\begin{aligned} (\mathbf{Z})_\delta &= (\mathbf{XY})_\delta \\ &= (\mathbf{X})_\delta \mathbf{Y}. \end{aligned} \quad (\text{A.11})$$

This is easily extended to more than one multiplication. Now suppose \mathbf{X} is a block circulant matrix with blocks of size M by N . Let \mathbf{Z} be the multiplication of this matrix by a vector \mathbf{y} . A shift of M positions can be accomplished in two different ways. The first method is to shift \mathbf{X} by M positions as in Equation A.11. A second method is to shift \mathbf{y} by N positions so that

$$(\mathbf{Z})_M = \mathbf{X}(\mathbf{y})_N. \quad (\text{A.12})$$

This can also be extended to more than one multiplication (c.f. Section 3.3.1).

Appendix B

Filter Coefficients of the Subband Trees

This appendix contains the filter coefficients for each of the subband trees designed in this thesis. The coefficients for each filter given, are listed with the highest order tap given first. The filter are referenced as follows. Each level in the analysis tree is denoted by a letter starting with “A” for the initial two-band split. A five stage tree, therefore, would contain levels A, B, C, D, and E. Within each level, the filters are numbered in sequence starting with one. For example, at level two, the filters are denoted by B1, B2, B3, and B4 with B1 and B2 being associated with A1 and the other two with A2. This continues throughout the remainder of the tree. For example, consider the subband associated with the filter E14. The filters along the branch leading to that subband are A1, B2, C4, D7, and E14.

Only one filter from each QMF pair is given. For example, D3 and D4 will form a QMF pair so only the coefficients of D3 are given. D4 can be determined by using Equation 2.27. Additionally, the filter given is not necessarily the low pass filter from that particular QMF pair.

Finally, for the multiuser and multipath subband trees, only the coefficients for the filters in the top half of the tree are given. Since the channel is symmetric in the frequency domain, the resulting codes can be grouped in pairs similar to a QMF subband pair. Each of the codes resulting from the bottom half of the subband tree can be generated by first calculating the codes from the top half of the tree and then, using Equation 2.27, find the corresponding code for the subband in the bottom half.

B.1 Filter Coefficients for Section 4.1.2

Structure - Full Binary Tree, Five Stages

Filters - Four Tap FIR Filters

Objective - Energy Compaction

Interference - Single Interference Ranging From $[\pi/8, \pi/4]$

A1=[0.56925516692869 0.75889929443112 0.25299512228665 -0.18977324346751]
B1=[0.76328748691989 0.18100823204623 0.14310345596798 -0.60344811967495]
B3=[0.75002156247275 0.43292553383075 0.24997842636258 -0.43307496387644]
C1=[0.59985790044806 0.72482148765989 0.26103005288342 -0.21602690061248]
C3=[0.50982676519455 0.81482823194596 0.23390718251047 -0.14635249189917]
C5=[0.53533210930287 0.79228318886575 0.24257473290723 -0.16390357040624]
C7=[0.49222354566689 0.82926344443128 0.22757638296929 -0.13508186679085]
D1=[0.53057731163895 0.79664135706782 0.24100821001652 -0.16051575408323]
D3=[0.63827544793489 0.67525324493361 0.26863033723363 -0.25391977031074]
D5=[0.49669334312602 0.82568012506479 0.22920866325186 -0.13788198815501]
D7=[0.54287426101372 0.78521599745753 0.24500957010884 -0.16939210324886]
D9=[0.51043300627073 0.81431535358826 0.23412040834030 -0.14675246307451]
D11=[0.52007840654593 0.80600833193658 0.23746733705778 -0.15322625011454]
D13=[0.48777312910708 0.83277744193495 0.22593518929341 -0.13233441338244]
D15=[0.51108280000201 0.81376443053153 0.23434858965682 -0.14718206996990]
E1=[0.54711942544432 0.78115252761416 0.24635196891874 -0.17254498055887]
E3=[0.54616218471888 0.78207429011022 0.24605108407845 -0.17182996466225]
E5=[0.54429625828327 0.78386184371678 0.24546153275339 -0.17044303776370]
E7=[0.54429960586605 0.78385864759230 0.24546259402037 -0.17044551793940]
E9=[0.56297558895191 0.76540092952591 0.25117452519218 -0.18474647833902]
E11=[0.52488438722928 0.80176351183554 0.23910186297758 -0.15653098824064]
E13=[0.54531007508860 0.78289211571430 0.24578235155466 -0.17119548133393]
E15=[0.50850146659434 0.81594569932904 0.23343988326487 -0.14548091026674]
E17=[0.52006279383827 0.80602200647280 0.23746198782715 -0.15321559936333]
E19=[0.53655484748613 0.79115043009290 0.24297369579608 -0.16478372423167]
E21=[0.54561115170487 0.78260344268087 0.24587739878382 -0.17141944874324]
E23=[0.54924264744859 0.77909645179513 0.24701552573159 -0.17413949328976]
E25=[0.70710678118770 0.00000000000041 0.00000000000041 0.70710678118769]
E27=[0.50393468877447 0.81975739557703 0.23181772480576 -0.14250678758256]
E29=[0.53546117530565 0.79216385463876 0.24261692123105 -0.16399630080356]
E31=[0.000000000000594 0.70710678119271 0.70710678118039 -0.000000000000595]

B.2 Filter Coefficients for Section 4.2.2.1

Structure - Full Binary Tree, Three Stages

Filters - Eight Tap FIR Filters

Objective - Minimize Cross Correlations

Interference - Multiuser Interference

A1=[0.06139303854177 -0.01702240455379 -0.09015611352235 0.33174685245139
0.76915511255569 0.51893443118977 -0.03469806409340 -0.12514210737434]
B1=[0.07418392437531 -0.08322970440740 -0.07281265709927 0.43229813020650
0.77978182048409 0.42168194055606 -0.07280228248762 -0.06488980174643]
C1=[0.19912252579444 -0.16031981420496 -0.02576729462679 0.07094930070005
-0.10902554059585 0.09696553059470 0.59747383151588 0.74208231226756]
C3=[0.07959130894727 -0.11474922047559 -0.06471939162881 0.45444111766106
0.77984853184655 0.39354638615846 -0.06750888287818 -0.04682489633979]

B.3 Filter Coefficients for Section 4.2.2.4

Structure - Full Binary Tree, Three Stages

Filters - Eight Tap FIR Filters

Objective - Minimize Cross Correlations and Autocorrelations

Interference - Multiuser and Multipath Interference, $\alpha = .8$

A1=[-0.05911448630152 0.10187908985342 0.04849141298087 -0.20114190203630
-0.09869017910996 0.44073504190888 0.74371278352434 0.43153309690105]
B1=[-0.01795020725105 -0.05342912399986 0.00240918206924 0.17079705181030
-0.04218460652784 -0.67889478306441 0.67361150973633 -0.22630852428887]
C1=[0.18572289980417 -0.21532379774293 -0.26266893764112 0.18523085266579
0.70150154292065 0.53342874609285 0.14989979310017 0.12929283500677]
C3=[-0.16355236661009 -0.16332366503577 0.00691707310682 0.03976362439386
0.06568936056508 0.07189850169291 -0.68343014184950 0.68438714677306]

Structure - Full Binary Tree, Three Stages

Filters - Eight Tap FIR Filters

Objective - Minimize Cross Correlations and Autocorrelations

Interference - Multiuser and Multipath Interference, $\alpha = .6$

A1=[-0.05911448630152 0.10187908985342 0.04849141298087 -0.20114190203630
-0.09869017910996 0.44073504190888 0.74371278352434 0.43153309690105]
B1=[0.00847057563847 0.02725312912747 -0.01759146552161 -0.14257834574333
0.06327265927773 0.66420006779596 -0.69742013330167 0.21676593404349]

C1= [0.13292755623553 -0.23181380063902 -0.16441168899916 0.25598833922434
0.79078920813276 0.44641800318453 0.09260211042549 0.05310025635739]
C3= [-0.11613764173520 -0.14116086050454 -0.00798902726174 0.03133100430738
0.08751068812377 0.10769249752515 -0.75120538651545 0.61804116056317]

Structure - Full Binary Tree, Three Stages

Filters - Eight Tap FIR Filters

Objective - Minimize Cross Correlations and Autocorrelations

Interference - Multiuser and Multipath Interference, $\alpha = .4$

A1=[0.00076202191380 -0.04003599787824 -0.99839799400399 0.03990502628101
-0.00235680887663 0.00013503171274 -0.00000721911404 -0.00000013740964]
B1=[-0.46831215893045 0.64129851484526 0.51293951721567 0.25324146759773
0.10569241232339 0.15331644144742 -0.06996219810043 -0.05109032264603]
C1=[-0.58179988541997 -0.34737585639643 0.54037088751192 -0.40194332285231
0.13838146339107 -0.26052357197524 -0.00823136658461 0.01378624348119]
C3=[-0.15642098953557 -0.02089547451648 -0.61799220126938 -0.14529298807407
-0.14296314422715 -0.51693489480963 -0.07061383899778 0.52860663978821]

B.4 Filter Coefficients for Section 4.2.2.6

Structure - Full Binary Tree, Five Stages

Filters - Eight Tap FIR Filters

Objective - Minimize Cross Correlations Over Limited Set of Time Shifts and Autocorrelations

Interference - Multiuser and Multipath Interference, $\alpha = .7$

A1=[-0.21359361393253 -0.04200549364874 0.50492951429500 0.73929394303632
0.36655965106061 -0.04374993282931 -0.02349413575564 0.11946526338282]
B1=[-0.09533119258461 -0.14151100726811 0.04852644884045 0.19157802433650
-0.09798410604555 -0.35512216489134 0.74000081527981 -0.49851358983369]
C1=[0.18438608855810 0.09767598597987 -0.36955792092046 -0.70770361636661
-0.52339052018188 0.00461699311069 0.09939494236292 -0.18763101760277]
C3=[-0.10425486996888 -0.14840274139847 0.04917680978848 0.19624487488344
-0.10199341998006 -0.36161308971138 0.72498917483712 -0.50931439297704]
D1=[0.15687635384402 -0.10503623732347 0.08739048045484 0.37379315656622
0.79309983403068 0.36045873340715 -0.13405877471346 -0.20022282132098]
D3=[-0.09582515495590 0.01616308188318 -0.01433100817897 -0.28644511646105
-0.79266367680502 -0.47162496648105 0.03990174020321 0.23656320407326]
D5=[-0.19594538533495 -0.06917599341445 0.42488183217842 0.69980252895005
0.50030403372568 -0.05823273043921 -0.06036136236176 0.17097738429839]

D7=[-0.11924139613643 -0.14199938954771 0.06083552016496 0.17473489118001
-0.12631963924206 -0.31278495134626 0.69244845909081 -0.58147095758751]
E1=[0.35726793968229 0.20273450479324 0.27450611170414 -0.17552162537932
0.59675921921949 -0.39120085095114 -0.22934024216418 0.40415377682155]
E3=[-0.00019389311448 0.00155143566703 0.01707612580017 -0.07615879233128
-0.24215152812457 -0.94826434039879 0.18843716309968 0.02355023030270]
E5=[-0.00142350418149 0.00530174784689 -0.01805015899213 -0.01466072678289
-0.21186637879770 0.94447522648760 0.24146438866725 0.06483249993699]
E7=[-0.00147288403473 -0.00273109792938 0.02141973652705 -0.03438959792140
-0.07277046267087 -0.99329092279117 -0.07055875858176 0.03805241397896]
E9=[-0.00053445106876 0.00152379861464 0.03606424375635 -0.06255558122686
-0.20804131785974 -0.97004267189379 0.09678463449951 0.03394585797006]
E11=[-0.00214326351182 0.00604620259715 -0.01588506851328 -0.03356035659143
-0.20719308599725 0.94865809359034 0.22244413560980 0.07885220374949]
E13=[-0.00119002793754 -0.00423228530333 -0.00143694178820 0.04672301670476
0.38581673132215 0.87256181459036 -0.28488638725668 0.08010394752743]
E15=[0.01182025421925 0.01683239348255 -0.12438942230497 -0.20652298519614
-0.49987802126206 -0.38735003813615 0.60223242518676 -0.42290719808582]

Appendix B:

Proceedings of the SPIE, 1997

Performance of Filter Bank-Based Spreading Codes for Cellular and Micro-Cellular Channels

Kenneth J. Hetling, Gary J. Saulnier, and Pankaj Das

Electrical, Computer, and Systems Engineering Department
Rensselaer Polytechnic Institute
Troy, New York 12180-3590

ABSTRACT

Recently, a new class of spreading codes has been developed based upon the time-frequency duality of multirate filter bank structures. Unlike the maximal length sequences, these new codes are not limited to being binary valued. Instead, the elements of the sequences are determined by an optimization process which emphasizes certain desirable code properties. In this paper, spreading codes based upon multi-rate filter banks are developed for use in a cellular or micro-cellular channel in which partial synchronization is maintained between the users. This situation allows the cross-correlation between the codes to be optimized over a fraction of the total range of possible phase shifts between the codes. Codes are designed for an example set of channel conditions and bit error rate results are generated. These results show that the new codes perform better than conventional Gold codes.

1 INTRODUCTION

Traditionally, the DSSS/CDMA systems utilize maximal length sequences (m-sequences) as the spreading codes.¹ As an alternative, Perfect Reconstruction Quadrature Mirror Filter (PR-QMF) based spread spectrum codes have been proposed.² Whereas the m-sequences are limited to being two-valued codes, no restriction is placed upon the individual "chip" values in the PR-QMF based codes. Instead, the values are determined to provide the certain code properties. Finally, instead of using binary feedback shift registers for code generation, the codes are generated within the framework of a PR-QMF subband tree.

Consider the typical filter bank structure shown in Figure 1. The spreading codes considered are generated by taking the impulse response of each of the subbands of the PR-QMF synthesis stage. The codes are then used to modulate (i.e. spread) the data prior to transmission. The receiver can de-spread the data in one of two ways. One method is to use the analysis bank to process the received signal. In the absence of noise and other interference, all of the signal energy will be isolated to a single subband which can then be sent to a threshold device. This method is similar to a trans-multiplexer using subband tree structures.³ A second and more computationally efficient method is to simply correlate the received signal with a synchronized locally-generated copy of the spreading

*This work partially supported by the Air Force Materiel Command, Rome Laboratory contract no. F30602-95-C-0167

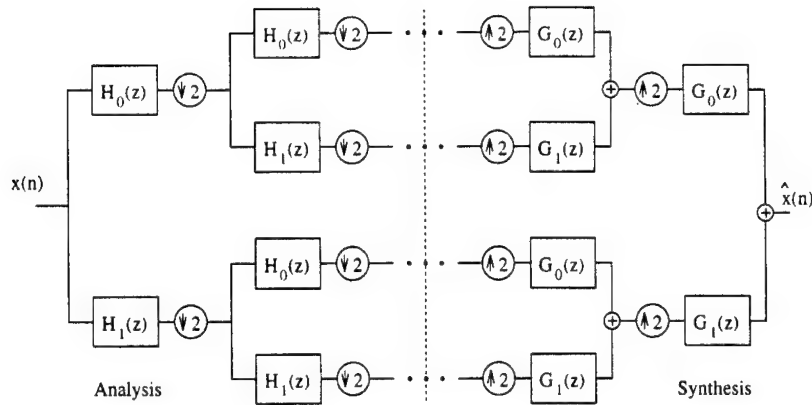


Figure 1: Four-band tree structure

code. The result of the correlation can then be sent to the threshold device.

Since the spreading codes which modulate the message bits are the impulse responses from a PR-QMF synthesis tree, the tap weights used in the filters from which the tree is constructed have a direct impact upon the structure and performance of the codes. Previous studies have focused upon the performance of codes optimized for a channel characterized by interference such as narrowband or multipath interference.⁴⁻⁶ In this paper, a new set of codes is designed for use in a coarsely-synchronized cellular or micro-cellular environment. The performance of the new codes is compared to that for Gold codes.

2 MULTIUSER CHANNEL WITH COARSE SYNCHRONIZATION

In many communication systems, synchronization between the users is achieved through the use of a beacon or timing signal transmitted by a base station. For example, consider the mobile to base transmissions as shown in Figure 2. In earlier work, it was assumed that an asynchronous system occurred because of both transmit clock differential and variances in the propagation paths. Suppose, however, that the base station is transmitting a timing signal which each mobile unit can use to synchronize their respective transmit clocks. The only cause for different delay times, therefore, would be the different propagation paths between the users and the base station.

The *microcell*⁷ trend in cellular communications has the effect of shortening this distance and thus the delay times as well. Originally proposed to increase capacity in a Personal Communication System (PCS) environment, the microcell architecture limits the physical size of a cell. Under these conditions, partial synchronization between the users is possible and there are some delay times which need not be considered in the filter design.

2.1 Alternate Representation of Spreading Code Shifts

As in the previous work,⁶ the filter design, and therefore the spreading code design, will be accomplished via a multivariable constrained optimization using the filter coefficients as the optimization variables.^{4,5} Once again, the constraints will be the perfect reconstruction conditions for a QMF filterbank.^{8,9} The problem, therefore, is

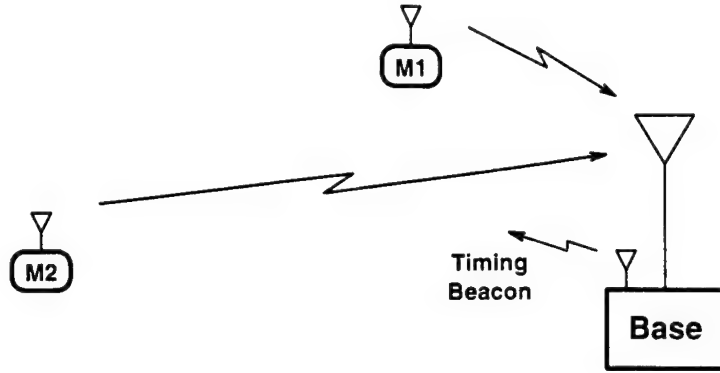


Figure 2: Mobile to Base Communications System

to formulate a suitable objective function for the scenario described above.

Although the formulation of this objective function would seem to be a straightforward extension of our previous work, the use of progressive optimality in a hierarchical tree structure prevents this. Previously, the goal was to produce codes which were completely orthogonal over all time shifts. Linear processing by subsequent decimation did not negate any orthogonality which was already attained between two codes and, therefore, the progressively optimal approach worked. In this case, however, the codes are not completely orthogonal. It must therefore be determined how the final objective, i.e. codes with low cross correlations over a subset of all possible time shifts, affects the design of filters in the earlier stages of the tree.

In previous work, the spreading codes were represented in terms of operator matrices which correspond to the filters along a particular subband path which produced the code. The objective function then used these code representations to formulate cross correlations between the codes subject to various phase shifts (delay values) of the codes.⁴ A similar approach will be used here with a slight modification.

In order to “backtrack” the objective through the tree, the expressions for a circular shift of a code must be redefined in a more complex format. This is best seen by first looking at an example prior to giving the formula for the general case. Consider a code generated by a full binary subband tree structure with three levels and eight tap filters in each decimator. The equation for this code is

$$\mathbf{c} = \mathbf{A}_1^T \mathbf{A}_2^T \mathbf{A}_3^T \mathbf{x} \quad (1)$$

where \mathbf{x} is a unit vector and \mathbf{A}_l for $l = 1, 2, 3$, is an operator matrix representing a decimation using the filter $A_l(z)$.⁵ The filters $A_1(z)$, $A_2(z)$ and $A_3(z)$ are the filters along the branch associated with spreading code \mathbf{c} and $A_1(z)$ is associated with the first split in the subband tree. To represent a circular shift of the code we can use

$$(\mathbf{c})_\delta = (\mathbf{A}_1)_\delta^T \mathbf{A}_2^T \mathbf{A}_3^T \mathbf{x} \quad (2)$$

where $(\cdot)_\delta$ is a circular shift (downward) of the vector or matrix.

An alternative and more complex method of representing the circular shift involves performing a shift on more than one matrix or vector in the right hand side of Equation 2. For the code under consideration, this alternative method has the form

$$(\mathbf{c})_\delta = (\mathbf{A}_1)_{\delta_1}^T (\mathbf{A}_2)_{\delta_2}^T (\mathbf{A}_3)_{\delta_3}^T (\mathbf{x})_{\delta_x}^T \quad (3)$$

Each of the matrix shift indicators, δ_1 , δ_2 , and δ_3 , can take on a value of either zero or one. The values allowable for δ_x is dependent upon the filter length. In this example since each of the filters are of length eight, the matrix

\mathbf{A}_3 has eight rows and four columns. The vector \mathbf{x} , therefore, must be of length four and the shift indicator, δ_x , can take on values of zero, one, two, or three.

The effect on each of the shift indicators on δ is as follows. If δ_1 is a one then \mathbf{c} will be circularly shifted by one position. If δ_2 is a one then \mathbf{c} will be circularly shifted by two positions. Finally, if δ_3 is a one then \mathbf{c} will be circularly shifted by four positions. For the unit vector shift, δ_x , number of shifted positions of the spreading code is equal to $8 \cdot \delta_x$. Other shift values for $(\mathbf{c})_\delta$ are generated by combining different values of the shift indicators on the right hand side of Equation 3. For example, if a shift of 19 is desired, the indicators would be $\delta_1 = 1$, $\delta_2 = 0$, $\delta_3 = 1$, and $\delta_x = 2$. Notice that the maximum shift which can be indicated is when $\delta_1 = \delta_2 = \delta_3 = 1$ and $\delta_x = 3$. In this case δ will equal 31. Since a code generated by a three stage full binary tree using eight tap filters is of length 32, it is possible to specify every shift using the above notation. Notice that although it is possible for each δ_i to take on values other than zero or one, those two values are the only ones necessary to represent each possible shift.

Now consider the general case of a code generated by a full binary tree with L stages and N -tap filters in each decimator. Let the filters along the branch generating the code be $A_1(z), A_2(z), \dots, A_L(z)$ with $A_1(z)$ occurring in the first split. A shift of δ positions of the code \mathbf{c} can be represented by

$$(\mathbf{c})_\delta = \left[\prod_{l=1}^L (\mathbf{A}_l)_{\delta_l}^T \right] (\mathbf{x})_{\delta_x}. \quad (4)$$

The shift indicators are chosen so that

$$\delta = \delta_x 2^L + \sum_{l=1}^L \delta_l 2^{l-1}. \quad (5)$$

The allowable values for the shift indicators are

$$\delta_l \in \{0, 1\} \quad (6)$$

$$\delta_x \in \{0, 1, 2, \dots, \frac{N}{2}\}. \quad (7)$$

This formulation, though somewhat complex, is necessary to consider how a given shift of a code will effect every filter in the branch generating that code.

2.2 Objective Functions for Coarse Synchronization

2.2.1 First Stage Optimization

Now that the new representation of a circularly shifted code has been developed, it can be combined with an expression for the cross correlations between the codes. The first case which will be considered is the design of the QMF pair which occurs at the first split in a hierarchical subband tree structure as shown in Figure 3. The cross correlation between two spreading codes with a relative time shift of δ can be expressed as

$$\rho_\delta = (\mathbf{c}_c)_\delta^T \mathbf{c}_b \quad (8)$$

for the case when the polarity of the code \mathbf{c}_c does not change (case 1) and

$$\rho_\delta^- = (\mathbf{c}_b)_\delta^T \mathbf{K}_\delta \mathbf{c}_c \quad (9)$$

for the case where the polarity of the code \mathbf{c}_c does change (case 2), indicating a change in data bit polarity. See Figure 4 for an illustration of the two polarity cases. \mathbf{K}_δ is a diagonal matrix whose first δ diagonal elements are

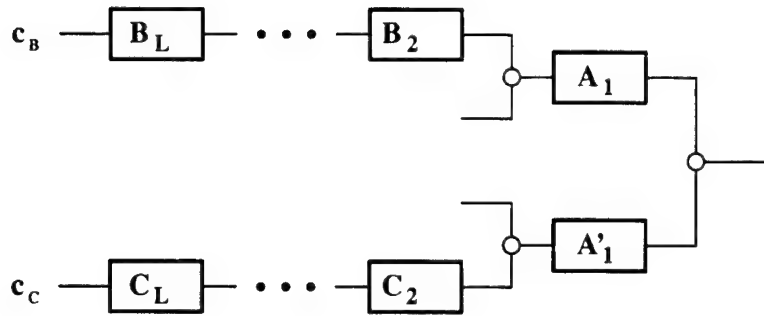


Figure 3: Branch Split at Stage 1

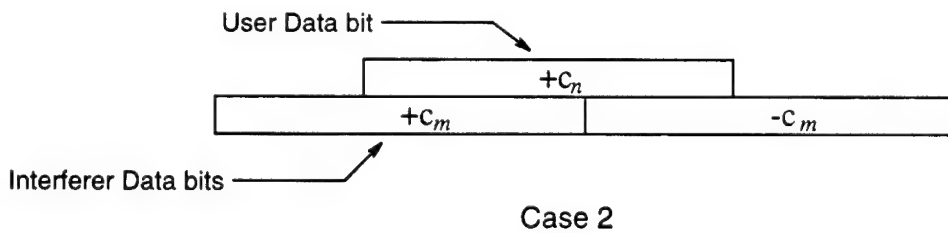
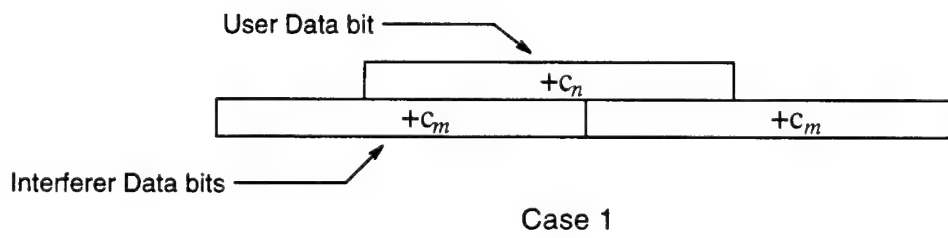


Figure 4: Illustration of the Two Polarity Cases

negative one and the remaining elements are positive one.

Consider the cross correlations between two codes generated by the branches shown in Figure 3. For polarity case one substitution of Equation 4 into Equation 8 gives

$$\begin{aligned}\rho_\delta &= \left((\mathbf{A}_1)_{\delta_1}^T \left[\prod_{l=2}^L (\mathbf{C}_l)_{\delta_l}^T \right] (\mathbf{x})_{\delta_x} \right)^T \left((\mathbf{A}'_1)^T \left[\prod_{l=2}^L (\mathbf{B}_l)^T \right] \mathbf{x} \right) \\ &= (\mathbf{x})_{\delta_x}^T \left[\prod_{l=L}^2 (\mathbf{C}_l)_{\delta_l} \right] (\mathbf{A}_1)_{\delta_1} (\mathbf{A}'_1)^T \left[\prod_{l=2}^L (\mathbf{B}_l)^T \right] \mathbf{x}.\end{aligned}\quad (10)$$

For polarity case two, a similar result is attained by substitution of Equation 4 into Equation 9

$$\begin{aligned}\rho_\delta &= \left((\mathbf{A}_1)_{\delta_1}^T \left[\prod_{l=2}^L (\mathbf{C}_l)_{\delta_l}^T \right] (\mathbf{x})_{\delta_x} \right)^T \mathbf{K}_\delta \left((\mathbf{A}'_1)^T \left[\prod_{l=2}^L (\mathbf{B}_l)^T \right] \mathbf{x} \right) \\ &= (\mathbf{x})_{\delta_x}^T \left[\prod_{l=L}^2 (\mathbf{C}_l)_{\delta_l} \right] (\mathbf{A}_1)_{\delta_1} \mathbf{K}_\delta (\mathbf{A}'_1)^T \left[\prod_{l=2}^L (\mathbf{B}_l)^T \right] \mathbf{x}\end{aligned}\quad (11)$$

The filter coefficients for $A_1(z)$ are contained in the two terms in the middle of the above equations

$$\mathbf{V}_\delta = (\mathbf{A}_1)_{\delta_1} \mathbf{A}'_1^T \quad (12)$$

$$\mathbf{V}_\delta^- = (\mathbf{A}_1)_{\delta_1} \mathbf{K}_\delta \mathbf{A}'_1^T \quad (13)$$

As discussed above, the shift indicator can be only a zero or a one. Since the operator matrices are generated from a QMF pair, the result for $\delta_1 = 0$ is $\mathbf{V}_\delta = \mathbf{V}_\delta^- = 0$. For $\delta_1 = 1$, the multiplications result in matrices which are dependent upon δ .

Since every element in the matrices \mathbf{V}_δ and \mathbf{V}_δ^- contributes to the cross correlation values, these are the terms which should be minimized. For computational simplicity, the objective will be to minimize the squares of the elements. The objective function thus becomes

$$F_{CS} = \min \left\{ \sum_{\delta} \sum_i \sum_j ([\mathbf{V}_\delta]_{i,j}^2 + [\mathbf{V}_\delta^-]_{i,j}^2) \right\} \quad (14)$$

where $[\cdot]_{i,j}$ represents the i th row and the j th column of the matrix inside the brackets. The outer summation should only be performed over the shifts δ which are of interest.

Once again, the resulting objective function is very computationally intensive and unrealistic given current processing capabilities. For this reason, approximations are made by not including every element of \mathbf{V}_δ^- . Due to the structure of the operator matrices, \mathbf{V}_δ is a circulant matrix. Additionally, an analysis of \mathbf{V}_δ^- shows that nearly every row is identical to, within a circular shift, or an additive inverse of, the same row which comprises \mathbf{V}_δ . Therefore, an objective function which approximates the one given by Equation 14, yet is able to be implemented, is

$$F_{CS} = \min \{ \mathbf{v} \mathbf{v}^T \} \quad (15)$$

where \mathbf{v} is a vector which represents the row that can be used to construct \mathbf{V}_δ . Using this approximation, some of the rows unique to \mathbf{V}_δ^- are not being considered. Generation of the vector \mathbf{v} is easily accomplished by using Equation 12, with $\delta_1 = 1$ and then extracting the first row of \mathbf{V}_δ .

2.2.2 Subsequent Stage Optimizations

The optimization for subsequent stages becomes even more complex than the first stage optimization discussed above. Things are again simplified, however, by not considering the matrices generated under polarity case two and using only Equation 8. Again, although this is only an approximation, it allows for optimization function which can be calculated using current processing capabilities.

Consider the design of a filter at stage M as shown in Figure 5. The two codes generated by the two different

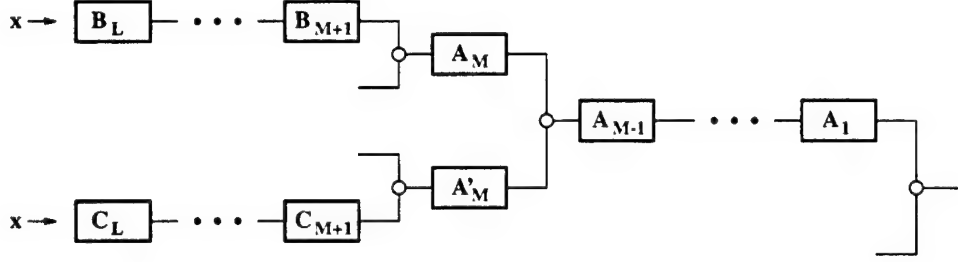


Figure 5: Spreading Code Branches

subbands depicted in the figure can be represented by

$$\mathbf{c}_b = \left[\prod_{i=1}^{M-1} (\mathbf{A}_i)^T \right] \mathbf{A}_M^T \left[\prod_{j=M+1}^L (\mathbf{B}_j)^T \right] \mathbf{x} \quad (16)$$

and

$$\mathbf{c}_c = \left[\prod_{i=1}^{M-1} (\mathbf{A}_i)^T \right] \mathbf{A}'_M{}^T \left[\prod_{j=M+1}^L (\mathbf{C}_j)^T \right] \mathbf{x}. \quad (17)$$

Using both of these expressions in Equation 8 along with Equation 4 gives

$$\begin{aligned} \rho_\delta &= \left(\left[\prod_{i=1}^{M-1} (\mathbf{A}_i)_{\delta_i}^T \right] (\mathbf{A}_M)_{\delta_M}^T \left[\prod_{j=M+1}^L (\mathbf{B}_j)_{\delta_j}^T \right] (\mathbf{x})_{\delta_x} \right)^T \\ &\quad \left(\left[\prod_{i=1}^{M-1} (\mathbf{A}_i)^T \right] \mathbf{A}'_M{}^T \left[\prod_{j=M+1}^L (\mathbf{C}_j)^T \right] \mathbf{x} \right) \\ &= (\mathbf{x})_{\delta_x}^T \left[\prod_{j=L}^{M+1} (\mathbf{B}_j)_{\delta_j} \right] (\mathbf{A}_M)_{\delta_M} \mathbf{W}_\delta \mathbf{A}'_M{}^T \left[\prod_{j=M+1}^L (\mathbf{C}_j)^T \right] \mathbf{x} \end{aligned} \quad (18)$$

where

$$\mathbf{W}_\delta = \left[\prod_{m=M-1}^1 (\mathbf{A}_m)_{\delta_m} \right] \left[\prod_{m=1}^{M-1} (\mathbf{A}_m)^T \right] \quad (19)$$

and represents the filters in Figure 5 which have already been designed. Once again, it is the middle of Equation 18 which is of interest since that contains the filter coefficients to be optimized. Therefore, let

$$\mathbf{V}_\delta = (\mathbf{A}_M)_{\delta_M} \mathbf{W}_\delta \mathbf{A}'_M{}^T \quad (20)$$

As in the previous section, for any particular δ , the rows of \mathbf{V}_δ are identical except for a circular shift. Let \mathbf{v}_δ be a row from \mathbf{V}_δ . Since the shift indicators on the right hand side of the above equation can take on only one of two values and since there are M of these indicators, there are 2^M different possibilities for \mathbf{v}_δ . The objective function then becomes

$$F_{CS} = \min \left\{ \sum_{\delta} \mathbf{v}_\delta \mathbf{v}_\delta^T \right\} \quad (21)$$

which again provides an approximation which can be implemented.

2.2.3 Final Stage Optimization

At the L th stage of the subband tree, shown in Figure 6, each of the filters along the branch except for the final QMF pair will already have been designed. Equation 18 then becomes

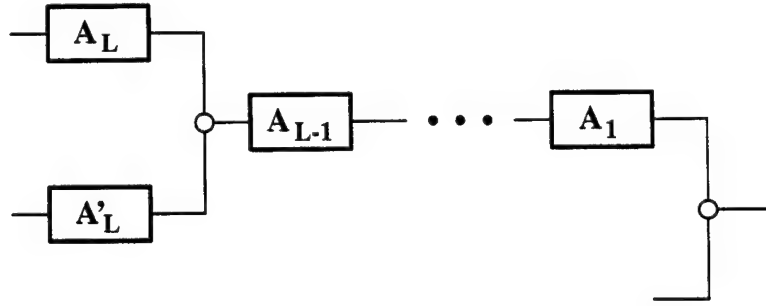


Figure 6: Final Stage Split

$$\rho_\delta = (\mathbf{x})_{\delta_x}^T (\mathbf{A}_L)_{\delta_L} \left[\prod_{l=L-1}^1 (\mathbf{A}_l)_{\delta_l} \right] \left[\prod_{l=1}^{L-1} (\mathbf{A}_l)^T \right] \mathbf{A}'_L{}^T \mathbf{x} \quad (22)$$

$$= (\mathbf{x})_{\delta_x}^T (\mathbf{A}_L)_{\delta_L} \left[\prod_{l=L-1}^2 (\mathbf{A}_l)_{\delta_l} \right] (\mathbf{A}_1)_{\delta_1} \mathbf{A}'_1{}^T \left[\prod_{l=2}^{L-1} (\mathbf{A}_l)^T \right] \mathbf{A}'_L{}^T \mathbf{x} \quad (23)$$

$$= \mathbf{x}^T \mathbf{A}_L \left[\prod_{l=L-1}^2 (\mathbf{A}_l) \right] (\mathbf{A}_1)_\delta \mathbf{A}'_1{}^T \left[\prod_{l=2}^{L-1} (\mathbf{A}_l)^T \right] \mathbf{A}'_L{}^T \mathbf{x} \quad (24)$$

$$= \mathbf{A}_L^T \mathbf{P}^T \mathbf{Q}_\delta \mathbf{P} \mathbf{A}'_L \quad (25)$$

where

$$\mathbf{P} = \left[\prod_{l=2}^{L-1} (\mathbf{A}_l)^T \right]. \quad (26)$$

and

$$\mathbf{Q}_\delta = (\mathbf{A}_1)_\delta \mathbf{A}'_1{}^T. \quad (27)$$

2.3 Example Design and Results

A set of subband trees were designed for a system where some synchronization between the users is maintained. These trees consist of a full binary tree with five stages and eight tap filters at each stage, resulting in 32 spreading codes each of length 128. Assume that maximum distance between the transmitters and the base station receiver is three kilometers. If a timing beacon is transmitted from the base station, the maximum round trip delay time is six kilometers divided by the speed of light or 20 microseconds. If the vocoder operates at 9.6 kilobits per second and each data bit is spread by a code of length 128, then the chip duration is 813.8 nanoseconds and the delay times can vary over only the first 25 values of the spreading code. For example, suppose that the user transmitting the signal of interest is co-located with the base station and the interfering user is located three kilometers away. The differential delay between the start of each users bit interval will be twenty microseconds or 25 chips. Due to physical symmetry (i.e. the two mobile units swap positions), there is uncertainty over the last 25 chips as well. For simplicity, assume every possible delay in the ± 25 chip range is equally likely.

Under these conditions, a five stage tree was constructed using an objective function which weights multiuser performance by 0.7 and multipath performance by 0.3. After extracting the codes from the tree, the cross correlations between all of the codes were calculated. A histogram of these cross correlations are shown in Figure 7. The lower histogram is the same calculation for 127 chip Gold codes. The histogram for the PR-QMF

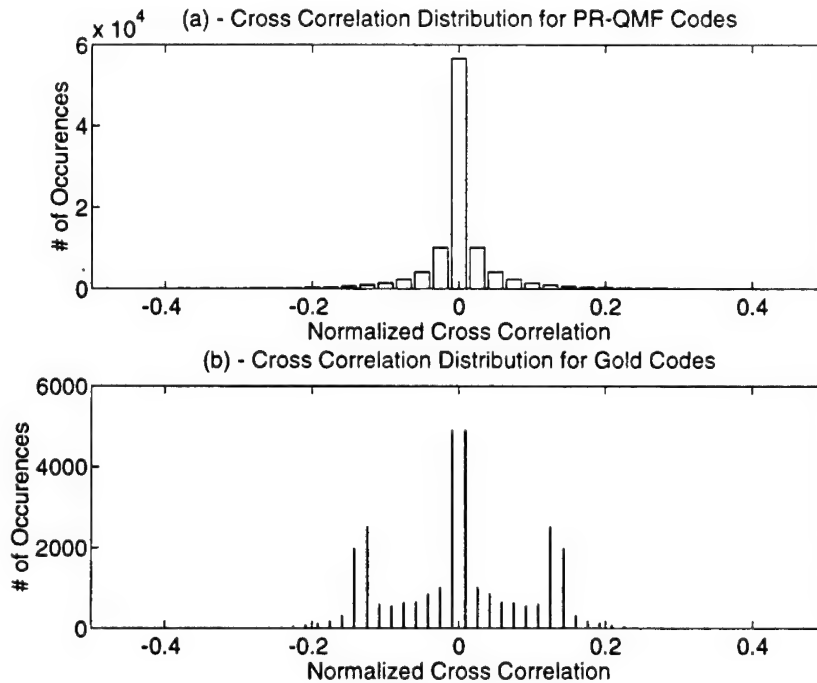


Figure 7: Cross Correlation Results for Codes With Partial Synchronization

based codes shows a much narrower spread than that of the Gold codes. Note that only the cross correlations possible in the above scenario were calculated and plotted. Cross correlations not included in the minimization were ignored. A cursory look at these "unimportant" values showed many which were well above the values shown in the figure.

After extracting the codes from the tree, the capacity, i.e. the number of users in the channel at a given

BER, was calculated and is plotted in Figure 8. The same calculations were again performed for 127 chip Gold

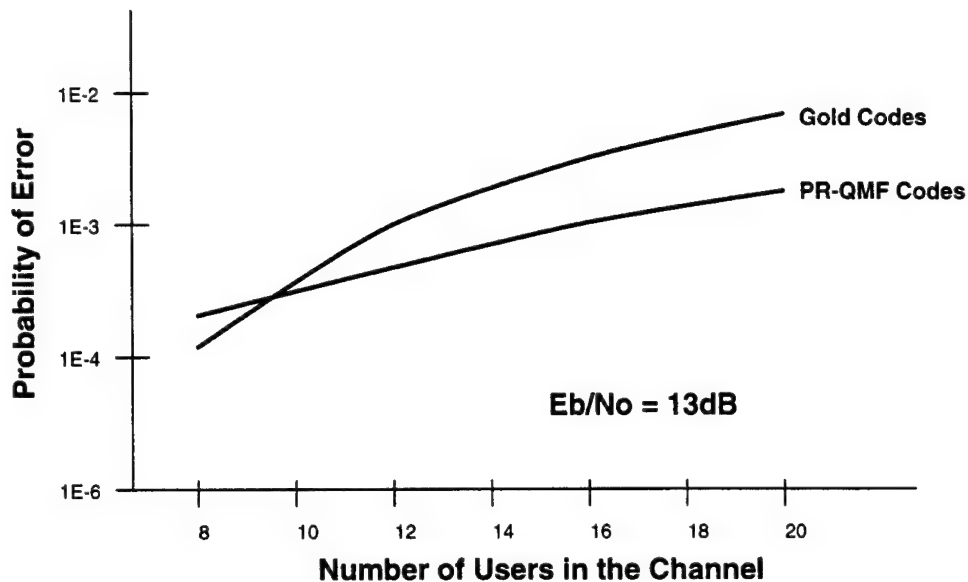


Figure 8: Capacity Results for Codes With Partial Synchronization

codes. The improvement attained by the PR-QMF based codes demonstrates both the validity of the partial synchronization objective function, as well as, the ability of the PR-QMF based technique to extend to practical length spreading codes.

Figure 9 shows the cross correlations between the codes that were generated. The cross correlation values are plotted versus the delay between the two codes. Although some of these values are considerably large, the values over the range of interest, the first 25 and the last 25, were successfully minimized. This demonstrates the ability of two or more codes to attain low cross correlation properties using both time domain and frequency orthogonality.

One final interesting result is the frequency response of two codes which were optimized for partial synchronization. The response of two codes generated by two adjacent subbands (one from each decimator of a QMF pair) are plotted in Figure 10. Notice that the frequency response of the two codes almost completely overlap.

3 CONCLUSIONS

This paper describes a method for designing non-binary spreading codes for multiuser communications through the use of multi-rate filter bank techniques. Example results are presented for a quasi-synchronous cellular system and the codes designed specifically for the case under consideration out-perform conventional Gold codes by producing less multiuser interference.

4 REFERENCES

- [1] R. Dixon. *Spread Spectrum Systems With Commercial Applications*. John Wiley and Sons, Inc.; 1994.

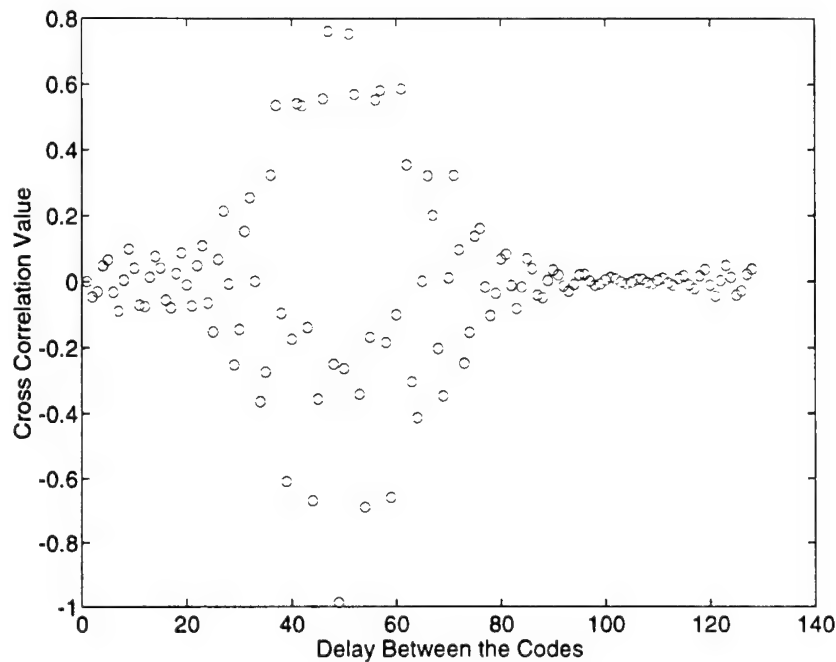


Figure 9: Cross Correlations of Two Codes Designed For Partial Synchronization

- [2] K. Hetling, M. Medley, G. Saulnier, and P. Das. A PR-QMF (wavelet) based spread spectrum communications system. In *The Proceedings of the IEEE Conference on Military Communications*, pages 760–764, 1994.
- [3] M. Vetterli. A theory of multirate filter banks. *IEEE Transactions on ASSP*, 35(3):356–372, March 1987.
- [4] K. Hetling, G. Saulnier, and P. Das. Optimized PR-QMF based codes for multiuser communications. In H. Szu, editor, *SPIE Proceedings - Wavelet Applications*, pages 248–259, 1995.
- [5] K. Hetling, G. Saulnier, and P. Das. Optimized filter design for PR-QMF based spread spectrum communications. In *The Proceedings of the IEEE International Conference on Communications*, pages 1350–1354, 1995.
- [6] K. Hetling, G. Saulnier, and P. Das. PR-QMF based codes for multipath/multiuser communications. In *The Proceedings of the IEEE Global Telecommunications Conference*, 1995.
- [7] R. Steele and M. Nofal. Teletraffic performance of microcellular personal communication networks. *Proceedings of the Institute of Electrical Engineering*, 139(8), August 1992.
- [8] M. Smith and T. Barnwell. A procedure for designing exact reconstruction filter banks for tree-structured subband coders. In *The Proceedings of the IEEE ICASSP*, 1984.
- [9] M. Smith and T. Barnwell. Exact reconstruction techniques for tree-structured subband coders. *IEEE Transactions on ASSP*, 34(6):434–441, June 1986.

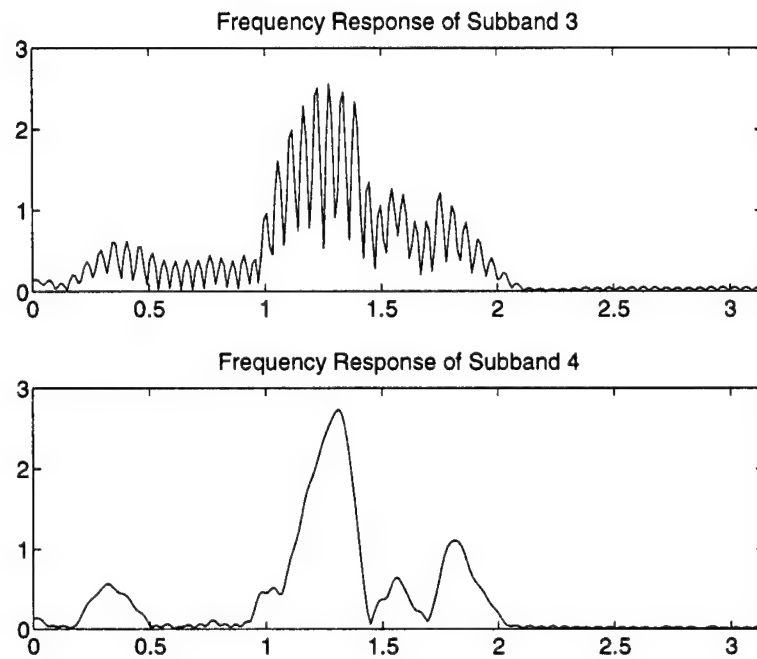


Figure 10: Frequency Response of Codes With Partial Synchronization

Appendix C: IEEE DSP Workshop, 1996

An OFDM Spread Spectrum System using Lapped Transforms and Partial Band Interference Suppression

Gary J. Saulnier, V. A. Alanzo Whyte, and Michael J. Medley
Electrical, Computer, and Systems Engineering Department
Rensselaer Polytechnic Institute
Troy, New York 12180-3590

ABSTRACT

A system that uses orthogonal frequency division multiplexing (OFDM) as a spread spectrum modulation is introduced and its performance is evaluated in the presence of tone interference. Interference excision, in which some of the transform bins are removed in the detection process, is used in the receiver. The BER performance obtained using a number of block transforms is compared to that obtained using the Modulated Lapped Transform (MLT) and it is shown that the MLT provides much better performance due to its ability to confine the interference energy to a few transform bins.

1. INTRODUCTION

Orthogonal frequency division multiplexing (OFDM), often called multi-carrier modulation, is a method designed to efficiently utilize channels with non-flat frequency responses and/or non-white noise. The information to be transmitted is divided up among the many carriers in the system in a manner which optimizes the capacity for a given channel. This technique has been implemented for a variety of applications, including high-speed transmission over telephone lines. It has recently found application as the signaling standard for asymmetric digital subscriber lines (ADSL) [1].

In this paper, we study the use of OFDM as a *spread spectrum* modulation, where, rather than dividing up the information among the carriers, the *same* information is sent on all the carriers in the system. In effect, this technique spreads the signal bandwidth by a factor equal to the number of carriers in the system, assuming that the carriers are grouped together in the spectrum. Processing gain is obtained by coherently combining the signals on the various carriers in the receiver. In the presence of partial-band interference, a decision can be made to exclude some of the carriers from the coherent combiner if those carriers have been "jammed" by the interference. By excluding these carriers, the effect of the interference can be diminished and the performance of the system enhanced. This technique is similar to transform domain excision which has been studied extensively [2, 3, 4, 5].

To a large extent, multi-carrier systems have relied upon sinusoidal carriers to convey information. These systems can be implemented efficiently using the discrete Fourier transform (DFT) implemented efficiently as the fast Fourier transform (FFT). In the modulator, an inverse FFT is used to place the information on the equally-spaced carriers while, at the receiver, a forward FFT is used to frequency translate all the carriers to baseband. One problem with the FFT approach is that there is considerable spectral overlap with a large number of adjacent carriers, a problem which is often mitigated in multipath channels through the use of a cyclic prefix [6]. In the partial-band interference scenario the problem is magnified because processing by a rectangularly-windowed FFT will result in interference components being spread over a much larger portion of the band. To combat this problem, we propose to use non-sinusoidal carriers which are based on Lapped Transforms (LT) and, in particular, Modulated Lapped Transforms (MLT)[7]. This approach is similar to the wavelet-based OFDM system that was proposed by Sanberg [?]. With LTs, the basis vectors are not restricted in length as they are in conventional block transforms like the DFT and discrete cosine transform (DCT). Indeed, whereas the lengths of the block transform basis vectors are limited to the number of transform domain cells, or bins, the LT basis vectors have length, L , that is equal to some even integer multiple of the number of bins, i.e. $L = 2KM$, where M is the number of bins and K is the *overlapping factor* [7]; the inputs to successive transforms are produced by overlapping segments of the received signal. Thus, in comparison to traditional length- M basis vectors, the basis vectors associated with LTs typically yield improved stopband attenuation in the frequency domain for a given filter bandwidth. Fortunately, there exist efficient filter bank structures that allow these longer basis vectors to be used while only moderately increasing the number of required arithmetic operations [7]. The improved stopband attenuation will contain partial-band interference to fewer transform bins, allowing the interference to be suppressed by removing fewer bins.

The remainder of the paper discusses the MLT and describes how it can be used in an OFDM system. Bit-error-rate (BER) performance results are presented

which compare the performance of the MLT-based OFDM system to systems using the FFT, DCT and a full-binary tree (FBT) subband decomposition.

2. MODULATED LAPPED TRANSFORMS

To be consistent with the development of LTs as presented in [8, 7], modulated lapped transforms are considered here as a subset of general LTs with $K = 1$. The basic premise of the MLT is to use a $2M$ -tap lowpass filter as a subband filter prototype which is shifted in frequency to produce a set of orthogonal bandpass FIR filters spanning the frequency domain. Denoting the lowpass prototype as $h[n]$, the sinusoidally modulated basis vectors can be expressed as [7]

$$\psi_k[n] = h[n] \sqrt{\frac{2}{M}} \cos \left[\left(n + \frac{M+1}{2} \right) \left(k + \frac{1}{2} \right) \frac{\pi}{M} \right], \quad (1)$$

where $0 \leq n \leq 2M - 1$ and $0 \leq k \leq M - 1$.

Of central importance to the development of the MLT is the design of the lowpass prototype, $h[n]$. To meet the perfect reconstruction requirements $h[n]$ must satisfy the following requirements [7],

$$h[2M - 1 - n] = h[n] \quad 0 \leq n \leq M - 1 \quad (2)$$

and

$$h^2[n] + h^2[n + M] = 1 \quad 0 \leq n \leq M/2 - 1. \quad (3)$$

Note that the range over n in the last equation is limited to $M/2 - 1$ due to the symmetry of $h[n]$ as suggested by Eq. 2. Although there are many solutions to the above equations, the half-sine windowing function [7],

$$h[n] = -\sin \left[\left(n + \frac{1}{2} \right) \frac{\pi}{2M} \right], \quad (4)$$

is used exclusively throughout the remainder of this paper as the MLT lowpass filter prototype. Figure 1 illustrates the frequency response associated with the half-sine windowing function for $M = 64$. Whereas non-windowed FFT basis vectors yield sidelobes that are roughly 13 dB down from the main lobe, the sidelobe energy level obtained using the MLT approximately 23.5 dB below that of the main lobe.

3. MLT OFDM SYSTEM

A spread spectrum OFDM system using block transforms and interference excision is shown in Figure 2. The input data is fed into an inverse transform and the result is transmitted passed through the channel to the receiver. It is assumed that the up- and down-conversion processes in the transceiver are transparent and that the receiver has symbol timing. At the receiver, a forward transform is performed to effectively frequency translate all the carriers to baseband. An exciser determines which carriers are predominantly interference and removes them and the remaining carriers are summed. A decision is then made on the current data bit.

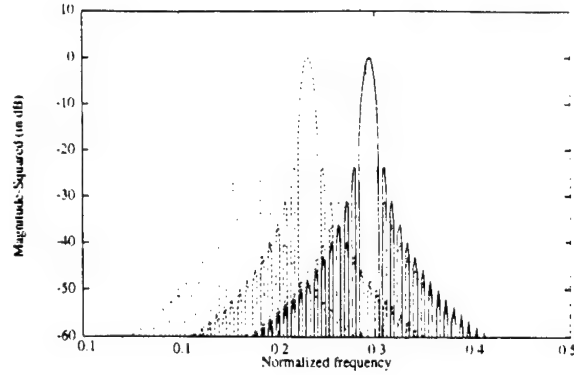


Figure 1. Typical magnitude-squared frequency response of the MLT subband filters.

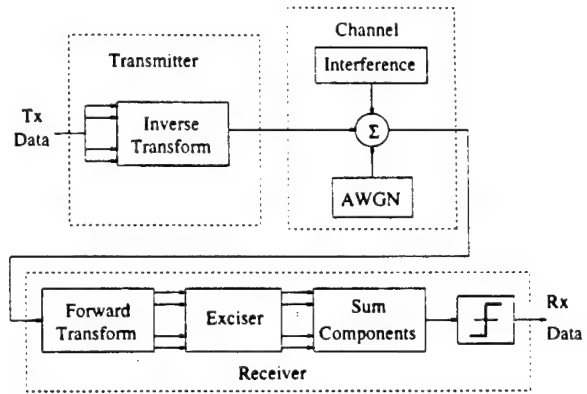


Figure 2. OFDM system using block transforms and interference excision

When a MLT is used in place of the block transform, the length of the basis vectors is double that for block transforms for a given number of carriers. Consequently, if the arrangement of Figure 2 were used to produce an MLT-based OFDM system, each data bit would produce a segment of the transmitted signal of length $2M$ samples when there are M carriers. In the case of block transform-based systems, the each data bit produced a transmitted signal containing the same number of samples as there are carriers. As a result, it would seem that the data rate would have to be cut in half to maintain the channel rate. However, due to the orthogonality properties of the MLT basis vectors, it is possible to overlap and sum sequential output vectors from the inverse MLT in the transmitter. When the overlap is 50%, the overlapping tails from adjacent data bits will be orthogonal to the present data bit, meaning that they will not affect detection performance. As a result of the overlap, M new samples are transmitted for every data bit when M carriers are used.

Figure 3 shows the processing that replaces the inverse and forward transforms in Figure 2 when the MLT is used. For simplicity, the signals shown are considered

to be vectors of length M . The upper diagram shows

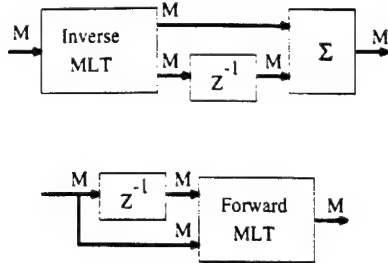


Figure 3. Transmitter (top) and receiver (bottom) processing in a MLT-based OFDM system

the processing that replaces the inverse transform in the transmitter. A vector of length M is input into the inverse MLT, producing an output vector of length $2M$ which is shown as two vectors of length M . One of these vectors represents the "upper" M vector elements and the other represents the "lower" M vector elements. A delay is used to allow the lower M elements from one inverse transform output to be summed with the upper M elements from the next inverse transform output, producing an M element vector for transmission. One of these M element vectors will be transmitted for each data bit.

The lower part of Figure 3 shows the processing which replaces the forward transform in the receiver of Figure 2 when the MLT is used. As is evident from the transmitter processing described above, only one-half of a particular inverse MLT output vector is transmitted at a given time. As a result, the receiver must observe two received vectors of length M in order to assemble the $2M$ vector elements needed for the forward transform. As the figure shows, the $2M$ length vector is produced by using the current received vector as the lower M element and a delayed received vector as the upper M elements for the forward MLT.

4. RESULTS

Simulation has been used to determine the performance of the OFDM spread spectrum system with a number of different transforms, including the FFT, DCT, MLT and a full binary tree (FBT) using 4-tap Daubechies filter coefficients[9]. In all cases a 64-bin transform was used. In the presence of AWGN only, all the systems provide the theoretical BPSK performance, as expected. A more interesting comparison is occurs when a tone jammer is used along with excision. The particular exciser that was used excises, i.e. sets to zero, any bins that exceed a fixed threshold along with a set number of adjacent bins. The removal of these adjacent bins produces a desired "notch width". To generate the BER results that are presented, Monte Carlo simulations were performed for each of the test systems and data was collected for a range of threshold and notch width values. All the data points presented below are the best results obtained for the threshold and notch width values tested. The re-

sults, then, represent a "best case" performance.

Figure 4 shows the BER performance as a function of normalized jammer frequency over the range of 0.125 to 0.140625. The normalization is to a sampling frequency of unity. These frequencies span the range between adjacent bin centers in the transforms. For this plot, the energy per bit to one-sided noise power spectral density E_b/N_o is 4 dB and the jammer-to-signal power ratio (JSR) is 30 dB. As expected, the results show some sym-

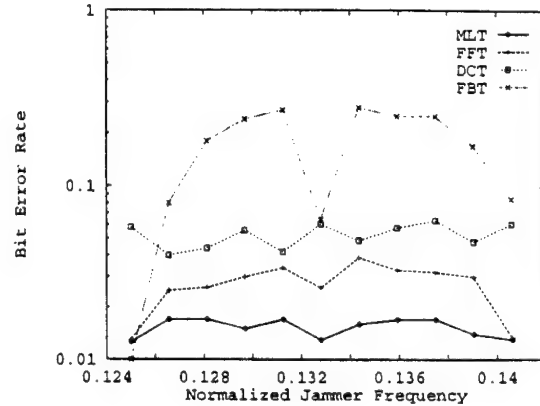


Figure 4. Ber performance as a function of jammer frequency with excision; $E_b/N_o = 4$ dB, JSR = 30 dB.

metry around the center frequency value, since each end value places the jammer frequency at a bin center. For the most part, the transforms perform best when the jammer occurs at a bin center due to the fact that these jammer frequencies minimize the spectral spreading due to windowing. For example, the FFT of a signal having a frequency that is a bin center frequency will be confined to a single bin even with rectangular windowing of the input. For other jammer frequencies, additional bins must be excised in order to remove the jammer energy, resulting in additional loss of signal energy and the increasing of the BER.

The MLT significantly outperforms the other transforms, maintaining a BER very near of 0.125, which is the value for AWGN alone with $E_b/N_o = 4$ dB. This excellent performance is due to the ability to the MLT transform in the receiver to contain the jammer energy to a few bins. It was observed that the best performance for MLT at all the frequencies tested was obtained when the notch width was between one and five bins. The FFT did not perform as well as the MLT, largely due to the fact that more bins had to be excised in order to remove the jammer. In this case the best performance was obtained when the notch width was between 15 and 17 bins except for the frequencies of 0.125 and 0.140625, where excising a single bin provided the best performance. The DCT also required a wide notch width, yet did not perform as well as the FFT. Finally, the FBT performed particularly poorly due to the fact that it cannot confine the jammer energy to a few bins.

Figure 5 shows the BER performance as a function

of E_b/N_o for the various transforms in the presence of a tone jammer with JSR = 30 dB and a normalized frequency of 0.135. Without excision, all the system perform very poorly in the presence of this jammer, with BER performance approaching 0.5. With excision, the MLT provides the best performance.

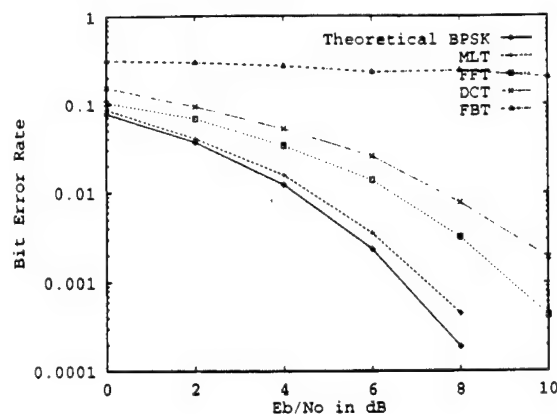


Figure 5. Performance of different transforms with excision as the SNR is increased; JSR = 30dB, normalized jammer frequency = 0.135.

Figure 6 shows how the performance of the systems varies with JSR. Once again, $E_b/N_o = 4$ dB and the normalized jammer frequency is 0.135. When JSR is low, i.e. in there is virtually no jamming, all the transforms provide the same performance of 0.0125. As the JSR increases towards 50 dB, the performance of each of the systems except the MLT degrades to nearly 0.5 BER, with the performance of the FBT falling off first, followed by the DCT and FFT. The spectral containment provided by the MLT again enables outperform the other transforms.

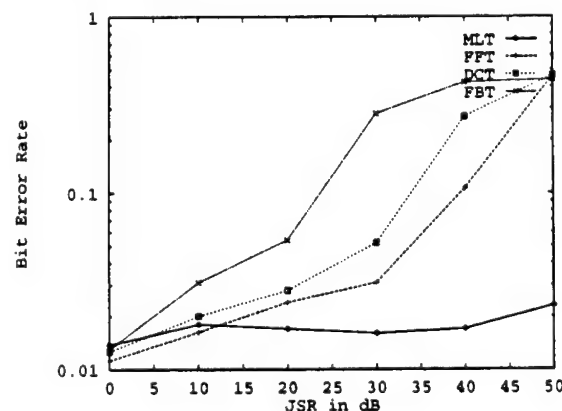


Figure 6. Performance of different transforms with excision as the JSR is increased; $E_b/N_o = 4$ dB, normalized jammer frequency = 0.135

5. CONCLUSIONS

This paper shows how a OFDM spread spectrum system can be constructed using the MLT. The performance of this MLT OFDM system is compared to that for OFDM systems implemented using block transforms when the channel introduces a tone jammer and the receiver performs interference excision. The superiority of the MLT-based system is clear demonstrated by the fact that, in the presence of a jammer, the BER performance remains near that for a channel for AWGN alone with little sensitivity to jammer frequency and JSR value.

The techniques used to implement the MLT-based system can be extended to transforms which use larger overlaps, such as the Extended Lapped Transform (ELT) [7]. By lengthening the basis functions further, even greater frequency selectivity can be obtained and, presumably, better performance in the presence of narrowband interference.

REFERENCES

- [1] *Asymmetric Digital Subscriber Line (ADSL) Metallic Interface*. ANSI T1E1.4/94-007R8, 1994.
- [2] L. B. Milstein and P. K. Das. An analysis of a real-time transform domain filtering digital communication system - Part I: Narrowband interference rejection. *IEEE Transactions on Communications*, COM-28(6):816-824, June 1980.
- [3] J. Gevargiz, M. Rosenmann, P. Das, and L. B. Milstein. A comparison of weighted and non-weighted transform domain processing systems for narrowband interference excision. In *IEEE MILCOM '84*, pages 32.3.1-32.3.4, October 1984.
- [4] L. B. Milstein and P. K. Das. An analysis of a real-time transform domain filtering digital communications system - Part II: Wideband interference rejection. *IEEE Transactions on Communications*, COM-31:21-27, June 1983.
- [5] M. Rosenmann, J. Gevargiz, P. Das, and L. B. Milstein. Probability of error measurement for an interference resistant transform domain processing receiver. In *IEEE MILCOM '83*, pages 638-640, October 1983.
- [6] J. G. Proakis. *Digital Communications*. McGraw-Hill, New York, 3rd edition, 1995.
- [7] H. S. Malvar. *Signal Processing with Lapped Transforms*. Artech House, Boston, 1992.
- [8] H. S. Malvar. Modulated QMF filter banks with perfect reconstruction. *Electronics Letters*, 26:906-907, June 1990.
- [9] I. Daubechies. Orthonormal basis of compactly supported wavelets. *Communications in Pure and Applied Mathematics*, XLI:909-996, 1988.

Appendix D: ICC, 1997

OFDM Spread Spectrum Communications using Lapped Transforms and Interference Excision*

Gary J. Saulnier and V. A. Alanzo Whyte
ECSE Dept, Rensselaer Polytechnic Institute
Troy, New York 12180-3590

Michael J. Medley
Rome Laboratory C3BB
Rome, New York 13441-4505

ABSTRACT: Two systems that use orthogonal frequency division multiplexing (OFDM) as a spread spectrum technique are described and their performance is evaluated in the presence of tone and pulsed Gaussian interference. One system obtains frequency diversity by sending the same data bit simultaneously on all the carriers while a second system obtains both time and frequency diversity by sequentially sending a given data bit on different carriers until it is sent on all possible carriers. Interference excision, in which some of the transform bins are removed in the detection process, is used in the receivers. Simulated BER performance in AWGN and interference is presented for systems that use a number of different block transforms and the Modulated Lapped Transform (MLT) and it is shown that the MLT provides much better performance due to its ability to confine the interference energy to a few transform bins.

1. INTRODUCTION

Orthogonal frequency division multiplexing (OFDM), often called multi-carrier modulation, is a method designed to efficiently utilize channels with non-flat frequency responses and/or non-white noise. The information to be transmitted is divided up among the many carriers in the system in a manner which optimizes the capacity for a given channel. This technique has been implemented for a variety of applications, including high-speed transmission over telephone lines. It has recently found application as the signaling standard for asymmetric digital subscriber lines (ADSL) [1].

In this paper, we study the use of OFDM as a *spread spectrum* modulation, where, rather than dividing up the information among the carriers, the *same* information is sent on all the carriers in the system. In effect, this technique spreads the signal bandwidth by a factor equal to the number of carriers in the system, assuming that the carriers are grouped together in the spectrum. Processing gain is obtained by coherently combining the signals on the various carriers in the receiver. In the presence of partial-band interference, a decision can be made to exclude some of the carriers from the coherent combiner if those carriers have been "jammed" by the interference. By excluding these carriers, the effect of the interference can be diminished and the performance of the system enhanced. This technique is similar to transform domain excision which has been studied extensively [2, 3, 4, 5]. This paper also discusses a variation to this technique in which a given data bit is sent *sequentially* on all the carriers rather than *simultaneously*. Consequently, at a given instant, a different data bit is being sent on each of the M carriers. Each data bit is also sent M times, once on each of the M different carriers, and the received energy for a given data bit is coherently combined to make a decision. It will be shown that this approach provides a performance gain when coupled with the exciser in the presence

of pulsed Gaussian interference.

To a large extent, multi-carrier systems have relied upon sinusoidal carriers to convey information. These systems can be implemented efficiently using the discrete Fourier transform (DFT) implemented as the fast Fourier transform (FFT). In the modulator, an inverse FFT is used to place the information on the equally-spaced carriers while, at the receiver, a forward FFT is used to frequency translate all the carriers to baseband. One problem with the FFT approach is that there is considerable spectral overlap with a large number of adjacent carriers, a problem which is often mitigated in multipath channels through the use of a cyclic prefix [6]. In the partial-band interference scenario the problem is magnified because processing by a rectangularly-windowed FFT will result in interference components being spread over a much larger portion of the band. To combat this problem, we propose to use non-sinusoidal carriers which are based on Lapped Transforms (LT) and, in particular, Modulated Lapped Transforms (MLT)[7]. This approach is similar to the wavelet-based OFDM system that was proposed by Sandberg [8]. With LTs, the basis vectors are not restricted in length as they are in conventional block transforms like the DFT and discrete cosine transform (DCT). Indeed, whereas the lengths of the block transform basis vectors are limited to the number of transform domain cells, or bins, the LT basis vectors have length, L , that is equal to some even integer multiple of the number of bins, i.e. $L = 2KM$, where M is the number of bins and K is the *overlapping factor* [7]; the inputs to successive transforms are produced by overlapping segments of the received signal. Thus, in comparison to traditional length- M basis vectors, the basis vectors associated with LTs typically yield improved stopband attenuation in the frequency domain for a given filter bandwidth. Fortunately, there exist efficient filter bank structures that allow these longer basis vectors to be used while only moderately increasing the number of required arithmetic operations [7]. The improved stopband attenuation will contain partial-band interference to fewer transform bins, allowing the interference to be suppressed by removing fewer bins.

The remainder of the paper discusses the MLT and describes how it can be used in an OFDM system. Bit-error-rate (BER) performance results are presented which compare the performance of the MLT-based OFDM system to systems using the FFT, DCT and a full-binary tree (FBT) subband decomposition.

2. MODULATED LAPPED TRANSFORMS

To be consistent with the development of LTs as presented in [9, 7], modulated lapped transforms are considered here as a subset of general LTs with $K = 1$. The basic premise of the MLT is to use a $2M$ -tap lowpass filter as a subband filter prototype which is shifted in frequency to produce a set of orthogonal bandpass FIR filters spanning the frequency domain. Denoting the lowpass prototype as $h[n]$, the sinusoidally modulated basis vectors can

*This work partially supported by the Air Force Materiel Command, Rome Laboratory contract no. F30602-95-C-0167

be expressed as [7]

$$\psi_k[n] = h[n] \sqrt{\frac{2}{M}} \cos \left[\left(n + \frac{M+1}{2} \right) \left(k + \frac{1}{2} \right) \frac{\pi}{M} \right], \quad (1)$$

where $0 \leq n \leq 2M-1$ and $0 \leq k \leq M-1$.

Of central importance to the development of the MLT is the design of the lowpass prototype, $h[n]$. To meet the perfect reconstruction requirements $h[n]$ must satisfy the following requirements [7],

$$h[2M-1-n] = h[n] \quad 0 \leq n \leq M-1 \quad (2)$$

and

$$h^2[n] + h^2[n+M] = 1 \quad 0 \leq n \leq M/2-1. \quad (3)$$

Note that the range over n in the last equation is limited to $M/2-1$ due to the symmetry of $h[n]$ as suggested by Eq. 2. Although there are many solutions to the above equations, the half-sine windowing function [7],

$$h[n] = -\sin \left[\left(n + \frac{1}{2} \right) \frac{\pi}{2M} \right], \quad (4)$$

is used exclusively throughout the remainder of this paper as the MLT lowpass filter prototype. Figure 1 illustrates the frequency response associated with the half-sine windowing function for $M = 64$. Whereas non-windowed FFT basis vectors yield sidelobes that are roughly 13 dB down from the main lobe, the sidelobe energy level obtained using the MLT approximately 23.5 dB below that of the main lobe.

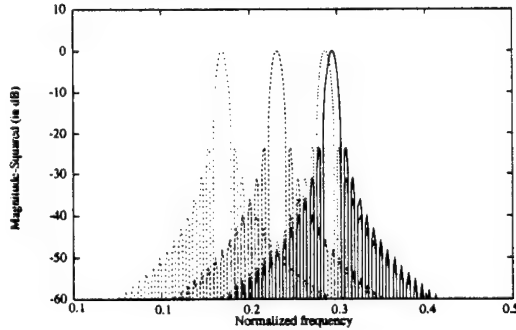


Figure 1. Typical magnitude-squared frequency response of the MLT subband filters.

3. OFDM SPREAD SPECTRUM SYSTEM

A spread spectrum OFDM system which includes interference excision in the receiver is shown in Figure 2. The input data is fed into an inverse transform and the result is passed through the channel to the receiver. It is assumed that the up- and down-conversion processes in the transceiver are transparent and that the receiver has symbol timing. At the receiver, a forward transform is performed to effectively frequency translate all the carriers to baseband. An exciser determines which carriers are predominantly interference and removes them and the remaining carriers are summed. A decision is then made on the current data bit.

When a MLT is used as the transform, the length of the basis vectors is double that for block transforms for a given number of carriers. However, the overlap processing as part of the transform makes it so that there are the same number of samples to transmit

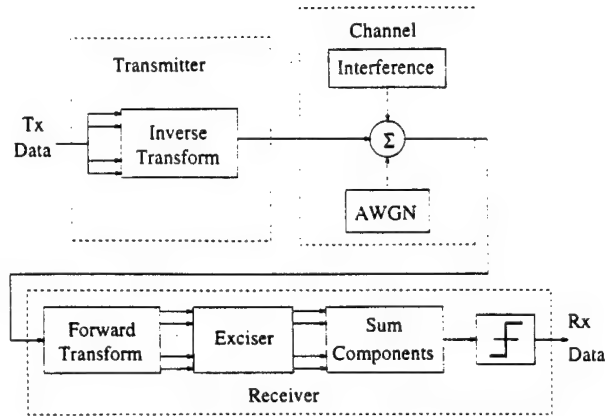


Figure 2. OFDM system using block transforms and interference excision

as with a block transform. This overlap processing within the inverse and forward transforms when the MLT is used is shown in Figure 2. For simplicity, the signals shown are considered to be vectors of length M . The upper diagram shows the processing that replaces the inverse transform in the transmitter. A vector of length M is multiplied by a $M \times 2M$ matrix, producing a vector of length $2M$ which is shown as two vectors of length M . One of these vectors represents the "upper" M vector elements and the other represents the "lower" M vector elements. A delay is used to allow the lower M elements from one inverse transform output to be summed with the upper M elements from the next matrix multiplication output, producing an M element vector for transmission. One of these M element vectors will be transmitted for each data bit.

The lower part of Figure 3 shows the processing which replaces the forward transform in the receiver of Figure 2 when the MLT is used. As is evident from the transmitter processing described above, only one-half of a particular inverse MLT output vector is transmitted at a given time. As a result, the receiver must observe two received vectors of length M in order to assemble the $2M$ vector elements needed for the forward transform. As the figure shows, the $2M$ length vector is produced by using the current received vector as the lower M element and a delayed received vector as the upper M elements for the forward MLT.

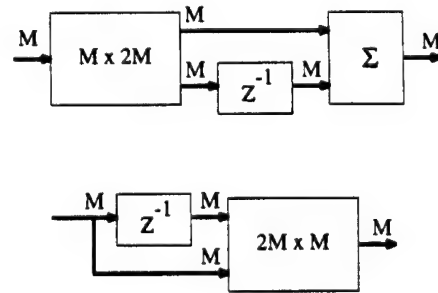


Figure 3. Transmitter (top) and receiver (bottom) processing in a MLT-based OFDM system

4. MODIFIED OFDM SYSTEM

The system of Figure 2 can be modified to insert some additional *time diversity* into the signal. The basic idea is that, rather than sending the same data on all the carriers simultaneously, a given data bit can sequence through the carriers in some pseudo-random pattern. As before, all the carriers in the system would always be carrying data but, now, a number of different data bits would be modulating carriers at a given time. For instance, each of the M carriers could be modulated by a different data bit and each data bit could modulate a different carrier in M successive intervals. In this case, the same amount of energy would be transmitted for each data bit as before, except that energy would now be spread over M data bit intervals rather than one. Of course, a given data bit could modulate a number of different carriers in each interval and be spread over a shorter time interval, if desired. Coherently combining all of the energy from the received carriers that are modulated by the same data bit would provide the same performance as the earlier system in AWGN.

There are several advantages of this new approach:

- The resulting signal would be much more "random" since the actual transmitted waveform would be the function of multiple data bits. Whereas, the original system would be simply sending the same waveform, inverted or non-inverted, during each data bit interval, this new system would have up to 2^M different waveforms which are chosen depending on sequence of data bits being sent. This property would make the signal more suitable for low probability of detection and low probability of intercept (LPD/LPI) applications.
- The time diversity would make the signaling scheme less susceptible to time-varying interference since segments of the signal can be lost while still retaining information from all the data bits.

Figure 4 shows the block diagram of the new system. The

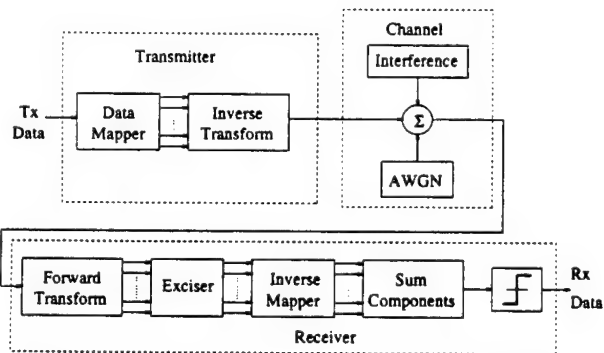


Figure 4. Modified OFDM spread spectrum system with time diversity.

new functions are a block in the modulator which maps the input data bits onto the carriers and a block in the demodulator which undoes this mapping operation and re-aligns in time all the energy corresponding to a single data bit. The primary feature of these blocks is that they have memory.

5. RESULTS

5.1. Original System

Simulation has been used to study the performance of the original OFDM spread spectrum system with a number of different

transforms, including the FFT, DCT, MLT and a full binary tree (FBT) using 4-tap Daubechies filter coefficients[10]. In all cases a 64-bin transform was used. In the presence of AWGN only, all the systems provide the theoretical BPSK performance, as expected. A more interesting comparison occurs when a tone jammer is used along with excision. The particular exciser that was used excises, i.e. sets to zero, any bins that exceed a fixed threshold along with a set number of adjacent bins. The removal of these adjacent bins produces a desired "notch width". To generate the BER results that are presented, Monte Carlo simulations were performed for each of the test systems and data was collected for a range of threshold and notch width values. All the data points presented below are the *best* results obtained for the threshold and notch width values tested. The results, then, represent a "best case" performance.

Figure 5 shows the BER performance as a function of normalized jammer frequency over the range of 0.125 to 0.140625. The normalization is to a sampling frequency of unity. These frequencies span the range between adjacent bin centers in the transforms. For this plot, the energy per bit to one-sided noise power spectral density E_b/N_0 is 4 dB and the jammer-to-signal power ratio (JSR) is 30 dB. As expected, the results show some

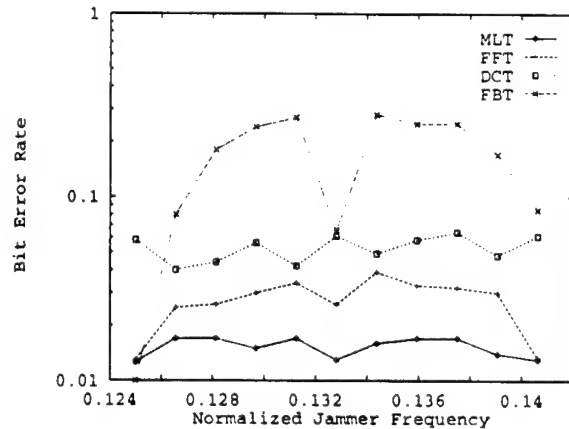


Figure 5. BER performance as a function of jammer frequency with excision; $E_b/N_0 = 4$ dB, JSR = 30 dB.

symmetry around the center frequency value, since each end value places the jammer frequency at a bin center. For the most part, the transforms perform best when the jammer occurs at a bin center due to the fact that these jammer frequencies minimize the spectral spreading due to windowing. For example, the FFT of a signal having a frequency that is a bin center frequency will be confined to a single bin even with rectangular windowing of the input. For other jammer frequencies, additional bins must be excised in order to remove the jammer energy, resulting in additional loss of signal energy and the increasing of the BER.

The MLT significantly outperforms the other transforms, maintaining a BER very near of 0.0125, which is the value for AWGN alone with $E_b/N_0 = 4$ dB. This excellent performance is due to the ability to the MLT transform in the receiver to contain the jammer energy to a few bins. It was observed that the best performance for MLT at all the frequencies tested was obtained when the notch width was between one and five bins. The FFT did not perform as well as the MLT, largely due to the fact that more bins had to be excised in order to remove the jammer. In this case the best performance was obtained when the notch width

was between 15 and 17 bins except for the frequencies of 0.125 and 0.140625, where excising a single bin provided the best performance. The DCT also required a wide notch width, yet did not perform as well as the FFT. Finally, the FBT performed particularly poorly due to the fact that it cannot confine the jammer energy to a few bins.

Figure 6 shows the BER performance as a function of E_b/N_o for the various transforms in the presence of a tone jammer with JSR = 30 dB and a normalized frequency of 0.135. Without excision, all the systems perform very poorly in the presence of this jammer, with BER performance approaching 0.5. With excision, the MLT provides the best performance.

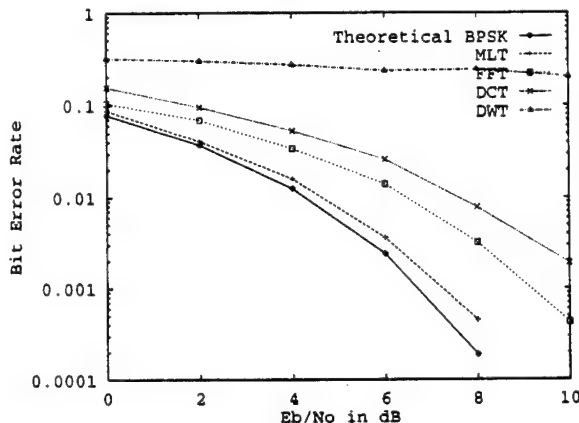


Figure 6. Performance of different transforms with excision as the SNR is increased; JSR = 30dB, normalized jammer frequency = 0.135.

Figure 7 shows how the performance of the systems varies with JSR. Once again, $E_b/N_o = 4$ dB and the normalized jammer frequency is 0.135. When JSR is low, i.e. in there is virtually no jamming, all the transforms provide the same performance of 0.0125. As the JSR increases towards 50 dB, the performance of each of the systems except the MLT degrades to nearly 0.5 BER, with the performance of the FBT falling off first, followed by the DCT and FFT. The spectral containment provided by the MLT again enables outperform the other transforms.

5.2. Modified System

Based on the superior performance of the MLT demonstrated above, the modified system was simulated using only the MLT. In this simulation, the data mapper simply stepped a data bit through the all 64 carriers, i.e. each data bit modulated a different carrier for each of 64 sequential data bit intervals. Initial simulations in AWGN showed that the system performance matched that of BPSK in AWGN, as expected. Additionally, simulations with tone jamming showed that both systems performed virtually the same. This result is expected since the additional time diversity of the modified system does not provide any advantage for a continuous-tone jammer.

Both systems were also tested in the presence of pulsed Gaussian jamming. In this case, the jammer consisted of gated white Gaussian noise with duty factors of 10% and 25% and a repetition period of 7.8125 times the data bit interval. With this repetition period and duty factors, the high-power Gaussian noise does not affect every transform in the receiver. While *time-domain excision*, in which time segments of the received signal are excised, would be the preferable approach to suppressing this type

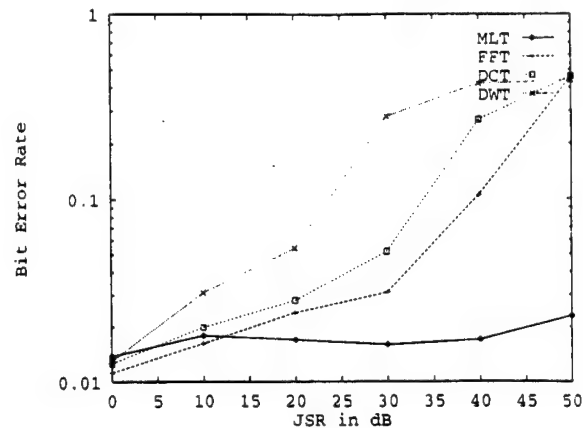


Figure 7. Performance of different transforms with excision as the JSR is increased; $E_b/N_o = 4$ dB, normalized jammer frequency = 0.135

of jammer, the performance of the original and modified systems with the transform domain excision was studied.

Figures 8 and 9 show the performance of the two systems in the presence of a pulsed Gaussian jammer with JSR = 30dB and a duty factors of 0.1 and 0.25, respectively. As the figures show,

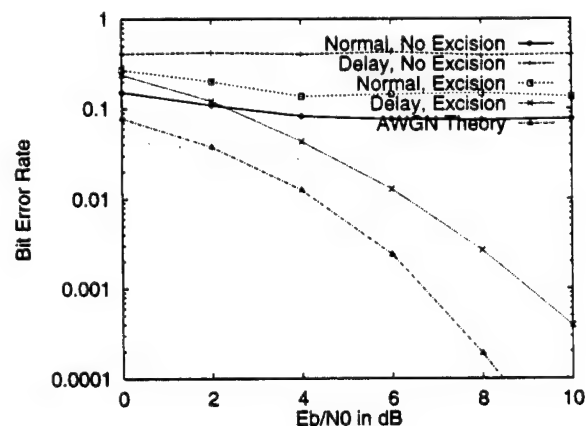


Figure 8. Performance of the systems with a pulsed Gaussian jammer; JSR = 30dB, duty factor = 0.1, repetition rate = 7.8125 times the bit duration.

the modified system (labeled as "delay") performs worse than the original system (labeled as "normal") when excision is not used. This performance difference occurs because the pulsed jammer is able to affect all the data bits in the modified system due to the fact that a particular data bit modulates a carrier in 64 successive data bit intervals. In the original system, however, the jammer was inactive during some bit intervals, allowing the correct detection of some data bits. However, when excision is used, the situation is reversed and modified system is clearly superior. In fact, the same reason that the original system is better without excision makes the modified system better with excision. In the original system excision is totally ineffective because, if the pulsed jammer is active during a data bit, that data bit is simply lost; excision just removes both the data bit energy and the jammer. The

results with the exciser tended to only worsen the performance of the original system with this jammer. With the modified system, however, excision is very effective since removing jammed portions of the signal removes the contribution of these jammed carriers to the coherent combiner and allows detection to be performed using data bit energy contained in the unjammed carriers.

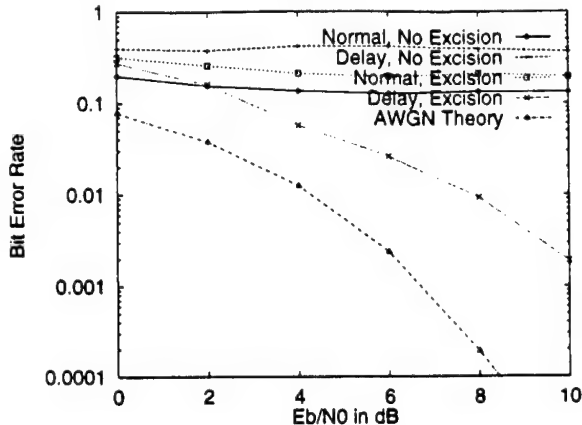


Figure 9. Performance of the systems with a pulsed Gaussian jammer; JSR = 30dB, duty factor = 0.25, repetition rate = 7.8125 times the bit duration.

Comparison of the two figures shows that, as the duty factor increases, the performance of the modified system with excision worsens. Figure 10 shows the BER performance for $E_b/N_o = 6\text{dB}$ and JSR = 30dB as the duty factor increases. As the duty

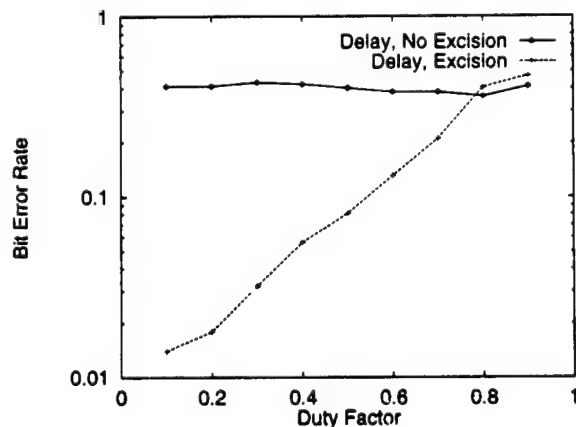


Figure 10. Performance of the modified system with and without excision as a function of the duty factor; $E_b/N_o = 6\text{dB}$, JSR = 30dB.

factor approaches unity, the jammer approaches a white Gaussian jammer and the excision technique becomes totally ineffective.

6. CONCLUSIONS

This paper shows how an OFDM spread spectrum system can be constructed using the MLT. The performance of this MLT OFDM system is compared to that for OFDM systems implemented using block transforms when the channel introduces a tone jammer and the receiver performs interference excision. The superiority of the

MLT-based system is clearly demonstrated by the fact that, in the presence of a tone jammer, the BER performance remains near that for a channel with AWGN alone, showing little sensitivity to jammer frequency and JSR value.

Additionally, the OFDM system was modified to spread the data bits in both time and frequency. In this way, it is possible to obtain protection from time-varying channel effects such as pulsed jamming. Results using a MLT and a transform domain exciser demonstrated this protection. Additional work will focus on applying a time-domain exciser under these conditions.

REFERENCES

- [1] *Asymmetric Digital Subscriber Line (ADSL) Metallic Interface*. ANSI T1E1.4/94-007R8, 1994.
- [2] L. B. Milstein and P. K. Das. An analysis of a real-time transform domain filtering digital communication system - Part I: Narrowband interference rejection. *IEEE Transactions on Communications*, COM-28(6):816-824, June 1980.
- [3] J. Gevargiz, M. Rosenmann, P. Das, and L. B. Milstein. A comparison of weighted and non-weighted transform domain processing systems for narrowband interference excision. In *IEEE MILCOM '84*, pages 32.3.1-32.3.4, October 1984.
- [4] L. B. Milstein and P. K. Das. An analysis of a real-time transform domain filtering digital communications system - Part II: Wideband interference rejection. *IEEE Transactions on Communications*, COM-31:21-27, June 1983.
- [5] M. Rosenmann, J. Gevargiz, P. Das, and L. B. Milstein. Probability of error measurement for an interference resistant transform domain processing receiver. In *IEEE MILCOM '83*, pages 638-640, October 1983.
- [6] J. G. Proakis. *Digital Communications*. McGraw-Hill, New York, 3rd edition, 1995.
- [7] H. S. Malvar. *Signal Processing with Lapped Transforms*. Artech House, Boston, 1992.
- [8] S. D. Sandberg and M. A. Tzannes. Overlapped discrete multitone modulation for high speed copper wire communications. *IEEE Journal on Selected Areas in Communications*, SAC-13(9):1571-1585, December 1995.
- [9] H. S. Malvar. Modulated QMF filter banks with perfect reconstruction. *Electronics Letters*, 26:906-907, June 1990.
- [10] I. Daubechies. Orthonormal basis of compactly supported wavelets. *Communications in Pure and Applied Mathematics*, XLI:909-996, 1988.

Appendix E: MILCOM, 1997

PERFORMANCE OF AN OFDM SPREAD SPECTRUM COMMUNICATIONS SYSTEM USING LAPPED TRANSFORMS

Gary J. Saulnier and Mike Mettke
ECSE Dept, Rensselaer Polytechnic Institute
Troy, New York 12180-3590

Michael J. Medley
Rome Laboratory, C3BB
Rome, New York 13441-4505

ABSTRACT

Two systems that use orthogonal frequency division multiplexing (OFDM) as a spread spectrum technique are described and their performance is evaluated in the presence of tone and pulsed Gaussian interference. One system obtains frequency diversity by sending the same data bit simultaneously on all the carriers while a second system obtains both time and frequency diversity by sequentially sending a given data bit on different carriers until it is sent on all possible carriers. Interference excision, in which some of the transform bins are removed in the detection process, is used in the receivers. Simulated BER performance in AWGN and interference is presented for systems that use a number of different block transforms and the Modulated Lapped Transform (MLT) and it is shown that the MLT provides much better performance due to its ability to confine the interference energy to a few transform bins.

1. INTRODUCTION

Orthogonal frequency division multiplexing (OFDM) has received considerable attention as a method to efficiently utilize channels with non-flat frequency responses and/or non-white noise. The information to be transmitted is divided up among the many carriers in the system in a manner which optimizes the capacity for a given channel. This technique has been implemented for a variety of applications, including high-speed transmission over telephone lines. It has recently found application as the signaling standard for asymmetric digital subscriber lines (ADSL) [1].

This paper considers the use of OFDM as a spread spectrum modulation wherein spectral spreading is accomplished by putting the same data on all the carriers, producing a spreading factor equal to the number of carriers. At the receiver, the energy from all the carriers is coherently combined to produce the decision variable. A benefit of this type of system arises can be felt the presence of partial-band interference since jammed carriers can be omitted from the coherent combining operation. This technique is similar to transform domain excision which has been studied extensively [2, 3, 4, 5] for use in direct sequence spread spectrum receivers. In these systems, a received signal with partial-band jamming is processed by a transform, most often a Fourier Transform or Fast Fourier Transform (FFT), and portions of the transform which are primarily jammer are "excised", i.e. set to zero. The effect is to remove most of the jammer energy and only a small amount of desired signal energy, producing improved receiver performance. In the system discussed in this paper, the excision is performed on a carrier-by-carrier basis, where jammed carriers are omitted from the decision process.

To a large extent, OFDM systems have been implemented efficiently using the discrete Fourier transform (DFT) implemented as the fast Fourier transform (FFT). In the modulator, an inverse

FFT is used to place the information on the equally-spaced carriers while, at the receiver, a forward FFT is used to frequency translate all the carriers to baseband. One problem with the FFT approach is that there is considerable spectral overlap among the orthogonal carriers. This overlap is not a problem unless the orthogonality is lost due to channel effects such as multipath fading, producing inter-carrier and inter-symbol interference. This problem is often mitigated through the use of a cyclic prefix [6]. In the partial-band interference case the problem is magnified because processing by a rectangularly-windowed FFT will result in interference energy falling into many transform bins even when this interference is confined to a small portion of the transmit spectrum. This problem is the result of the $\sin x/x$ frequency response of each bin of the FFT. To combat this problem, we propose to use carriers which are based on Lapped Transforms (LT) and, in particular, Modulated Lapped Transforms (MLT)[7]. This approach is similar to the wavelet-based OFDM system that was proposed by Sandberg [8]. With LTs, the basis vectors are not restricted in length as they are in conventional block transforms like the DFT and discrete cosine transform (DCT). Indeed, whereas the lengths of the block transform basis vectors are limited to the number of transform domain cells, or bins, the LT basis vectors have length, L , that is equal to some even integer multiple of the number of bins, i.e. $L = 2KM$, where M is the number of bins and K is the overlapping factor [7]; the inputs to successive transforms are produced by overlapping segments of the received signal. Thus, in comparison to traditional length- M basis vectors, the basis vectors associated with LTs typically yield improved stopband attenuation in the frequency domain for a given filter bandwidth. Fortunately, there exist efficient filter bank structures that allow these longer basis vectors to be used while only moderately increasing the number of required arithmetic operations [7]. The improved stopband attenuation will contain partial-band interference to fewer transform bins, allowing the interference to be suppressed by removing fewer bins. The use of LT's in place of FFT's produces a form of partial-response signaling since information derived from a particular data bit will affect each carrier for a period lasting multiple data bits in duration.

Kaleh proposed an OFDM spread spectrum system which has carriers with disjoint frequency support and studied its performance in partial-band Gaussian jamming [9]. He derived the optimal receiver and showed its performance and, in addition, showed a sub-optimal receiver which uses an exciser to remove jammed carriers. The system proposed here is similar to the sub-optimal system, though it differs in that it uses lapped transforms and also introduces time-diversity into the signal. This time diversity is produced by having a given data bit modulate only a subset of the carriers at a given time, therefore requiring multiple data bit intervals to modulate all the carriers. In a simple example, a given data bit may only modulate one carrier at a time, requiring M data bit intervals to step through each of the M carriers. It is important to emphasize that each data bit is still sent on each of

*This work partially supported by the Air Force Materiel Command, Rome Laboratory contract no. F30602-95-C-0167

the M carriers; the difference is that each data bit will not modulate all the carriers at the same time. At the receiver, energy from all the M carriers associated with a given data bit is still coherently combined to make a decision.

An advantage of inserting time diversity is that the signal can be less susceptible to time-varying interference, such as a pulsed jammer. Time segments of the received signal can be lost while still maintaining adequate performance. To illustrate this point, we will consider pulsed Gaussian jamming and a receiver equipped with a time-domain exciser, i.e. time segments of the received signal which are jammed will be set to zero. It will be shown that the introduction of time diversity provides a performance gain when coupled with this exciser in the presence of pulsed Gaussian interference.

The use of an OFDM spread spectrum signal rather than the conventional direct sequence signal opens up a number of possibilities:

- The transmitter can adjust the transmit spectrum in response to the jamming conditions by varying the power of each of the carriers.
- Coding can be used in place of simply sending the same data on all the carriers. In essence a repetition code can be replaced by a much better code.
- Inserting time diversity produces a transmitted waveform that is the function of multiple data bits. Consequently, there are up to 2^M different waveforms which are chosen depending on sequence of data bits being sent. This property could make the signal more suitable for low probability of detection and low probability of intercept (LPD/LPI) applications.

The remainder of the paper discusses the MLT and describes how it can be used in an OFDM system. Simulated bit-error-rate (BER) performance results are presented which compare the performance of the MLT-based OFDM system to a system using the FFT.

2. MODULATED LAPPED TRANSFORMS

Inherent in the design of LTs is the satisfaction of the *perfect reconstruction* (PR) criterion, which implies that for an input sequence, $x[n]$, the reconstructed signal samples, $\hat{x}[n]$, are equal to the original values to within a constant scale and delay adjustment, i.e.

$$\hat{x}[n] = cx[n - n'], \quad (1)$$

where c and n' are constants.

To be consistent with the development of LTs as presented in [10, 7], modulated lapped transforms are considered here as a subset of general LTs with $K = 1$. The basic premise of the MLT is to use a $2M$ -tap lowpass filter as a subband filter prototype which is shifted in frequency to produce a set of orthogonal bandpass FIR filters spanning the frequency domain. Denoting the lowpass prototype as $h[n]$, the sinusoidally modulated basis vectors can be expressed as [7]

$$\psi_k[n] = h[n] \sqrt{\frac{2}{M}} \cos \left[\left(n + \frac{M+1}{2} \right) \left(k + \frac{1}{2} \right) \frac{\pi}{M} \right], \quad (2)$$

where $0 \leq n \leq 2M - 1$ and $0 \leq k \leq M - 1$.

Of central importance to the development of the MLT is the design of the lowpass prototype, $h[n]$. To meet the perfect reconstruction requirements $h[n]$ must satisfy the following requirements [7],

$$h[2M - 1 - n] = h[n] \quad 0 \leq n \leq M - 1 \quad (3)$$

and

$$h^2[n] + h^2[n + M] = 1 \quad 0 \leq n \leq M/2 - 1. \quad (4)$$

Note that the range over n in the last equation is limited to $M/2 - 1$ due to the symmetry of $h[n]$ as suggested by (3). Although there are many solutions to the above equations, the half-sine windowing function [7],

$$h[n] = -\sin \left[\left(n + \frac{1}{2} \right) \frac{\pi}{2M} \right], \quad (5)$$

is used exclusively throughout the remainder of this paper as the MLT lowpass filter prototype. Figure 1 illustrates the frequency response associated with the half-sine windowing function for $M = 64$. Whereas non-windowed FFT basis vectors yield sidelobes that are roughly 13 dB down from the main lobe, the sidelobe energy level obtained using the MLT approximately 23.5 dB below that of the main lobe.

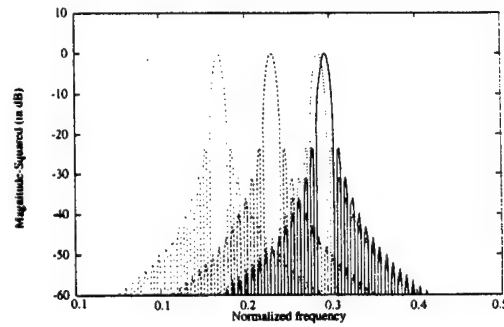


Figure 1. Typical magnitude-squared frequency response of the MLT subband filters.

The implementation of LT's and their inverses can be viewed in terms of either filter banks or transforms. Figure 2 shows the LT from a transform perspective. The implementation of the forward transform requires that segments of the input signal be overlapped in time, as shown in the top part of Figure 2. Here,

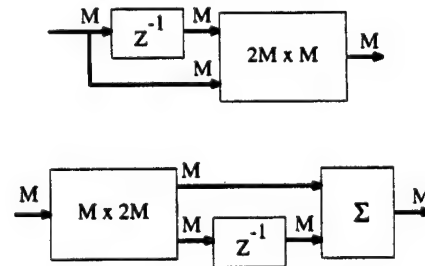


Figure 2. Forward (top) and Inverse (bottom) processing in the MLT

a M bin MLT is implemented, requiring an input data segment of length $2M$. Once the $2M$ length vector of input samples is assembled, the remainder of the transform can be implemented as a matrix multiply. The processing in the inverse transform is shown at the bottom of Figure 2.

3. OFDM SPREAD SPECTRUM SYSTEM

A spread spectrum OFDM system which includes both time and transform domain interference excision in the receiver is shown in Figure 3. The input data is fed into a data mapper block which

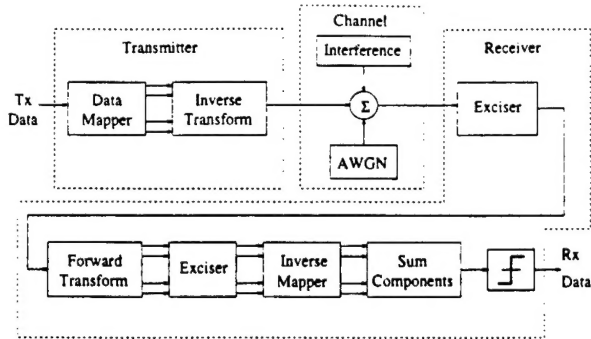


Figure 3. OFDM system using block transforms and interference excision

determines how the data is applied to the carriers. In a simple system without time diversity, this block simply applies the same data bit to all carriers concurrently. When time diversity is used, this data mapper block must have memory since a single data bit will affect one or more carriers over a number of bit intervals. The output of the data mapper goes to an inverse transform and the result is passed through the channel to the receiver. It is assumed that the up- and down-conversion processes in the transceiver are transparent and that the receiver has symbol timing. At the receiver, the signal first passes through a time domain exciser which removes time segments of the received signal that have power that is significantly above the average power of the signal. The purpose of this block is to remove pulsed interference. A forward transform is then performed to effectively frequency translate all the carriers to baseband. An transform domain exciser then determines which of the demodulated carriers are predominantly interference and removes them. The remaining demodulated carriers are fed to the inverse mapper which undoes the operation performed by the data mapper in the transmitter, thereby time-aligning all the information associated with a particular data bit. The components at the output of the inverse mapper are summed and a decision device is used to determine the data bit that was sent.

4. TEST SYSTEMS

Simulation has been used to study the performance of a binary OFDM spread spectrum system, both with and without time-diversity, when the transform is the FFT and MLT. In all cases a 64-bin transform was used and all carriers had equal power. In the presence of AWGN only, all four systems provide the theoretical BPSK performance, as expected. A more interesting comparison occurs when a jamming is used along with excision. The two types of jammers considered are fixed frequency tone jamming and pulsed broadband Gaussian jamming and the performance was measured for each of these jammers individually. The tone jammer is localized in frequency and is particularly amenable to frequency domain excision. The type of frequency domain exciser that was used sets to zero any bins that exceed a fixed threshold along with a set number of adjacent bins. The removal of these adjacent bins produces a desired "notch width". The pulsed broadband Gaussian jammer is localized in time and, therefore,

is well matched to a time domain exciser. The particular implementation of this exciser sets to zero any received signal samples having a power that exceeds the average signal power by a set amount. To generate the BER results that are presented, Monte Carlo simulations were performed for each of the test systems and data was collected for a range of exciser parameter values. All the data points presented below are the *best* results considering all the tested exciser parameter values, meaning the results represent a "best case" performance which may not be achievable when a practical exciser is used.

5. RESULTS

5.1. Tone Jammer

Figure 4 shows the BER performance as a function of normalized jammer frequency over the range of 0.125 to 0.140625. The normalization is to a sampling frequency (and chip rate) of unity. These frequencies span the range between adjacent bin centers in the transforms. For this plot, the energy per bit to one-sided noise power spectral density E_b/N_0 is 4 dB and the jammer-to-signal power ratio (JSR) is 30 dB. As expected, the results show

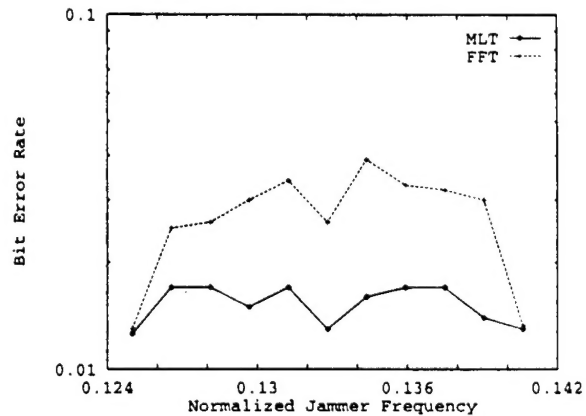


Figure 4. BER performance for a tone jammer as a function of jammer frequency with excision and without time-diversity; $E_b/N_0 = 4\text{dB}$, JSR = 30dB.

some symmetry around the center frequency value, since each end value places the jammer frequency at a bin center. Both transforms perform best when the jammer occurs at a bin center due to the fact that these jammer frequencies minimize the spectral spreading due to windowing. For example, the FFT of a signal having a frequency that is a bin center frequency will be confined to a single bin even with rectangular windowing of the input. For other jammer frequencies, additional bins must be excised in order to remove the jammer energy, resulting in additional loss of signal energy and the increasing of the BER.

The MLT significantly outperforms the FFT, maintaining a BER very near 0.0125, which is the value for AWGN alone with $E_b/N_0 = 4\text{dB}$. This excellent performance is due to the ability to the MLT transform in the receiver to contain the jammer energy to a few bins. It was observed that the best performance for MLT at all the frequencies tested was obtained when the notch width was between one and five bins. The FFT did not perform as well as the MLT, largely due to the fact that more bins had to be excised in order to remove the jammer. In this case the best performance was obtained when the notch width was between 15 and

17 bins except for the frequencies of 0.125 and 0.140625, where excising a single bin provided the best performance.

Figure 5 shows the BER performance as a function of E_b/N_o in the presence of the tone jammer with JSR = 30 dB and a normalized frequency of 0.135. Without excision, both systems perform very poorly in the presence of this jammer, with BER performance approaching 0.5. With excision, the MLT provides the best performance.

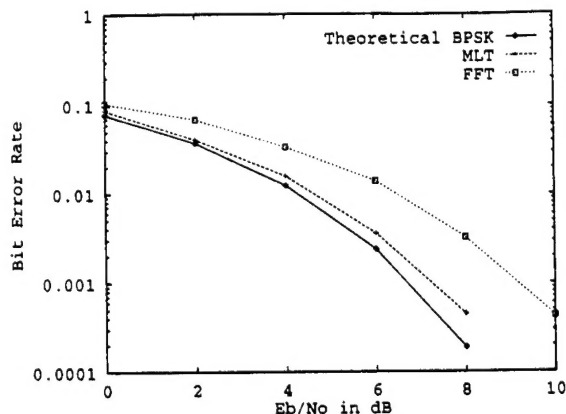


Figure 5. BER performance for a tone jammer as a function of E_b/N_o with excision and without time diversity; JSR = 30dB, normalized jammer frequency = 0.135.

Figure 6 shows how the performance of the systems varies with JSR. Once again, $E_b/N_o = 4$ dB and the normalized jammer frequency is 0.135. When JSR is low, i.e. when there is virtually no jamming, both transforms provide the same performance of 0.0125. As the JSR increases towards 50 dB, the performance of the FFT falls off first, heading toward a value of 0.5. The spectral containment provided by the MLT again enables outperform the FFT.

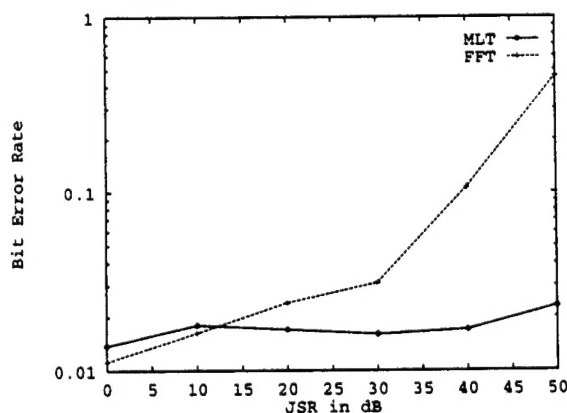


Figure 6. BER performance for a tone jammer as a function of JSR with excision and without time diversity; $E_b/N_o = 4$ dB, normalized jammer frequency = 0.135

The results presented above are for the case where time diversity is not used, meaning that a data bit is transmitted on all the

carriers simultaneously. Simulations using time diversity are not shown since they yielded nearly identical performance results as those shown. This is a sensible result since time diversity should not provide an advantage for a jammer that is active at all times.

5.2. Pulsed Gaussian Jammer

The systems were also tested in the presence of pulsed Gaussian jamming. In this case, the jammer consisted of gated white Gaussian noise with duty factors of 0.1, 0.25 and 0.4 and a repetition period of 7.8125 times the data bit interval. With this repetition period and these duty factors, the high-power Gaussian noise does not affect every transform in the receiver.

Figures 7, 8 and 9 show the performance of the two systems when the duty factors are 0.1, 0.25 and 0.4, respectively. Each plot shows the performance of the MLT and FFT systems both with and without diversity.

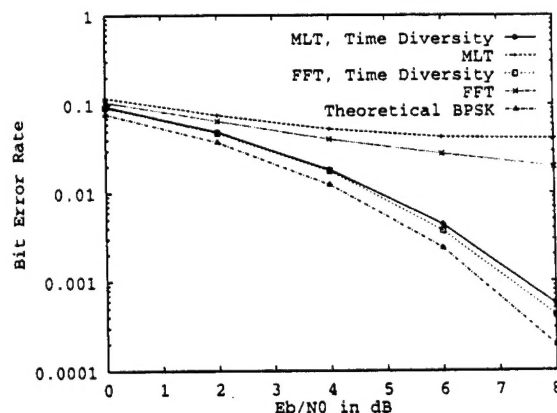


Figure 7. Performance of the systems with a pulsed Gaussian jammer; JSR = 30dB, duty factor = 0.1, repetition rate = 7.8125 times the bit duration.

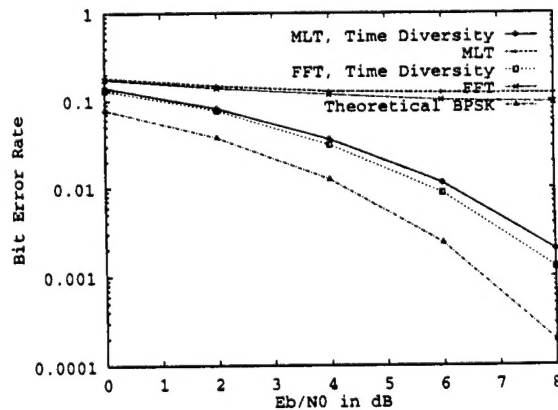


Figure 8. Performance of the systems with a pulsed Gaussian jammer; JSR = 30dB, duty factor = 0.25, repetition rate = 7.8125 times the bit duration.

For all the cases tested, the systems with time diversity provide much better performance than the systems without time diversity. This is an expected result since, without time diversity, loss of a

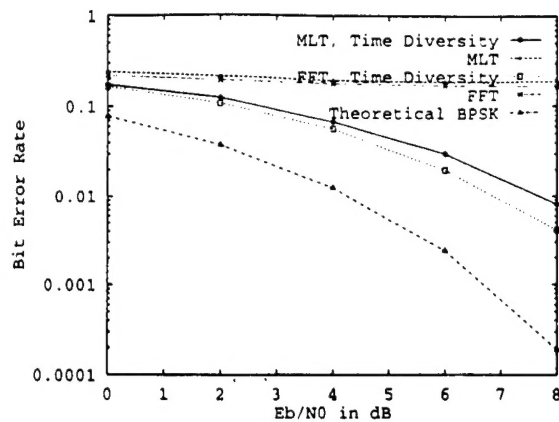


Figure 9. Performance of the systems with a pulsed Gaussian jammer; JSR = 30dB, duty factor = 0.4, repetition rate = 7.8125 times the bit duration.

time segment of the received signal can result in the loss of most, if not all, of the information associated with one or more data bits. For the repetition rate that was used, a duty factor of 0.1 makes the jammer active for time segments that are slightly less than a data bit interval while duty factors of 0.25 and 0.4 make the jammer active for segments greater than a data bit interval. With the time diversity used in the simulation, i.e. spreading a data bit over 64 data bit intervals, it is necessary to jam a time segment having a duration of 64 data bit intervals in order to lose all the information for a data bit. Consequently, the time domain excision of the pulsed jammer with time diversity tends to slightly reduce the received energy for a large number of data bits while, without time diversity, the excision tends to greatly reduce the received energy for a few data bits.

For all the duty factors tested, the FFT systems provide better performance than the MLT systems. This is due to the fact that excising a time segment of the waveform in the MLT case produces some inter-symbol interference (ISI). This ISI is the result of the fact that the MLT system produces partial response signals and loss of a time segment of the received signal results in incomplete cancellation of the overlapping data bits in the receiver.

As expected, the performance of all the systems decreases as the duty factor increases since time domain excision becomes less effective, removing more signal along with the jammer. With a greater duty cycle, the jammer approaches a white noise jammer.

6. CONCLUSIONS

This paper shows how an OFDM spread spectrum systems can be constructed using the MLT and FFT and how time and transform domain excision can be used with these systems to improve their performance in the presence of jamming. Transform domain excision is useful for narrowband jamming, since frequency segments of the received signal can be excised, thereby removing much of the jammer power and retaining much of the signal power. Time domain excision is useful for jammers that are localized in time.

The OFDM systems considered include some which introduce time diversity into the signal by having a given data bit modulate a subset of carriers over multiple data bit intervals. This time diversity provides a performance advantage with time-localized jamming.

The MLT system was shown to be better than the FFT system when tone jamming is used along with a transform transform do-

main exciser. This is due to the fact that the MLT does a better job at confining the jammer to a few transform bins, making it possible for the exciser to be more effective. The MLT is able to do this by having basis functions with greater time support, extending over 2 data bit intervals as opposed to one data bit interval for the FFT. This additional time support, however, proves to be a disadvantage with time-localized jamming. The result is that the FFT system performs better with a pulsed Gaussian jammer.

REFERENCES

- [1] *Asymmetric Digital Subscriber Line (ADSL) Metallic Interface*. ANSI T1E1.4/94-007R8, 1994.
- [2] L. B. Milstein and P. K. Das. An analysis of a real-time transform domain filtering digital communication system - Part I: Narrowband interference rejection. *IEEE Transactions on Communications*, COM-28(6):816-824, June 1980.
- [3] J. Gevargiz, M. Rosenmann, P. Das, and L. B. Milstein. A comparison of weighted and non-weighted transform domain processing systems for narrowband interference excision. In *IEEE MILCOM '84*, pages 32.3.1-32.3.4, October 1984.
- [4] L. B. Milstein and P. K. Das. An analysis of a real-time transform domain filtering digital communications system - Part II: Wideband interference rejection. *IEEE Transactions on Communications*, COM-31:21-27, June 1983.
- [5] M. Rosenmann, J. Gevargiz, P. Das, and L. B. Milstein. Probability of error measurement for an interference resistant transform domain processing receiver. In *IEEE MILCOM '83*, pages 638-640, October 1983.
- [6] J. G. Proakis. *Digital Communications*. McGraw-Hill, New York, 3rd edition, 1995.
- [7] H. S. Malvar. *Signal Processing with Lapped Transforms*. Artech House, Boston, 1992.
- [8] S. D. Sandberg and M. A. Tzannes. Overlapped discrete multitone modulation for high speed copper wire communications. *IEEE Journal on Selected Areas in Communications*, SAC-13(9):1571-1585, December 1995.
- [9] G. K. Kaleh. Frequency-diversity spread-spectrum communication system to counter bandlimited gaussian interference. *IEEE Transactions on Communications*, 44(7):886-893, July 1996.
- [10] H. S. Malvar. Modulated QMF filter banks with perfect reconstruction. *Electronics Letters*, 26:906-907, June 1990.

***MISSION
OF
AFRL/INFORMATION DIRECTORATE (IF)***

The advancement and application of information systems science and technology for aerospace command and control and its transition to air, space, and ground systems to meet customer needs in the areas of Global Awareness, Dynamic Planning and Execution, and Global Information Exchange is the focus of this AFRL organization. The directorate's areas of investigation include a broad spectrum of information and fusion, communication, collaborative environment and modeling and simulation, defensive information warfare, and intelligent information systems technologies.